

**Development of Lap Splices Using Headed Reinforcement**

**by**

**Antonio Lopez Ledesma, B.S.C.E.**

**Thesis**

Presented to the Faculty of the Graduate School of

The University of Texas at Austin

in Partial Fulfillment

of the Requirements

for the Degree of

**Master of Science in Engineering**

**The University of Texas at Austin**

**May 2000**

## **Development of Lap Splices Using Headed Reinforcement**

**Approved by**

**Supervising Committee:**

---

**John E. Breen**

---

**James O. Jirsa**

## **Dedication**

To my family

## **Acknowledgements**

I would like to thank Prof. John E. Breen and Prof. James O. Jirsa for their guidance and patience. Their support and advice throughout this study have been immeasurable.

Special thanks to M. Keith Thompson who was the Ph.D. student for this study and Michele Young who was also part of the research team. Without their help, I would not have been able to get this done. The staff of the Ferguson Structural Engineering Laboratory was invaluable in the completion of my research as were all of my fellow students who helped during the casting of my specimens.

Thanks to Dean VanLanduyt and the Texas Department of Transportation for sponsoring the project. Thanks to Headed Reinforcement Corporation and Erico, Inc. for supplying the headed reinforcement used in this study.

Finally, I would like to thank my parents who offer unconditional support in whatever I do.

May 5, 2000

## **Abstract**

### **Development of Lap Splices Using Headed Reinforcement**

Antonio Lopez Ledesma, M.S.E.

The University of Texas at Austin, 2000

Supervisor: John E. Breen

Recent progress in the fabrication of headed reinforcement provides opportunities for simplifying some details common to bridge structures. This study focused on the use of headed bars in lap splicing applications. Sixteen tests were evaluated to determine the behavior of unconfined headed bar lap splices. Variables included strength of staggered splices vs. adjacent splices, head size, head shape, bar spacing, lap length, and bar size. Conclusions were made concerning each variable and a model is proposed to determine the capacity of the lap splice.

## Table of Contents

<b>ACKNOWLEDGEMENTS.....</b>	<b>IV</b>
<b>ABSTRACT .....</b>	<b>V</b>
<b>LIST OF TABLES.....</b>	<b>IX</b>
<b>LIST OF FIGURES.....</b>	<b>X</b>
<b>CHAPTER 1: INTRODUCTION.....</b>	<b>1</b>
1.1 General .....	1
1.2 Conventional Lap Splices.....	3
1.3 AASHTO Code Recommendations .....	5
1.4 Headed Bars .....	7
1.5 Headed Bar Splice Applications .....	13
1.6 Background of Headed Bars .....	17
1.7 Objectives and Scope of Overall Study.....	18
1.8 Objectives and Scope of Thesis .....	18
<b>CHAPTER 2: TESTING PROCEDURE AND MATERIAL PROPERTIES .....</b>	<b>20</b>
2.1 Objectives.....	20
2.2 Variables.....	20
2.3 Nomenclature .....	23
2.4 Preparation of Test Specimens.....	24
2.5 Description of Test Specimens.....	28

2.6 Testing Setup.....	29
2.7 Instrumentation and Data Acquisition.....	31
2.7.1 Strain Gages .....	31
2.7.2 Load Measurement.....	32
2.7.3 Deflection Measurement .....	32
2.8 Materials.....	33
2.8.1 Concrete Properties .....	33
2.8.2 Steel Reinforcing Bar Properties.....	34
<b>CHAPTER 3: TEST RESULTS AND BEHAVIOR .....</b>	<b>36</b>
3.1 Introduction .....	36
3.2 Definitions of Terms .....	36
3.2.1 $P_{max}$ .....	36
3.2.2 $M_{max}$ .....	36
3.2.3 $P_y$ .....	36
3.2.4 $M_y$ .....	37
3.3 Specimen Failures .....	38
3.3.1 Failure of Specimens with #5 Bars .....	39
3.3.2 Failure of Non-Headed Bar Splices .....	41
3.3.3 Failure of Small Headed Bar Splices .....	44
3.3.4 Failure of Large Headed Bar Splices .....	47
3.4 Load-Deflection Response of Specimens with #8 Bars .....	53
3.5 Measured Strains .....	56
<b>CHAPTER 4: COMPARISON OF TEST RESULTS .....</b>	<b>60</b>
4.1 Introduction .....	60
4.2 Staggered vs. Adjacent Splice Arrangements .....	60
4.3 Head Size.....	61

4.4 Head Shape.....	68
4.5 Bar Spacing .....	70
4.6 Lap Splice Length .....	71
4.7 Bar Size .....	73
4.8 Comparison with Existing Models.....	73
4.8.1 Comparison with Orangun, Jirsa, and Breen.....	73
4.8.2 Comparison with AASHTO Basic Development Length Equation .....	75
4.8.2 Comparison with DeVries' Side Blowout Capacity Equation .....	79
4.8.3 Calculation of Moment Capacity Using Combination of DeVries' Model and the Modified AASHTO Development Length Equation .....	83
4.9 Recommendations for Further Research .....	88
<b>CHAPTER 5: SUMMARY AND CONCLUSIONS.....</b>	<b>89</b>
5.1 Summary .....	89
5.2 Conclusions .....	90
5.3 Recommendations for Further Research .....	93
<b>APPENDIX .....</b>	<b>94</b>
<b>BIBLIOGRAPHY .....</b>	<b>106</b>
<b>VITA.....</b>	<b>109</b>



## List of Tables

Table 1.1 – AASHTO Classification of Tension Lap Splices.....	6
Table 2.1 – Head Properties .....	22
Table 2.2 – Lap Splice Specimens .....	28
Table 2.3 – Concrete Strengths .....	34
Table 2.4 – Steel Reinforcing Bar Properties.....	35
Table 3.1 – Test Results of Lap Splice Specimens .....	37
Table 4.1 – Comparison of Measured Stress at the Head with Predicted Stress Using DeVries’ Side Blowout Model .....	82
Table 4.2– Predicted Moment Capacities Based on DeVries’ Side Blowout Model and the Modified AASHTO Development Length Equation .....	85

## List of Figures

Figure 1.1 – Conventional Lap Splice.....	2
Figure 1.2 – Transfer of Forces Between Bars in a Conventional Lap Splice .....	3
Figure 1.3 – Component Forces Acting on Bar .....	4
Figure 1.4 – Component Forces Acting on Concrete.....	4
Figure 1.5 – Splitting Cracks Caused by Radial Forces Acting on Concrete .....	5
Figure 1.6 – Friction-welded Heads .....	7
Figure 1.7 – Forged Head.....	8
Figure 1.8 – Threaded Head.....	8
Figure 1.9 – Development of Headed Bars .....	9
Figure 1.10 – Strut-and-Tie Model of Compression Strut Between Heads .....	11
Figure 1.11 – ASTM C496-96 Test .....	11
Figure 1.12 – Hypothesized Development of a Headed Bar Splice (Adjacent Splice Shown).....	12
Figure 1.13 – Closure Joint Details.....	13
Figure 1.14 – Existing Bent Cap Widening Using Headed Reinforcement.....	15
Figure 1.15 – Staged Construction Sequence Using Headed Reinforcement.....	16
Figure 2.1 – Staggered vs. Adjacent Spacing of Lap Splice .....	21
Figure 2.2 – Definition of Lap Length (Shown for Adjacent Splice) .....	22
Figure 2.3 – Specimen Nomenclature .....	23
Figure 2.4(a) – Reinforcement Layout for Staggered Specimens w/ #8 Bars.....	26
Figure 2.4(b) – Reinforcement Layout for Adjacent Specimens w/ #8 Bars.....	27

Figure 2.5 - Load Setup for Lap Splice Tests. ....	29
Figure 2.6 – Hydraulic Pump .....	30
Figure 2.7 – Loading Beam Resting on Pair of Hydraulic Rams.....	30
Figure 2.8 – Typical Strain Gage Instrumentation .....	31
Figure 3.1 – Failure of Specimen ULS-#5-1.5C-9.6-12 .....	39
Figure 3.2 – Load - Deflection for Specimens with Six #5 Bars, $s_{bar} = 6$ in. ....	40
Figure 3.3 – Load - Deflection for Specimens with Four #5 Bars, $s_{bar} = 10$ in. ....	40
Figure 3.4 - Failure of Specimen ULS-#8-0X-10S-5.....	41
Figure 3.5 - Failure of Specimen ULS-#8-0X-10S-8.....	42
Figure 3.6 – Cover Liftoff Caused by Bending of Specimen.....	43
Figure 3.7 – Failure of Specimen ULS-#8-1.2C–6S-3.....	44
Figure 3.8 – Wavy Crack Patterns Indicating Formation of Diagonal Compression Struts .....	45
Figure 3.9 – Specimens ULS-#8-1.2C-10S-5 and ULS-#8-1.2C-10S-8 Showing Development of Compression Struts .....	46
Figure 3.10 – Failure of Specimen ULS-#8-1.2C-10A-5.....	47
Figure 3.11 – Failure of ULS-#8-4.7R-6S-3 and ULS-#8-4.7R-10S-5 .....	48
Figure 3.12 – Failure of Specimen ULS-#8-4.7R-6S-5 .....	49
Figure 3.13 – Failure of Specimen ULS-#8-4.0C-10S-8 .....	51
Figure 3.14 – Failure of Specimen ULS-#8-4.7R-10S-8 .....	51
Figure 3.15 - Failure of Specimen ULS-#8-4.7R-10A-5 .....	52
Figure 3.16 – Load vs. Deflection of 25 in. Wide Specimens .....	53
Figure 3.17 – Load vs. Deflection of 36 in. Specimens w/ Staggered $L_s = 5$ in ..	54

Figure 3.18 – Load vs. Deflection of 36 in. Specimens w/ Adjacent $L_s = 5$ in. ....	54
Figure 3.19 – Load vs. Deflection of 36 in. Specimens w/ Staggered $L_s = 8$ in. ...	55
Figure 3.20 – Load-Deflection Response of ULS-#8-4.7R-10S-5.....	56
Figure 3.21 – Strains Outside of Splice at $M_{max}$ for Specimens w/ #8 Bars .....	57
Figure 3.22 – Strains at End of Splice at $M_{max}$ for Specimens w/ #8 Bars .....	58
Figure 3.23 – Location of Strain Gages in Relation to Cracks .....	59
Figure 4.1 – Beam Capacities with Staggered and Adjacent Splice Laps .....	61
Figure 4.2 – Beam Capacity vs. Head Size with $L_s = 3$ in. ....	63
Figure 4.3 – Beam Capacity vs. Head Size with $L_s = 5$ in. ....	64
Figure 4.4 – Beam Capacity vs. Head Size with $L_s = 8$ in. ....	65
Figure 4.5 – Strain Along Splice at $P = 7.2$ kips $b = 36$ in., $L_s = 5$ in., $s_{bar} = 10$ in., Staggered Splice .....	66
Figure 4.6 – Strain Along Splice at Failure $b = 36$ in., $L_s = 5$ in., $s_{bar} = 10$ in., Staggered Splice .....	68
Figure 4.7 – Beam Capacity vs. Head Shape .....	69
Figure 4.8 – Clear Cover of Headed Reinforcement.....	70
Figure 4.9 – Beam Capacities with 6 in. and 10 in. Bar Spacing.....	71
Figure 4.10 – Comparison of 5 in. and 8 in. Lap Lengths with Various Heads....	72
Figure 4.11 – Comparison of #5 Bar Specimens with O-J-B.....	74
Figure 4.12 – Comparison of #8 Bar Specimens with O-J-B.....	75
Figure 4.13 – Comparison with Modified AASHTO Equation .....	77
Figure 4.14 – Development of Headed Bar Splice.....	78
Figure 4.15 – Development that Parallels Modified AASHTO Equation.....	79

Figure 4.16 – Definition of Available Failure Area, $A_{bo}$ , for an Interior Headed Bar .....	81
Figure 4.17 – CEB Definition of Basic Blowout Failure Area, $A_{bon}$ , Shown for a Single Headed Bar .....	81
Figure 4.18 – Comparison of Measured Bar Stress at the Head with Predicted Bar Stress at the Head Using DeVries’ Side Blowout Model.....	83
Figure 4.19 – Comparison of Measured Moment Capacities of Headed Bar Specimens with Predicted Moment Capacities Using Eq. 4-9 .....	86
Figure 4.20 – Comparison of Measured Moment Capacities of Headed Bar Specimens with Capacities Predicted Using DeVries Side Blowout Model .....	87
Figure A.1 – Specimen ULS-#8-0X-10S-5 .....	94
Figure A.2 – Specimen ULS-#8-4.7R-10S-5 .....	95
Figure A.3 – Specimen ULS-#8-4.7R-10A-5 .....	96
Figure A.4 – Specimen ULS-#8-4.7R-6S-3 .....	97
Figure A.5 – Specimen ULS-#8-1.2C-10S-5 .....	98
Figure A.6 – Specimen ULS-#8-1.2C-10A-5 .....	99
Figure A.7 – Specimen ULS-#8-1.2C-6S-3 .....	100
Figure A.8 - Specimen ULS-#8-4.7R-6S-5.....	101
Figure A.9 – Specimen ULS-#8-0X-10S-8.....	102
Figure A.10 – Specimen ULS-#8-1.2C-10S-8 .....	103
Figure A.11 – Specimen ULS-#8-4.0C-10S-8 .....	104
Figure A.12 – Specimen ULS-#8-4.7R-10S-8 .....	105

# Chapter 1: Introduction

## 1.1 General

Recent progress in fabricating headed reinforcement provides opportunities for simplifying some details common to bridge structures. The goal of this study is to explore new uses for headed bars in structural concrete reinforcement applications.

One application that shows potential for use of headed bars is in lap splices. Lap splices are used in many ways in reinforced concrete structures. Large concrete structures usually require very long reinforcing bars in order to handle the tension forces present in structural elements. Due to transportation and handling limitations, reinforcing bars cannot always be made to the necessary lengths. Lap splices are typically used to provide continuity. In a lap splice, forces are transferred between the bars through the concrete surrounding the bars. The reinforcing bars are overlapped for a given length so that bar forces can be transferred through local bearing stresses on lugs and shearing stresses in the surrounding concrete as shown in Figure 1.1.

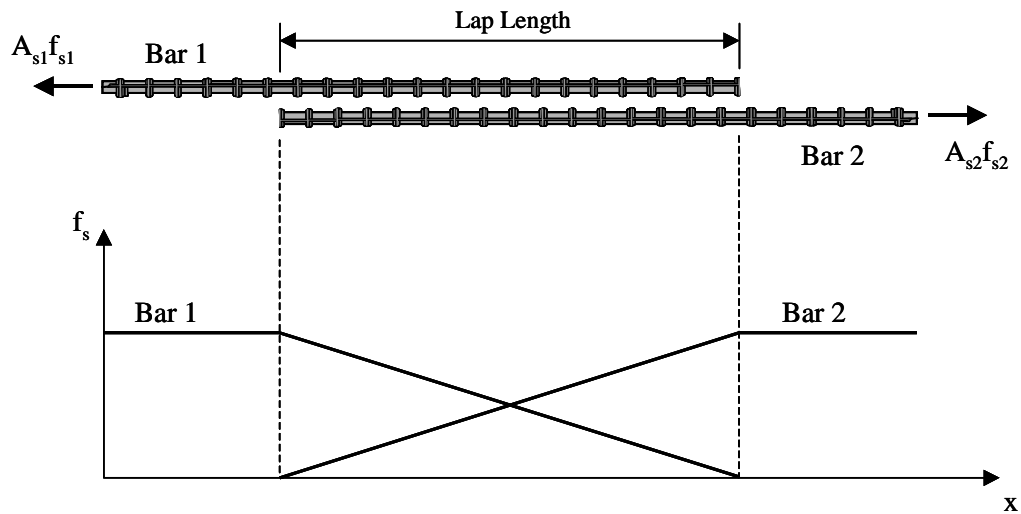


**Figure 1.1 – Conventional Lap Splice**

Lap splices are also used in retrofit applications. Although retrofit projects may be less numerous than new construction, the construction is often very labor intensive and expensive. Simplification of details may reduce project costs. One example of a retrofit application using lap splices is the widening of a bridge structure. In order to widen a bridge (see Fig. 1.14), the bent cap supporting the bridge deck must also be widened. To widen the bent cap, concrete must be removed to expose enough reinforcing steel so that a lap splice can effectively connect the new bent cap to the existing bent cap. Another alternative would be to use mechanical couplers that join the bars end-to-end. The problem with mechanical couplers is that they require space to align the bars properly and may result in congestion problems.

## 1.2 Conventional Lap Splices

Conventional lap splices work by transferring tensile forces in one bar to another bar through the surrounding concrete. For smooth bars, the transfer of forces is done primarily through adhesion between the concrete and the steel bar. However, once adhesion is lost, the bar pulls out at low stresses. In order to solve this problem, deformed bars are used. The force in the deformed bar is transferred by bearing against deformations, typically called lugs, as shown in Figure 1.2. Lugs create a wedge-type action with the concrete thus transferring forces between bars. However, the force in one bar is transferred gradually over some length of bar. The splice or overlap length is the distance needed for the force to be effectively transferred from one bar to the other.

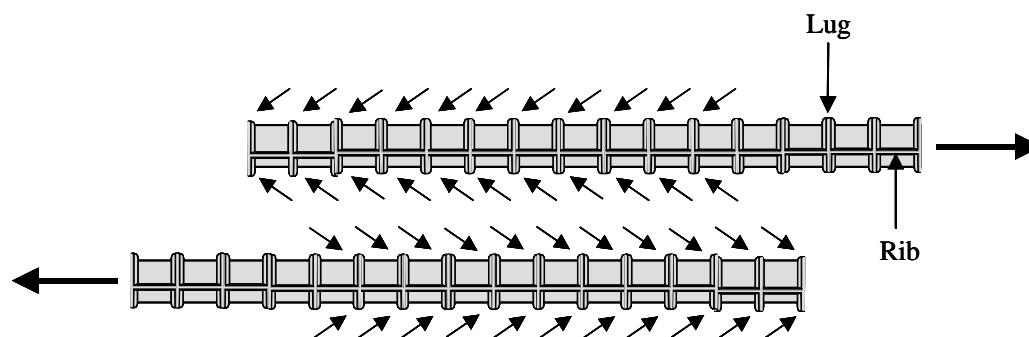


**Figure 1.2 – Transfer of Forces Between Bars in a Conventional Lap Splice**



Failures of conventional lap splices are generally governed by splitting caused by ring tension around the bar. Ring tension occurs because components of the bearing force from the lugs create an outward radial force, as shown in Figures 1.3-1.5. Once enough force is produced, the surrounding concrete splits in tension along its weakest plane. Splitting progresses until the reinforcing bar slips out of the concrete and can no longer transfer force between bars.

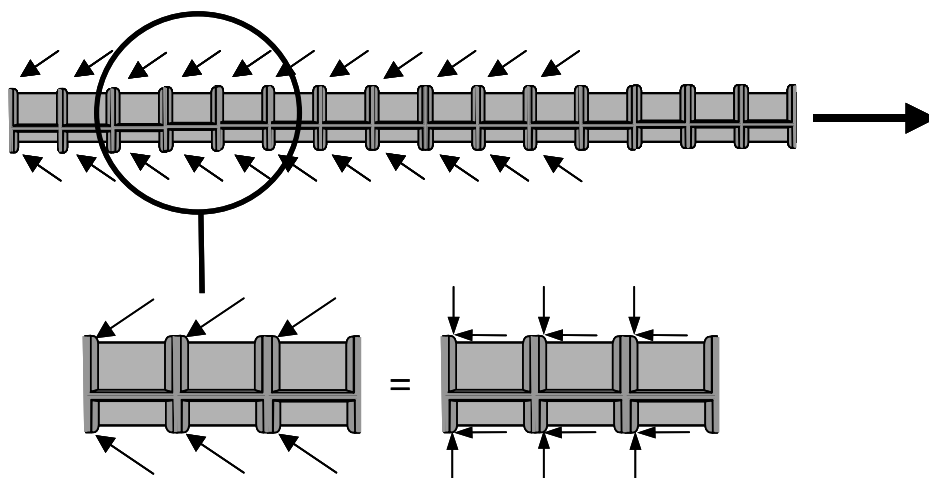


**Figure 1.3 – Component Forces Acting on Bar**

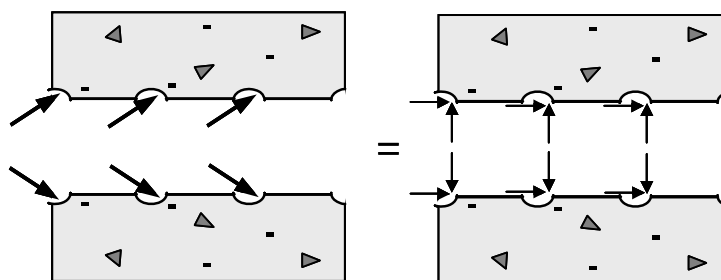
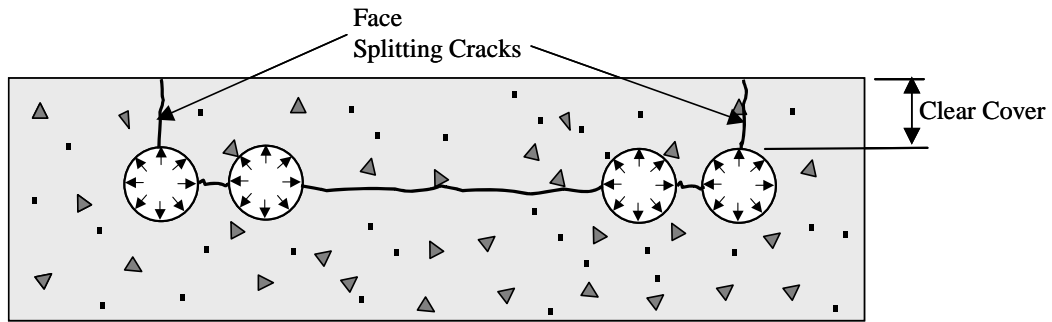
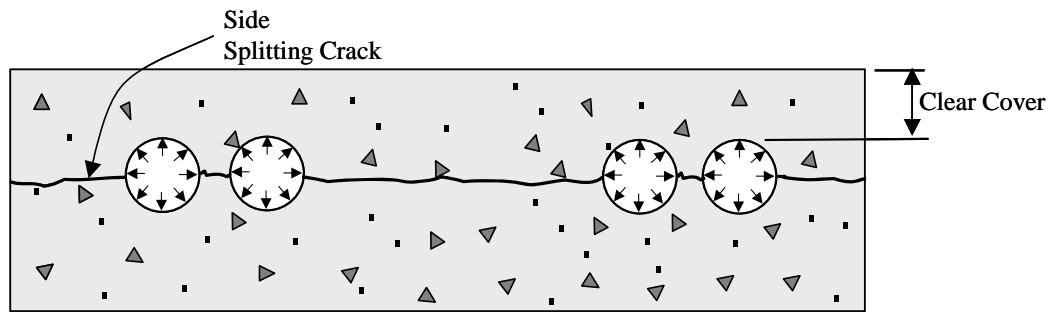


**Figure 1.4 – Component Forces Acting on Concrete**



(a) – Face Splitting Cracks



(b) - Side Splitting Cracks

**Figure 1.5 – Splitting Cracks Caused by Radial Forces Acting on Concrete**

### 1.3 AASHTO Code Recommendations

The requirements for development length of reinforcing bars can be found in Section 8.25 of AASHTO Standard Specifications for Highway Bridges [3].

The requirement for basic development length of #11 bars and smaller is:

$$l_d = \frac{0.04A_b f_y}{\sqrt{f'_c}}, \text{ but not less than } 0.0004d_b f_y \quad (\text{Eq. 1-1})$$

where  $l_d$  is the required development length in inches,  $A_b$  is the nominal area of the bar in  $\text{in}^2$ ,  $f_y$  is the yield strength of the bar in psi, and  $f'_c$  is the concrete strength in psi. The requirements for splices of reinforcement can be found in Section 8.32 of AASHTO. Lap splices are defined as Class A, B, or C splices. AASHTO definitions for splice class are given in Table 1.1. The minimum lap splice allowed by the code is 12 inches. Modification factors for each type of splice are as follows:

Class A splice	$1.0 * l_d$
Class B splice	$1.3 * l_d$
Class C splice	$1.7 * l_d$

**Table 1.1 – AASHTO Classification of Tension Lap Splices**

$(A_s \text{ provided}) / (A_s \text{ required})$	Maximum Percent of $A_s$ Spliced within Required Lap Length		
	50	75	100
Equal to or Greater than 2	Class A	Class A	Class B
Less than 2	Class B	Class C	Class C

The basic development length of a Class A splice using #8 bars and 4000 psi strength concrete would require a 30 in. lap splice. If the lap splice were used to connect precast elements, the splice would need to meet the requirements of a Class C splice. The Class C splice would then need to be over 50 inches in length

to meet the AASHTO development length requirements. Use of headed bars in lap splices would reduce the required lap lengths considerably.

#### **1.4 Headed Bars**

Use of headed bars may be a better solution than conventional straight bar development for some splicing applications. Progress in the manufacture of headed bars is allowing more ways of installing heads (heading) on reinforcing bars. Headed bars are fabricated by friction-welding plates on the ends of bars, forging heads on the ends of bars using portable devices, and using threaded heads after threading the bars (Figs. 1.6-1.8). Heads can be made in a variety of shapes such as square, rectangular, and circular.



**Figure 1.6 – Friction-welded Heads**



**Figure 1.7 – Forged Head**



**Figure 1.8 – Threaded Head**

The manner in which headed bars develop capacity is different than that of conventional non-headed bars. In addition to developing force through bearing on the lugs of the deformed bar, headed bars can also develop capacity through direct bearing of the head as shown in Figure 1.9. Because the head size can be varied, development of the bar's tensile capacity need not vary directly with lap length, as is the case for non-headed bars.

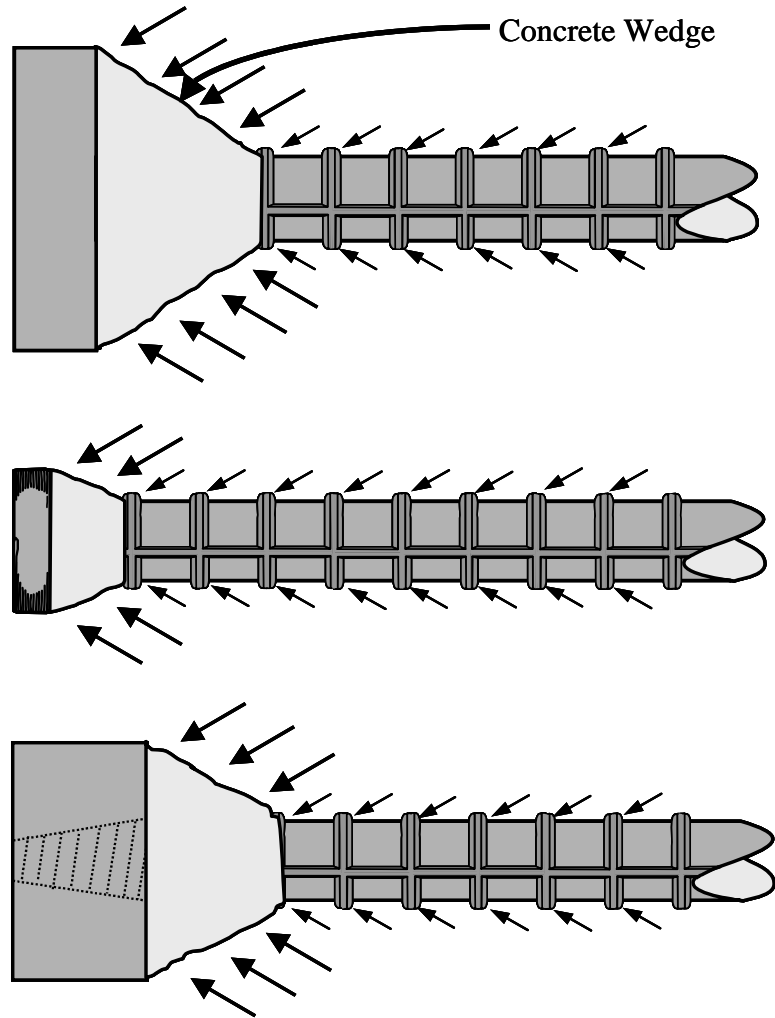


**Figure 1.9 – Development of Headed Bars**

In a headed bar lap splice, it is theorized that the bars develop by a combination of bearing of the head and bearing of the lugs on the surrounding concrete. The concrete between opposing heads acts like a compression member (compression strut). Failure of the compression strut occurs when cracks form and propagate from one head to the other or crushing of the concrete occurs. The crack that develops in the concrete between the heads can also be interpreted as failing in tension. The force being transferred from one head to the other head tends to spread out in a bottle-shape fashion. Tension stresses develop in the strut as the compressive forces spread out as shown in Figure 1.10. The concrete cracks when the tensile limit stress of the concrete is reached. A good example of a compression strut failure is the ASTM C496-96 [8] test used to determine the tensile strength of concrete. Figure 1.11 shows why the cylinder splits under compression loading. As load is applied to the cylinder, the compressive forces spread out as the width of the cylinder increases. As the cylinder decreases in width, the compressive forces must converge. As these forces spread out and converge, component forces induce tensile forces in the concrete. These tensile forces are responsible for failure of the concrete cylinder. Even though failures of the compression strut occur by tensile forces and shear planes, they are still referred to as compression failures.

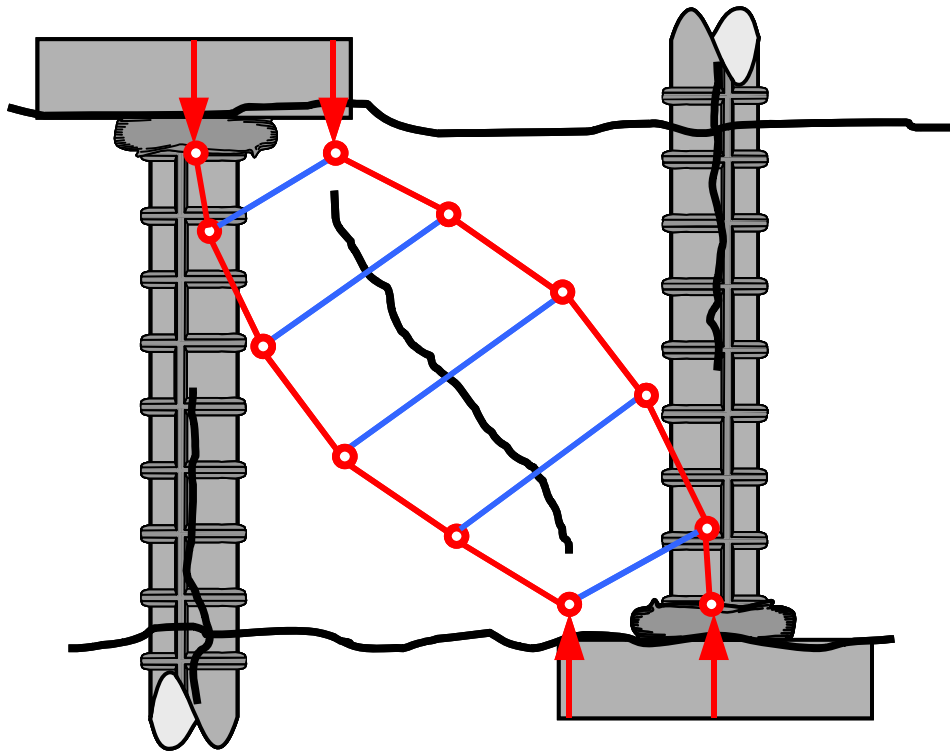


**Figure 1.10 – Strut-and-Tie Model of Compression Strut Between Heads**

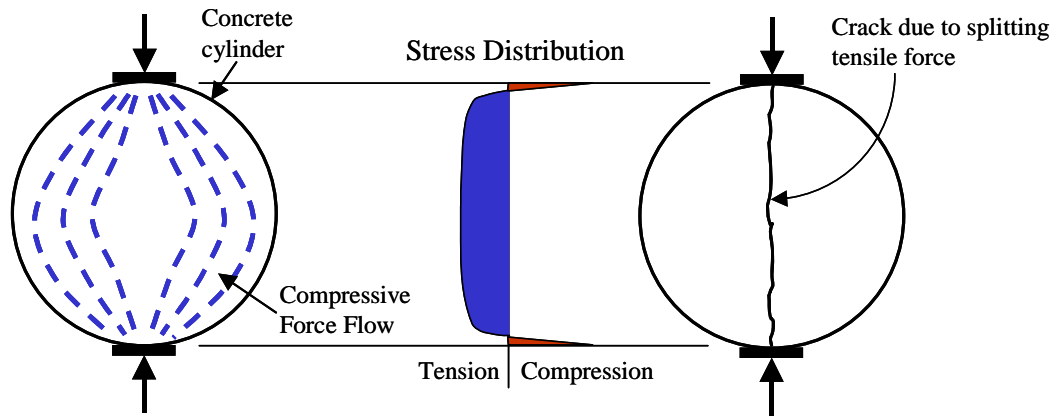


**Figure 1.11 – ASTM C496-96 Test**



Figure 1.12 shows the hypothesized development of a headed bar splice. The rate at which the lugs develop tension in the headed bar should be equal to the development rate of the lugs of a non-headed bar. Therefore the lap length should be reduced by the amount of development provided by the head. How large the head must be to provide significant development of the bar must be established. Is there a maximum head size that will develop the bar? Does the use of a head cause unknown types of failures and how would this affect the design of headed bar splices? What is the ideal spacing of headed bar splices? Does the head shape affect development? These are all questions that must be answered before headed bar laps can be used with confidence by practicing designers.

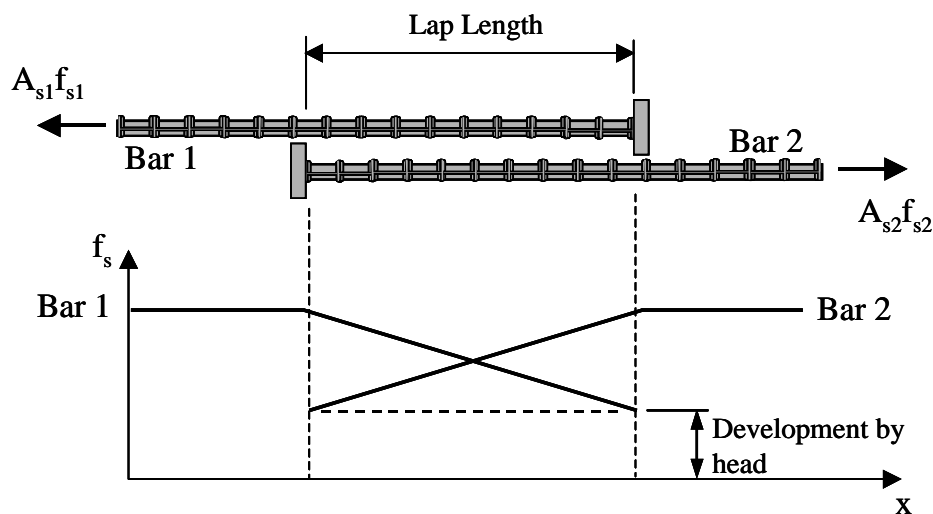


**Figure 1.12 – Hypothesized Development of a Headed Bar Splice (Adjacent Splice Shown)**

## 1.5 Headed Bar Splice Applications

There seem to be a number of details that show potential benefit from using headed bar lap splices. One possible use for headed bars in lap splice applications is the general detail of a closure joint between precast units as shown in Figure 1.13. Considerable savings can be made in time, formwork costs, material costs, and labor costs associated with constructing the cast-in-place joint by using headed bars to reduce the size of the joint. The use of headed bars to tie structural elements together can also make the use of other precast elements more widespread.

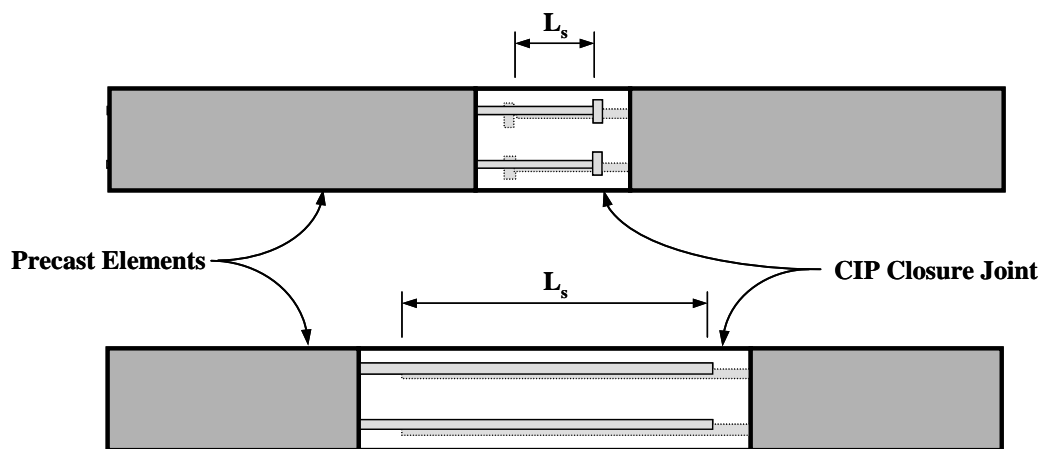
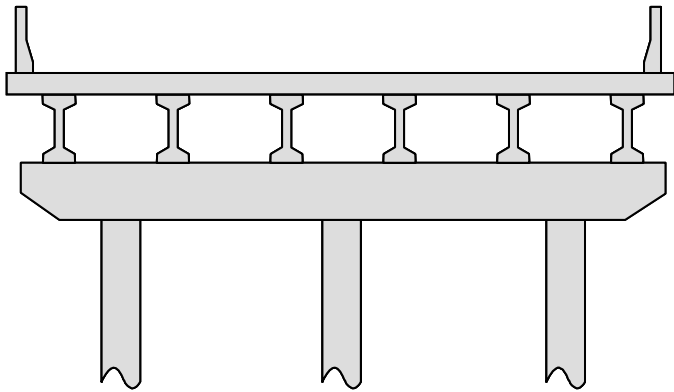


**Figure 1.13 – Closure Joint Details**

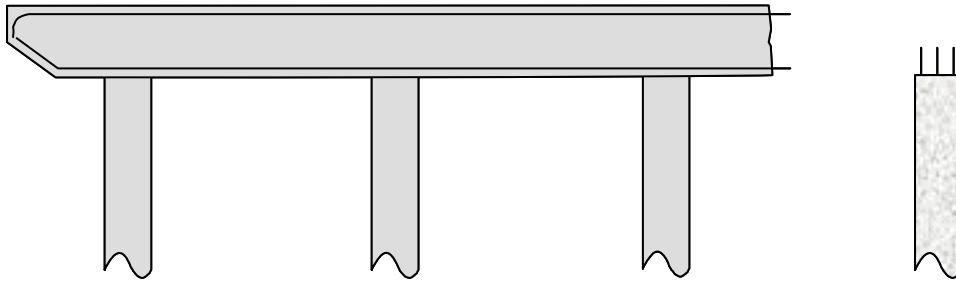
Another possible headed bar application is the idea mentioned earlier concerning the widening of bridge bent caps. Circumstances may warrant that an

existing bent cap be widened instead of replaced entirely. Concrete must be removed in order to expose enough reinforcing steel to effectively tie the structural elements together. Since the use of headed bars would shorten the required lap length, less concrete would have to be removed from the end of the bent cap. Figure 1.14 shows the process of a bent cap widening. Methods that would allow on-site heading of bars, such as forging heads or threading heads, would be ideal for use in retrofit applications.

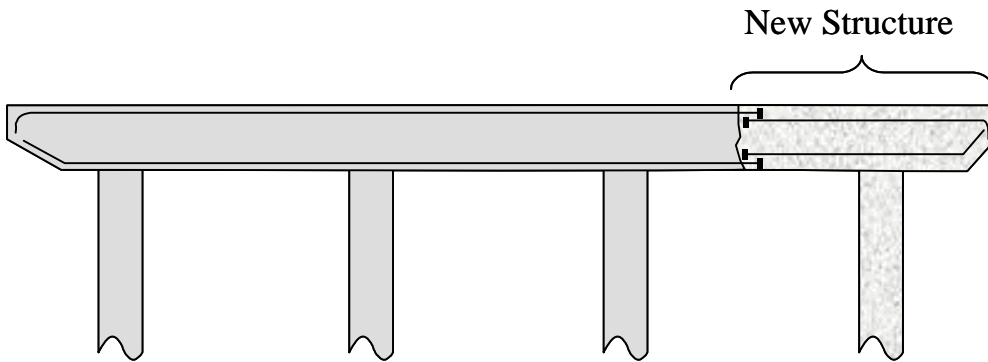
The use of headed bars could also be used in new construction. An example of using headed bars in new construction would be replacing an existing bridge with a new bridge. Stage construction of bridge bent caps and slabs are often used so that traffic can be shifted onto part of the new bridge as the existing bridge is torn down and replaced as shown in Figure 1.15. Clearance problems, such as the presence of existing structures, may limit the length of steel that can be exposed. Use of headed bars would shorten the length of exposed steel required. Shop fabricated heads, such as welded heads or threaded heads, would be ideal for these types of applications where the use of headed bars are anticipated. Shop fabricated heads are generally larger in size and detailing of connections can be incorporated into the design.



**(a) – Existing Bent Cap**

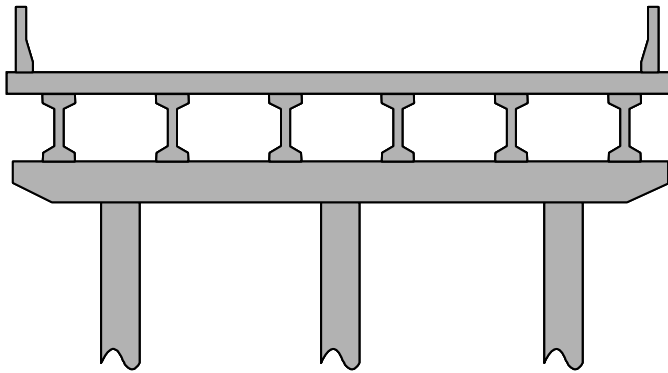


**(b) – Existing Bent Cap Steel and New Column Steel Exposed**

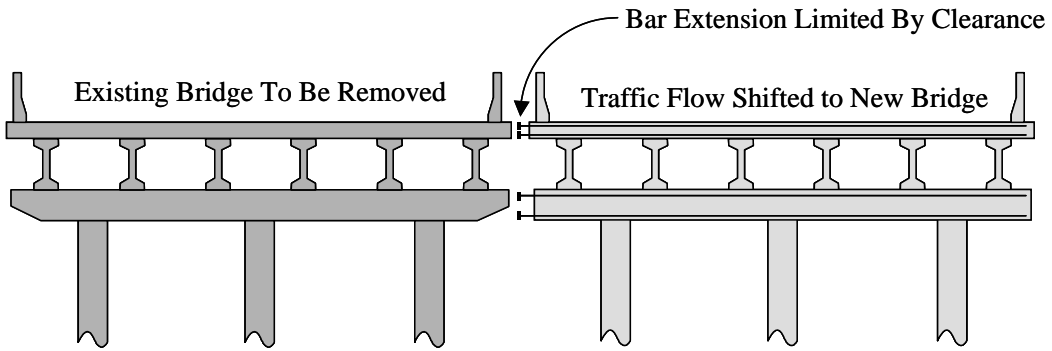


**(c) – Headed Lap Splice Used to Connect Bent Cap Extension**

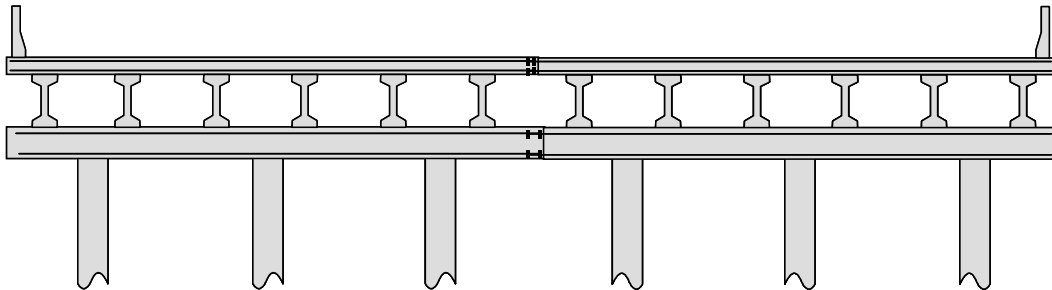
**Figure 1.14 – Existing Bent Cap Widening Using Headed Reinforcement**



(a) – Existing Bridge



(b) - Traffic Flow Shifted to New Bridge as Existing Bridge Torn Down



(c) - Finished Bridge

**Figure 1.15 – Staged Construction Sequence Using Headed Reinforcement**

## **1.6 Background of Headed Bars**

Headed bars were introduced in reinforced concrete construction because the provisions for anchorage of bars, splices, and continuity between elements pose significant difficulties for designers and contractors. Straight bar anchorages and lap splices are often so long that the resulting dimensions of elements are prohibitively large. The most common solution is to use hooked bars or to incorporate mechanical connectors. However, both options have drawbacks. Hooked bars create congestion problems and may make fabrication of reinforcement cages or placement and consolidation of concrete difficult when large amounts of reinforcement are required. Mechanical connectors require special construction operations and careful attention to tolerances. In order to reduce congestion problems, headed bars have been used instead of bent bars (hoops or ties) for shear reinforcement to anchor large diameter transverse reinforcement bars in the construction of reinforced concrete platforms for offshore development and petroleum production [10,16,20,24].

Considerable testing has been conducted on headed reinforcement. Recent work at the University of Texas at Austin aimed at providing data on basic anchorage characteristics of headed bars. Variables included depth or length of anchorage, size and shape of head, concrete cover, concrete strength, transverse reinforcement, and proximity of other headed bars [15]. Researchers in Norway

determined properties of headed bars in high strength concrete [17]. Some tests were conducted at the on beam-column joints where hooked bars were replaced by headed bars [9].

A few tests have been conducted on knee joints [13,19,21], mostly at a relatively small scale. One large knee joint specimen has been tested for CALTRANS [23] at the U.C. San Diego. Some fairly large tests have been conducted at U.C. Berkley in which headed reinforcement was used in the strengthening of models of existing bridge supports structures.

### **1.7 Objectives and Scope of Overall Study**

The research reported in this thesis is part of larger research investigation to explore new uses for headed bars in reinforced concrete structures. The objective of the overall study is to determine the general anchorage behavior of headed bars in lap splices and nodal zones of discontinuity regions. The behavior will be determined from large-scale tests of reinforced concrete specimens that mimic the structural details under study. Data from these tests will be used to develop design criteria for the anchorage of headed bars.

### **1.8 Objectives and Scope of Thesis**

The objectives and scope of this thesis are similar to those defined in the previous section. In this thesis, only the behavior of headed bars in lap splice applications will be examined. The factors that affect the performance of headed

bars will be evaluated and used to determine design criteria to ensure satisfactory performance of headed bars in lap splices. The scope of this study entailed fabricating and testing to failure 14 full depth slabs reinforced with headed bars. The widths of the slabs were limited due to floor space and cost considerations. The widths of the slabs were selected so that edge failures would not occur.



## **Chapter 2: Testing Procedure and Material Properties**

### **2.1 Objectives**

The main objectives of the testing procedure were to examine and evaluate several variables that affect the performance of headed bars in splicing applications. In order to effectively evaluate the variables, a total of 16 unconfined lap splice tests were performed. The test specimens were dimensioned so that edge failures, such as side blowout or side splitting, and yielding of the reinforcement in the specimens would not occur.

### **2.2 Variables**

Several variables were investigated for the lap splice specimens. Variables included strength of staggered vs. adjacent splice arrangements, head size, head shape, bar spacing, lap length, and bar size.

Staggered bar laps were spaced equal distances from each other as shown in Figure 2.1. Adjacent bar laps were spaced as so that the bars being spliced were as close together as the heads would allow. This spacing varied due to the size of the head attached to the bar.

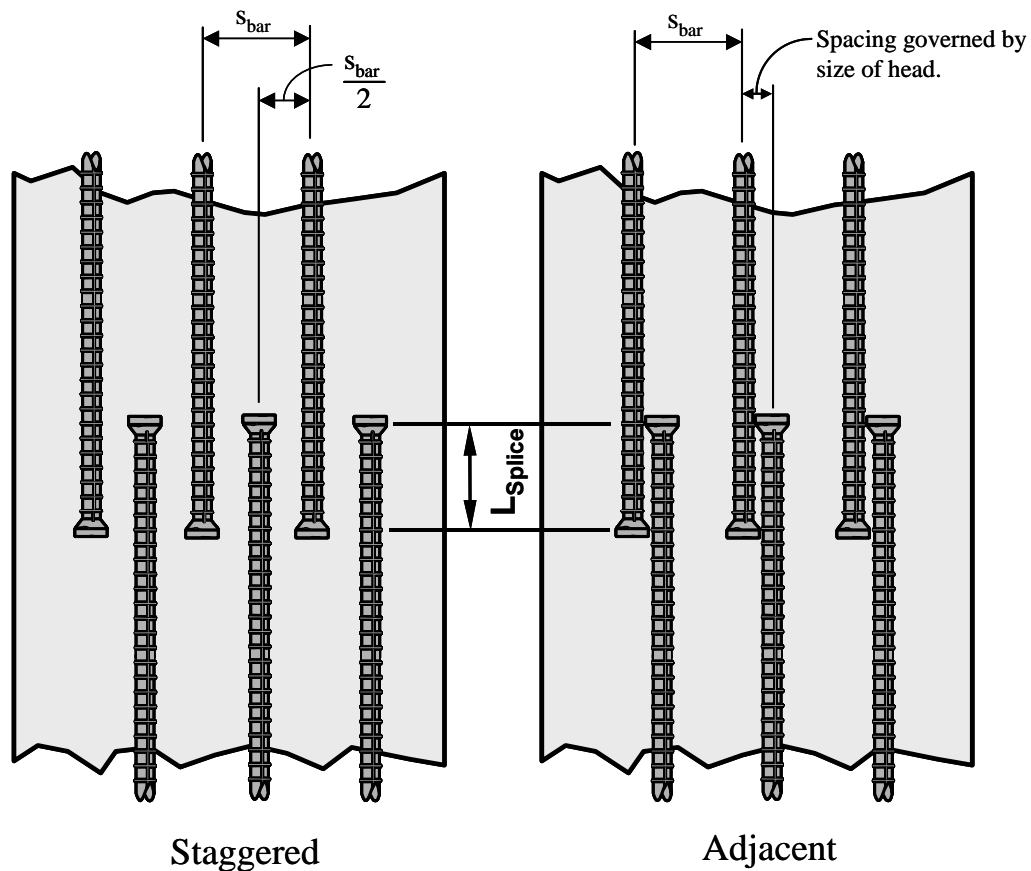


**Figure 2.1 – Staggered vs. Adjacent Spacing of Lap Splice**

Head size is defined as the ratio of the net head area to the nominal area of the bar. The net head area is determined by subtracting the nominal bar area from the gross area of the head. Head shapes used were: square, rectangular, and circular. Bars were spaced at  $s_{bar}$  of 6 in. or 10 in. on center. Table 2.1 shows the properties of the various heads used in this study. The distance inside the heads defines the lap length as shown in Figure 2.2. Bar sizes used in this study were

**Table 2.1 – Head Properties**

Head Type	Head Shape	Bar Size	$A_b$ (in <sup>2</sup> )	Head Size (in) Size	Diameter	$A_{head}$ (in <sup>2</sup> )	$A_n$ (in <sup>2</sup> ) ( $A_{head}-A_b$ )	$A_n/A_b$
Friction-welded	Square	#5	0.31	2x2	-	4.00	3.69	11.90
Forged	Circular	#5	0.31	-	1	0.79	0.48	1.53
Forged	Circular	#8	0.79	-	1.5	1.77	0.98	1.24
Threaded	Circular	#8	0.79	-	2.25	3.98	3.19	4.03
Friction-welded	Rectangular	#8	0.79	1.5x3	-	4.50	3.71	4.70

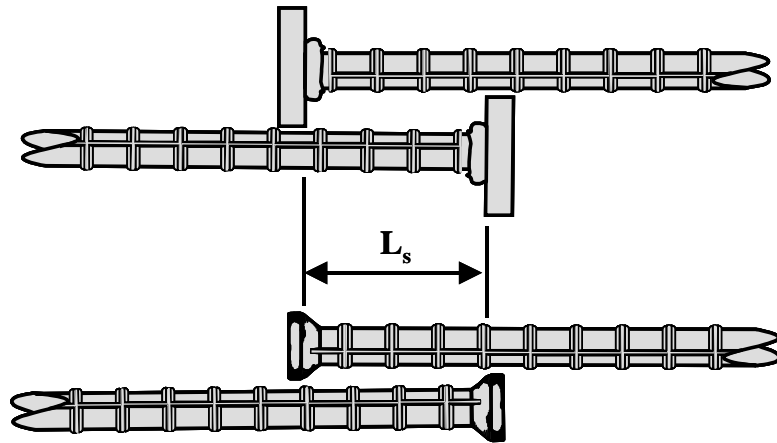


**Figure 2.2 – Definition of Lap Length (Shown for Adjacent Splice)**

#5's and #8's. Clear cover and edge distances were measured from the bar and not the head. Currently, headed reinforcement must meet requirements of ASTM A970-98 Standard Specifications for Welded or Forged Headed Bars for Concrete Reinforcement [4]. Many of the bars used in this program would not meet the

$A_n/A_b$  value of 10 required by the ASTM specification. Smaller sized heads were used for research purposes.

### 2.3 Nomenclature

A systematic method for identifying the test specimens was adopted so that the specimens would be readily identifiable and distinguishable. Because the lap splice study is part of an overall study exploring new uses for headed bars in structural concrete reinforcement applications, specimen identifiers were adopted so that the nomenclature would be consistent throughout the study. Specimen designation for the lap splice specimens is shown in Figure 2.3.

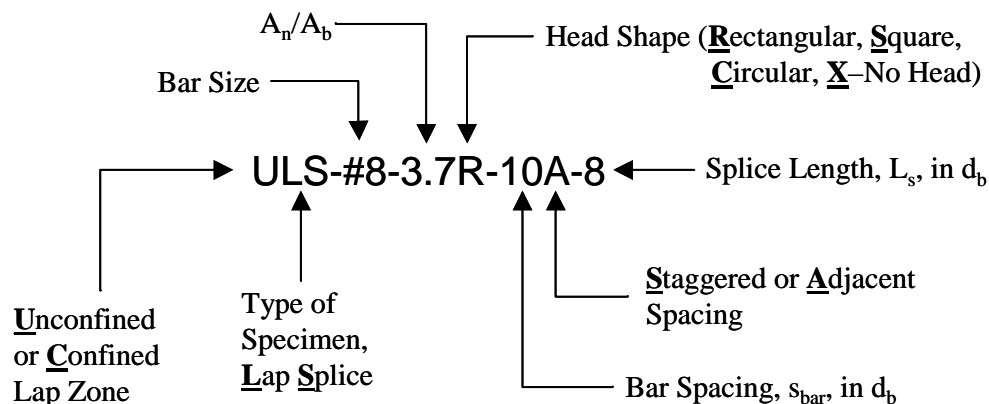


**Figure 2.3 – Specimen Nomenclature**

## **2.4 Preparation of Test Specimens**

All test specimens were cast in wooden forms so that slab size could be adjusted to various widths. The forms were sealed with a silicon caulk and sprayed with form oil to prevent bonding between the concrete and forms. Two lifting inserts were cast into the slab approximately two to three feet from each end of the specimen so that the specimen could be moved from the casting area to the test area using an overhead crane. In an attempt to save time and material cost, two initial specimens using #5 bars were cast so that two tests could be performed on each specimen. In order to use one specimen for two tests, lap splices were cast on both the top and the bottom of the slab. After one side was tested, the specimen was then flipped over so that the second lap splice could be tested. This technique did not achieve the desired results. The process of flipping over the specimens turned out to be rather dangerous. Additionally, cracks in the first test tended to initiate and influence cracking in the second test and seemed to reduce the overall capacity of the second test. This technique was abandoned for subsequent specimens containing #8 bars. Specimens with #8 bars were cast so that each specimen would provide one test.

All test specimens were reinforced with transverse reinforcement outside of the constant moment region containing the lap splice zone. The transverse reinforcement consisted of hoops made from #3 reinforcing bars and bent to the

proper configuration. The hoops were typically spaced from 4 in. to 5 in. on center. The specimens containing #8 bars were also reinforced with four #4 longitudinal bars 2½ in. from the bottom of the slab so that the specimens could be moved after the lap splices failed. Figures 2.4 (a and b) show typical reinforcing layouts for the test specimens. Specimens containing the #5 bars did not contain the additional longitudinal steel because those specimens had headed bars cast in the top and the bottom of the slabs. Reinforcement cages were properly positioned in the forms using steel chairs, which were used on the bottom and sides of the forms.

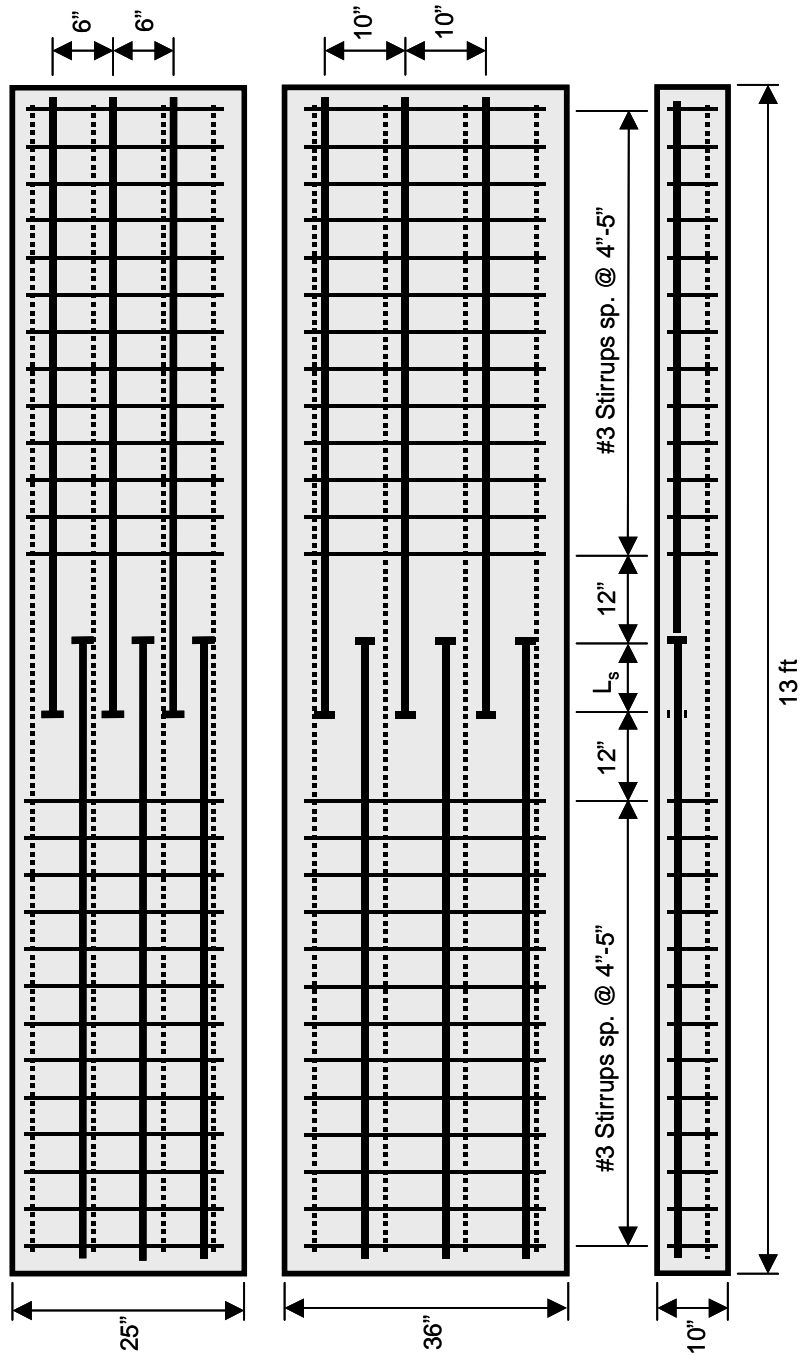


Figure 2.4(a) – Reinforcement Layout for Staggered Specimens w/ #8 Bars

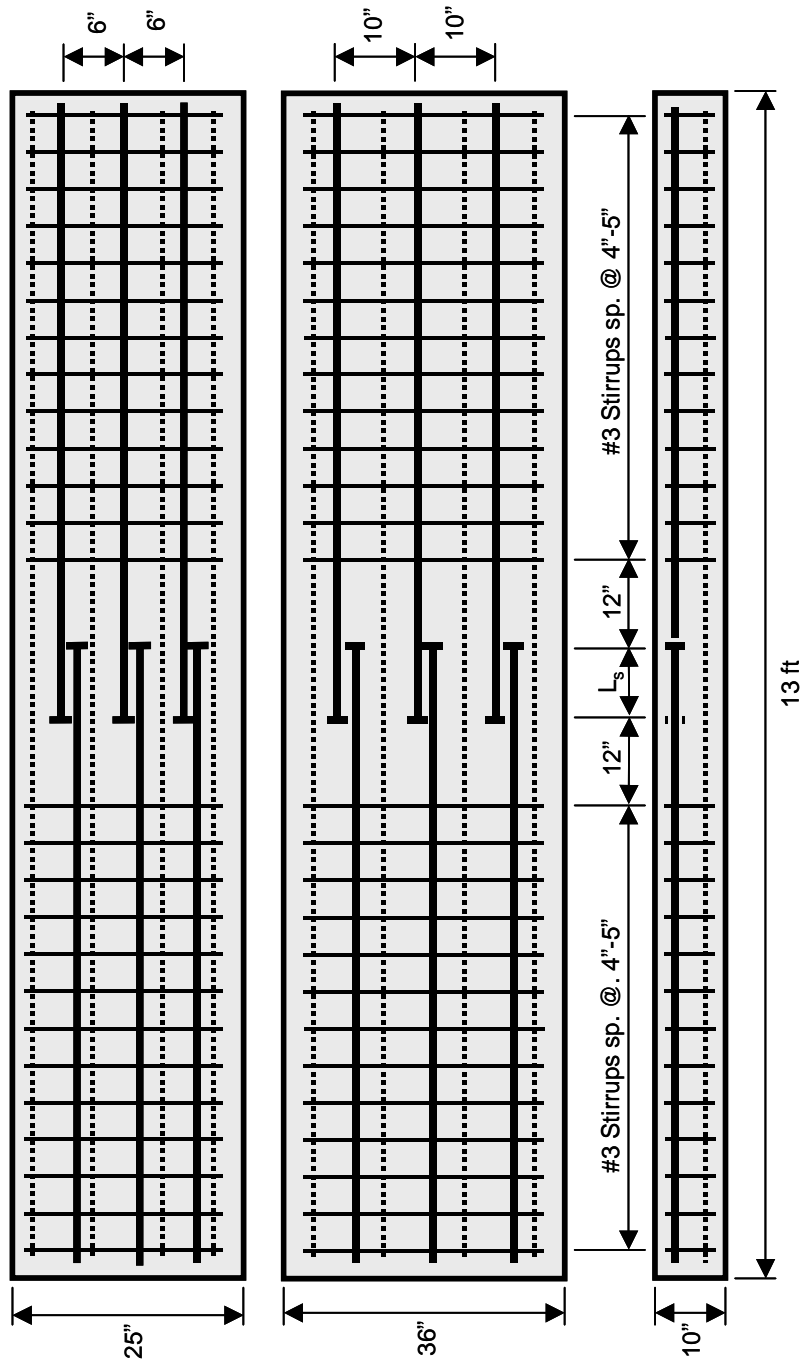


Figure 2.4(b) – Reinforcement Layout for Adjacent Specimens w/ #8 Bars



The specimens were cast in a series of four concrete placements. The two lap splice specimens containing #5 bars were cast first. The 12 specimens containing #8 bars were cast in the following three placements, with four specimens cast at a time.

## 2.5 Description of Test Specimens

The test specimens had the same basic dimensions but varied in width. All of the specimens were 13 feet in length and had a nominal depth of 10 inches. Table 2.2 shows the dimensions and variables for each specimen.

**Table 2.2 – Lap Splice Specimens**

Concrete Casting	Specimen	Slab Width (in)	S <sub>bar</sub> (in)	L <sub>s</sub> (in)	Top Clear Cover to Bar (in)	Side Clear Cover to Bar (in)
1	ULS-#5-1.5C-16A-12	40	10	7.5	2.2	3.9
	ULS-#5-1.5C-16A-12-R	40	10	7.5	2.2	3.9
	ULS-#5-11.9S-9.6A-11.2	40	6	7	2.2	3.7
	ULS-#5-1.5C-9.6A-12	40	6	7.5	2.2	3.7
2	ULS-#8-0X-10S-5	36	10	5	2.5	4.9
	ULS-#8-4.7R-10S-5	36	10	5	2.1	5.0
	ULS-#8-4.7R-10A-5	36	10	5	2.3	6.1
	ULS-#8-4.7R-6S-3	25	6	3	2.3	4.0
3	ULS-#8-1.2C-10S-5	36	10	5	2.0	5.0
	ULS-#8-1.2C-10A-5	36	10	5	2.1	6.8
	ULS-#8-1.2C-6S-3	25	6	3	2.3	4.5
	ULS-#8-4.7R-6S-5	25	6	5	2.1	4.5
4	ULS-#8-0X-10S-8	36	10	8	2.3	5.0
	ULS-#8-1.2C-10S-8	36	10	8	2.0	5.0
	ULS-#8-4.0C-10S-8	36	10	8	2.3	5.0
	ULS-#8-4.7R-10S-8	36	10	8	2.0	5.0

## 2.6 Testing Setup

Figure 2.5 shows the basic dimensions of the test setup. The lap splices were tested so that the lap zone would be at the top of the specimens. The specimens were then loaded from the bottom so that crack patterns could be easily observed. A two-point loading setup was used so that a constant moment region would be achieved throughout the lap zone. Load points were located 15 inches from the end of the splice. Prior to loading, the specimens rested on concrete support blocks. The specimens were loaded along two lines using two W6X12 beams. Two 30-ton hydraulic rams per load beam were used to load the specimens. Two W12X65 reaction beams with roller supports spaced 12 feet apart were tied down into the lab floor using a total of 16 one inch, high-strength steel, threaded rods.

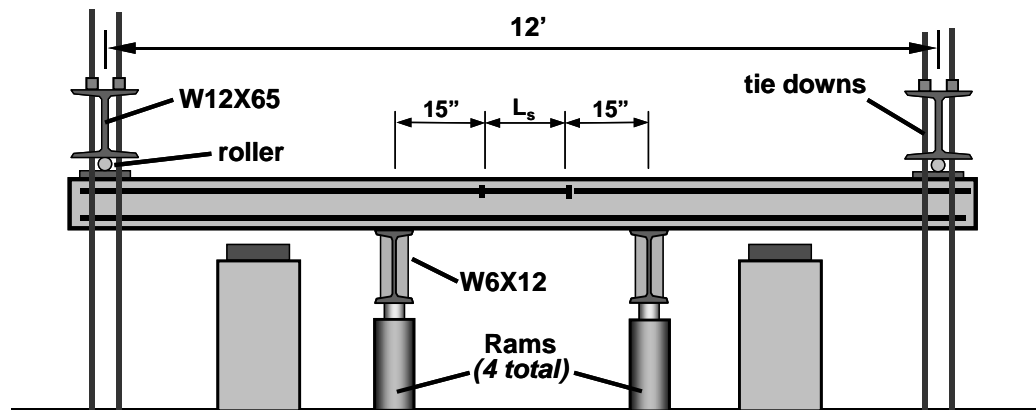
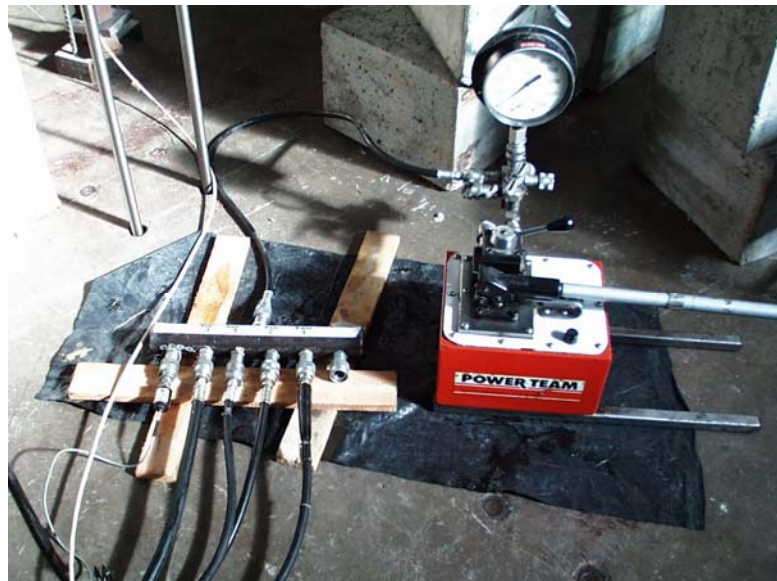


Figure 2.5 - Load Setup for Lap Splice Tests.



**Figure 2.6 – Hydraulic Pump**



**Figure 2.7 – Loading Beam Resting on Pair of Hydraulic Rams**

## 2.7 Instrumentation and Data Acquisition

### 2.7.1 Strain Gages

Electronic strain gages were used to determine strains along the bar. Strain gages were located at various points within the lap splice, at the end of the lap splice and outside of the lap splice. Figure 2.8 shows a typical instrumentation scheme.

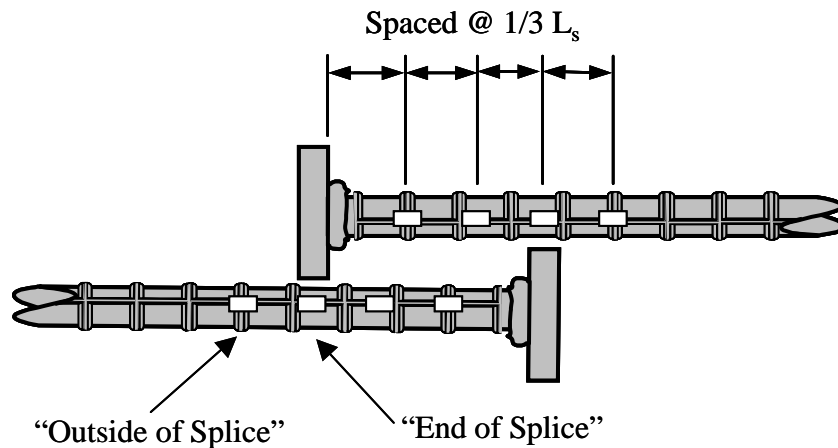


**Figure 2.8 – Typical Strain Gage Instrumentation**

All of the test specimens used type EA-06-250BG-120 strain gages from Micro Measurements Group©. The strain gages had a gage length of  $1/4$  in., a resistance of 120 ohms, and a gage factor of  $2.060 \pm 0.5\%$ . The rebar surface was prepared using a hand-held grinder to create a smooth area approximately one inch in length along the longitudinal rib of the bar. The area was further prepared

with light sanding using a 220 grit wet-dry sand paper and cleaned with acetone, a mild acid solution and neutralized with a mild base solution. The strain gages were attached to the bar using a two-part strain gage adhesive recommended by the manufacturer. The gages were protected with an acrylic coating, a layer of butyl rubber, and finally covered with a two-part, quick-setting epoxy.

### **2.7.2 Load Measurement**

The load was determined using an electronic pressure transducer connected in-line with the four hydraulic rams. Load was calculated by multiplying the measured pressure with the calculated area of the hydraulic rams. The area of the hydraulic rams was determined by calibrating the pressure transducer with the hydraulic rams using a 100 kip load cell.

### **2.7.3 Deflection Measurement**

Midspan deflection and deflection at the end supports were measured using linear potentiometers. The linear potentiometers used for midspan deflection measurement had a gage length of four inches. The linear potentiometers used to measure deflection at the end supports had gage lengths of either two or four inches.

## **2.8 Materials**

### **2.8.1 Concrete Properties**

The cement used in all test specimens was normal strength Type 1 cement with fly ash added. Three-quarter inch maximum size coarse aggregate was used. Slump typically ranged from 3 in. to 4 in. with the exception of the second casting, which had a slump of 7.5 in. All specimens were cast with ready mixed concrete procured from a local supplier.

Concrete strengths were determined by compression testing of 6 in. diameter concrete cylinders in accordance with ASTM C39-99 [5] within a few days of testing. Average concrete strengths at the time of testing for each cast are reported in Table 2.3. Specimens were tested between 28 and 42 days after casting. Modulus of elasticity and modulus of rupture tests were performed on the #4 cast according to test procedures defined in ASTM C469-94 [7] and ASTM C78-94 [6], respectively. Since the concrete strengths for the specimens with #8 bars did not vary significantly, average properties were used in the analysis. The average modulus of elasticity was estimated at 3,800,000 psi and the average modulus of rupture was estimated at 500 psi for the specimens with #8 bars. Modulus of elasticity and modulus of rupture tests were not performed on the concrete used for the specimens with #5 bars.

**Table 2.3 – Concrete Strengths**

<b>Concrete Casting</b>	<b>Specimen</b>	<b>Concrete Strength</b>
1	ULS-#5-1.5C-16A-12 ULS-#5-1.5C-16A-12-R ULS-#5-11.9S-9.6A-11.2 ULS-#5-1.5C-9.6A-12	5700 psi
2	ULS-#8-0X-10S-5 ULS-#8-4.7R-10S-5 ULS-#8-4.7R-10A-5 ULS-#8-4.7R-6S-3	3200 psi
3	ULS-#8-1.2C-10S-5 ULS-#8-1.2C-10A-5 ULS-#8-1.2C-6S-3 ULS-#8-4.7R-6S-5	3700 psi
4	ULS-#8-0X-10S-8 ULS-#8-1.2C-10S-8 ULS-#8-4.0C-10S-8 ULS-#8-4.7R-10S-8	4000 psi

### **2.8.2 Steel Reinforcing Bar Properties**

Steel bar specimens were tested in order to determine the yield stress and moduli of elasticity for the #5 and #8 bars used in the lap splices. Modulus of elasticity tests were not performed on the #5 compression bars used in the testing

of the #8 bar specimens. Two different suppliers provided reinforcing bars for the project. Table 2.4 shows the results of tests performed on the supplied bars.

**Table 2.4 – Steel Reinforcing Bar Properties**

<b>Bar Specimen</b>	<b>Nominal <math>A_{\text{bar}}</math> (in<sup>2</sup>)</b>	<b>Yield Strength (kips)</b>	<b>Yield Stress (ksi)</b>	<b>Modulus of Elasticity</b>
#5 – Supplier #1	0.31	22	71.0	28.1x10 <sup>6</sup> psi
#8 - Supplier #1	0.79	54	68.4	29.4x10 <sup>6</sup> psi
#8 – Supplier #2	0.79	48	60.8	29.4x10 <sup>6</sup> psi



## Chapter 3: Test Results and Behavior

### 3.1 Introduction

The results of the 16 lap splice tests are summarized and discussed in this chapter. The results are reported in terms of the maximum load,  $P_{\max}$ , maximum moment,  $M_{\max}$ , yield moment,  $M_y$ , and ratio of  $M_{\max}$  to  $M_y$ . Test results are summarized in Table 3.1.

### 3.2 Definitions of Terms

#### 3.2.1 $P_{\max}$

$P_{\max}$  is defined as the maximum measured load reached by the test specimen. The measured load is not the actual ram load applied to the specimen since the measured load also includes the dead load of the slab and the reaction beams located at each end of the specimen.

#### 3.2.2 $M_{\max}$

$M_{\max}$  is the calculated moment applied to the specimen at failure. The calculated moment takes into account the moment due to self-weight, moment due to the weight of the reaction beams, and the moment due to the applied load which was measured during the testing.

#### 3.2.3 $P_y$

$P_y$  is the calculated load required to yield the tension reinforcement of the specimens. The calculated yield load includes the dead load of the specimen and reaction beams.

### 3.2.4 $M_y$

$M_y$  is the calculated yield moment of the specimen. The yield moments were calculated assuming a rectangular stress block and a reinforcement stress based on the measured yield stress of the tensile bars as reported in Chapter 2, Section 2.8.2. The yield strength of all the #8 bars was 68 ksi except for those in specimen ULS-#8-4.0C-10S-8, which had bars with a yield capacity of 61 ksi.

**Table 3.1 – Test Results of Lap Splice Specimens**

Slab Width (in)	Specimen	$P_{max}$ (kips)	$P_y$ (kips)	$M_{max}$ (in-k)	$M_y$ (in-k)	$M_{max}/M_y$
40	ULS-#5-11.9S-9.6A-11.2	20.40	20.6	1000	970	1.03
	ULS-#5-1.5C-9.6A-12	17.20	20.6	830	970	0.86
	ULS-#5-1.5C-16A-12	15.60	14.8	740	660	1.12
	ULS-#5-1.5C-16A-12-R	15.90	14.8	760	660	1.15
25	ULS-#8-1.2C-6S-3	7.30	20.7	350	1070	0.33
	ULS-#8-4.7R-6S-3	8.50	20.7	420	1070	0.39
	ULS-#8-4.7R-6S-5	11.40	21.1	570	1070	0.53
36	ULS-#8-0X-10S-5	7.20	21.8	310	1070	0.29
	ULS-#8-1.2C-10S-5	10.20	21.8	480	1070	0.45
	ULS-#8-1.2C-10A-5	10.50	21.8	490	1070	0.46
	ULS-#8-4.7R-10S-5	12.10	21.8	580	1070	0.54
	ULS-#8-4.7R-10A-5	13.50	21.8	660	1070	0.62
	ULS-#8-0X-10S-8	10.40	22.4	470	1070	0.44
	ULS-#8-1.2C-10S-8	12.40	22.4	580	1070	0.54
	ULS-#8-4.0C-10S-8	14.20	20.6	670	980	0.68
	ULS-#8-4.7R-10S-8	14.00	22.4	660	1070	0.62

### **3.3 Specimen Failures**

In conventional lap splices, non-headed bars must transfer force from one bar to the lapped bar through local bearing stresses on lugs and shearing stresses in the surrounding concrete. To fully develop bars in tension when no transverse reinforcement present, the ring stresses around the bar must be kept below the tensile limits of the concrete. Therefore, overlap lengths need to be rather long to fully develop the spliced bars in tension. Headed bar laps transfer force between bars by direct bearing of the heads and lugs on the concrete. The concrete between the heads can be idealized as a compression strut. Failure of the strut occurs when compression stresses in the strut reach the effective compressive strength of the concrete that may be less than the compressive cylinder strength depending on the state of concrete cracking. Section 1.4 offers a more descriptive explanation of how failures can occur in compression struts. In the initial series with #5 bars, most of the specimens developed full yield strength of the reinforcement. Such failures indicate that the splice is fully effective but do not indicate whether a shorter lap length would have been equally effective. In the subsequent series of #8 bar specimens, the lap lengths were substantially reduced in order to provide more information on the mechanisms of splice development with headed reinforcement.

### 3.3.1 Failure of Specimens with #5 Bars

Four specimens reinforced with #5 bars were tested. One specimen (ULS-#8-1.5C-9.6A-12) with forged headed bars spaced at 6 in. and with a 7.5 in. splice length failed by splitting along an outer edge splice. Figure 3.1 shows the specimen at failure. The ordinary splice length for #5 bars with these covers as given by AASHTO 8.25.1 [3] is 12 inches or 19 bar diameters.

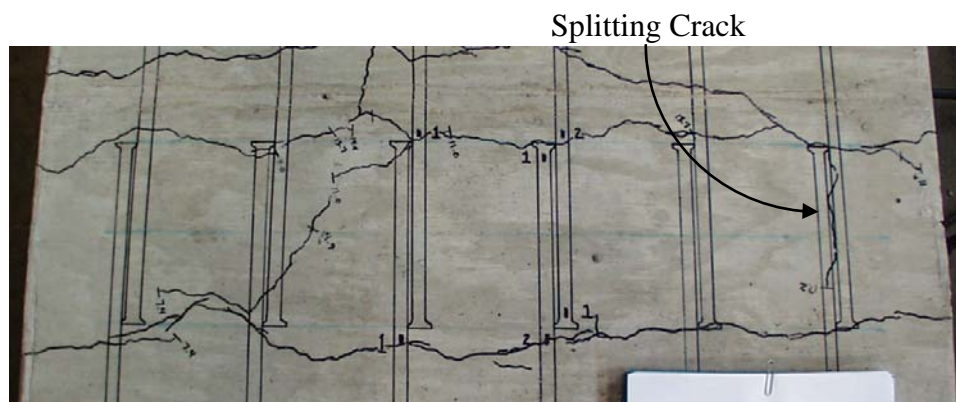


**Figure 3.1 – Failure of Specimen ULS-#5-1.5C-9.6-12**

Three of the specimens failed by yielding of the tensile reinforcement. Very little information can be deduced about the behavior from lap splices that yield other than the combination of lap length and head size was sufficient to cause yielding of the reinforcement. These specimens had lap lengths or 12 bar diameters or about 65% of the splice length required by AASHTO Basic Development Length Equation. This indicates great promise for lapped splices with headed bars.

Figure 3.2 shows the load vs. deflection response for the specimen reinforced with six #5 bars spaced at 6 in. and Figure 3.3 shows the response for the specimen reinforced with four #5 bars spaced at 10 in.

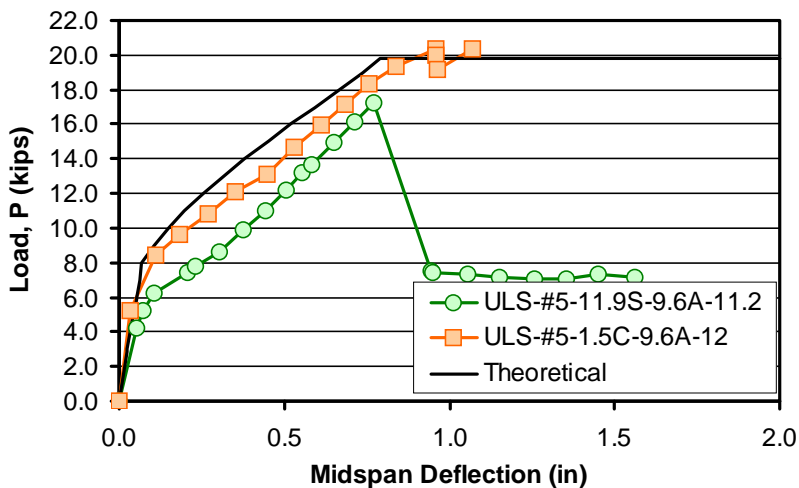


Figure 3.2 – Load - Deflection for Specimens with Six #5 Bars,  $s_{bar} = 6$  in.

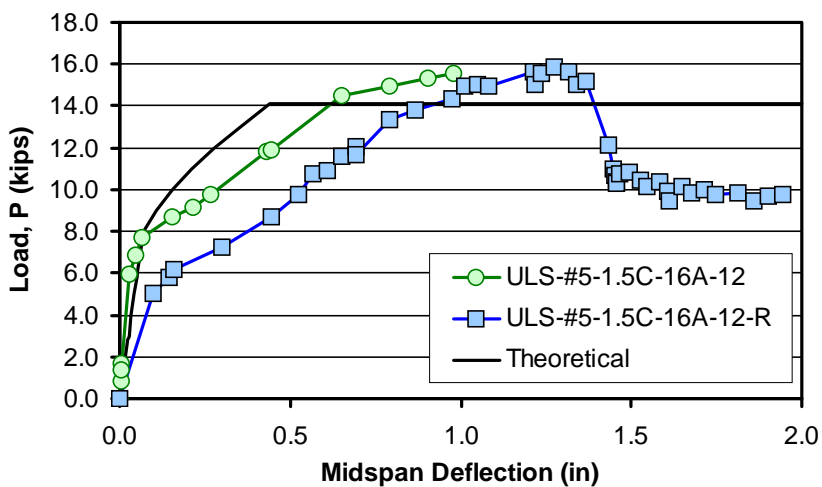
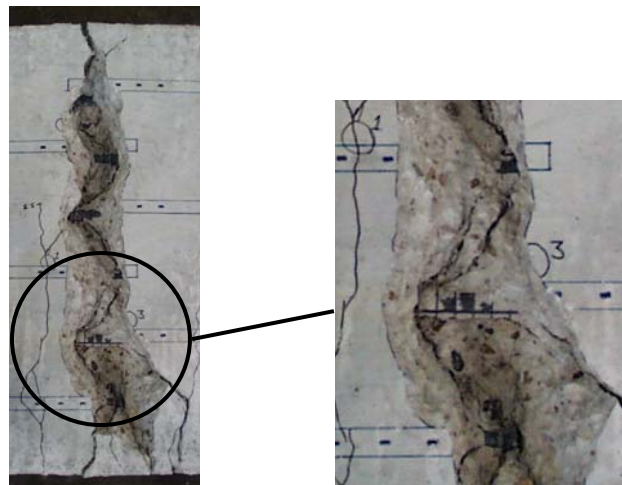


Figure 3.3 – Load - Deflection for Specimens with Four #5 Bars,  $s_{bar} = 10$  in.

### 3.3.2 Failure of Non-Headed Bar Splices

Two specimens with non-headed bar splices were tested as control specimens. Both specimens had #8 bars spaced at 10 in. with staggered splice arrangements, one with  $L_s = 5$  in. and the other with  $L_s = 8$  in. The ordinary splice length for #8 bars with these covers as given by AASHTO 8.25.1 [3] is 32 inches or 32 bar diameters. The greatly shortened splice lengths used were chosen to force splice failure before bar yield for research purposes. Figure 3.4 shows the failure of a non-headed bar splice with a lap length of 5 in. The specimen developed 29% of  $M_y$  although the lap length used was only  $5/32$  (16%) of the AASHTO requirement. The failure plane resembles a cone shape typically observed with shallow pullout tests of single bars. The failure planes follow lines



**Figure 3.4 - Failure of Specimen ULS-#8-0X-10S-5**

of principal compression between bars and cracks form due to high tensile stresses in the orthogonal direction. Figure 3.5 shows the failure of a non-headed splice with a lap length of 8 in. The specimen developed 44% of  $M_y$  although the lap length used was only 8/32 (25%) of the AASHTO requirement. The specimen failed after splitting cracks along the two outermost bars formed. The longer splice length allowed the specimen to reach a 50% higher maximum moment than the specimen with the 5 in. lap length before failure occurred. Under large deformations beyond the peak load, the combination of splitting and flexural cracks resulted in a cracking plane developing completely across the specimen. Upward forces at the ends of the bars due to bending of the specimen caused the cracked cover to lift from the bars as shown in Figure 3.6. It should be noted that

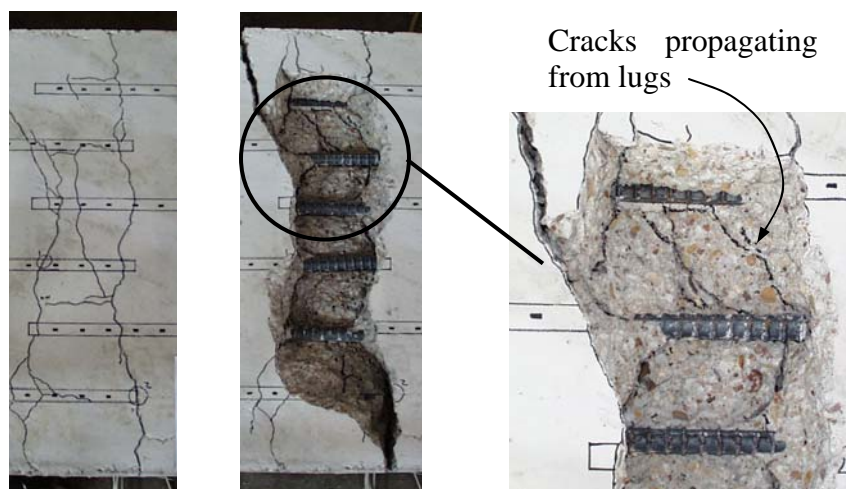


**Figure 3.5 - Failure of Specimen ULS-#8-0X-10S-8**

diagonal cracks were observed in the remaining concrete between the bars. These parallel cracks provide an indication of the development of multiple “struts” between the lugs of the spliced bars.

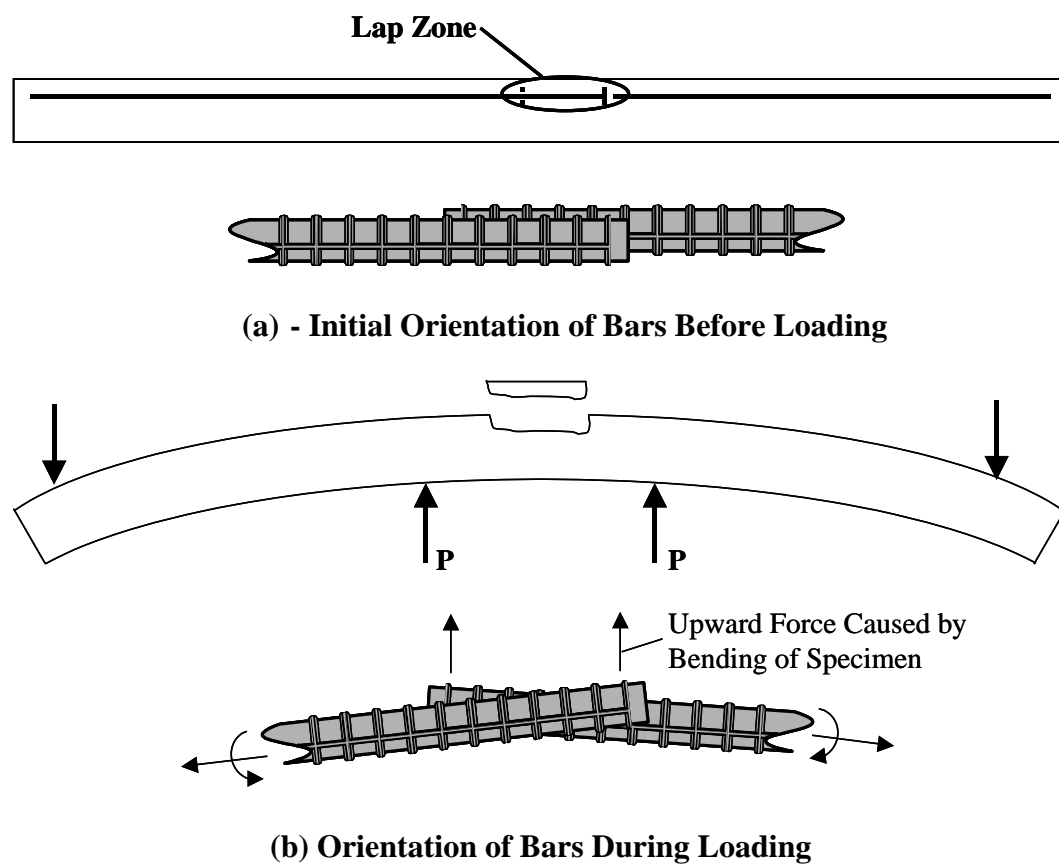


**Figure 3.6 – Cover Liftoff Caused by Bending of Specimen**



### 3.3.3 Failure of Small Headed Bar Splices

Four specimens reinforced with #8 bars with forged heads having  $A_n/A_b = 1.2$  were tested. The presence of a head allowed the force in the bars to be transferred through direct bearing of the head on the concrete in addition to bearing of the lugs on the concrete.

#### *Failure of Specimens With Staggered Spacing*

Three specimens were reinforced with #8 bars and had a staggered splice arrangement. These specimens experienced failures along the compression struts between the heads of the opposing bars. Figure 3.7 shows the failure of specimen ULS-#8-1.2C-6S-3. In spite of the small head size and very short lap length, the specimen developed 33% of  $M_y$  although the lap splice was only 3/32 (9%) of the

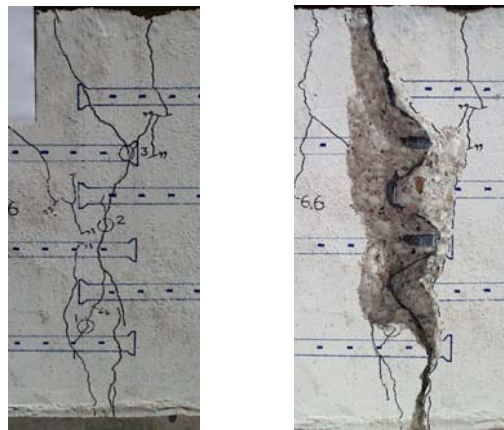


**Figure 3.7 – Failure of Specimen ULS-#8-1.2C-6S-3**

AASHTO requirement. When the cover was removed from this specimen, no cracks propagating from the lugs could be observed suggesting that most of the force was being transferred by bearing of the heads on the concrete.

When head size is increased, stresses in the compression strut were reduced due to the increased area of the compression strut. Therefore, higher loads are required in order to reach failure of the splice. Figure 3.8 shows “wavy” crack patterns between bar heads, which indicate that diagonal compression struts were forming. Figure 3.9 shows the two specimens after the cover was removed. Specimen ULS-#8-1.2C-10S-5 reached 45% of  $M_y$  although the lap splice was only 5/32 (16%) of the AASHTO requirement. Specimen ULS-#8-1.2C-10S-8

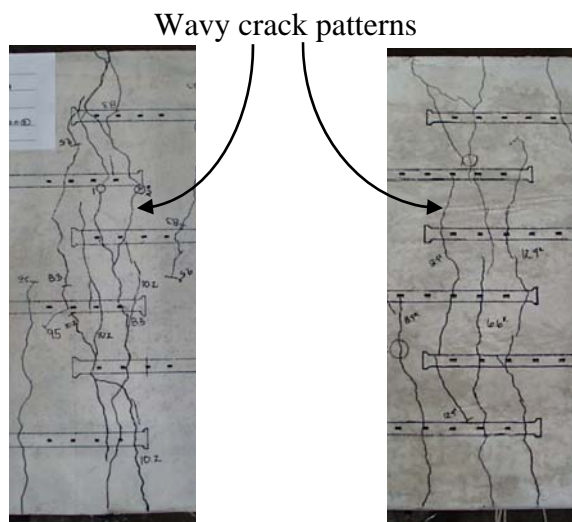


**Figure 3.8 – Wavy Crack Patterns Indicating Formation of Diagonal Compression Struts**

reached 54% of  $M_y$  although the lap splice was 8/32 (25%) of the AASHTO requirement. No cracks propagating from the lugs could be observed in the specimen with the 5 in. lap splice suggesting that the heads are responsible for most of the force transfer between bars. The specimen with the 8 in. lap length show cracks propagating from the lugs on the bar and from the heads. This suggests that force is being transferred in compression struts between bars by both the lugs and the heads.

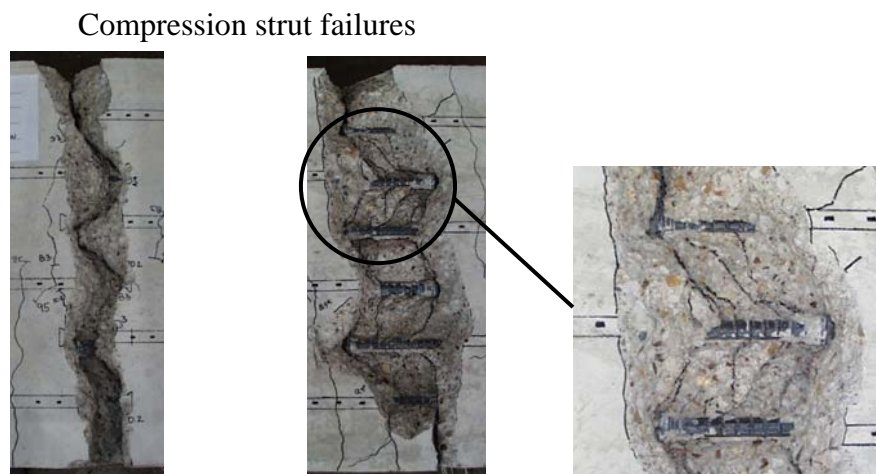


**Figure 3.9 – Specimens ULS-#8-1.2C-10S-5 and ULS-#8-1.2C-10S-8  
Showing Development of Compression Struts**

### ***Failure of Specimen With Adjacent Spacing***

The specimen with small headed bars adjacent to each other failed by splitting cracks which formed along the outermost bars as shown in Figure 3.10.

The specimen reached 46% of  $M_y$  although the lap length was only 5/32 (16%) of the AASHTO requirement. The splitting cracks may have developed due to the combination of ring tension surrounding the heads of the bar and ring tension surrounding the lugs of the bar. Since the bars are spaced adjacently, it is difficult to discern the action that initiated cracking.

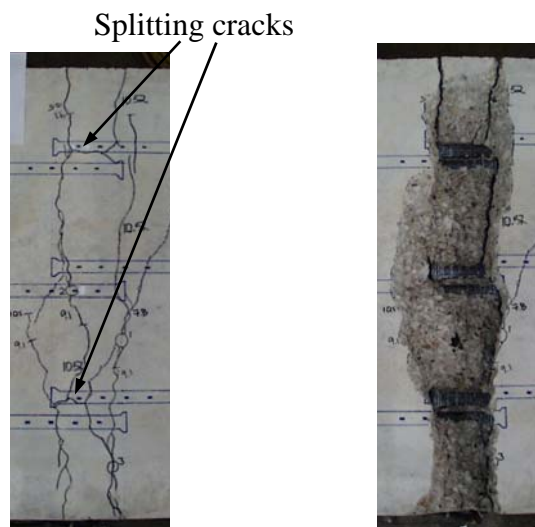


**Figure 3.10 – Failure of Specimen ULS-#8-1.2C-10A-5**

### **3.3.4 Failure of Large Headed Bar Splices**

#### ***Failure of Specimens with Staggered Spacing***

Six specimens reinforced with #8 bars had large heads with  $A_n/A_b$  from 4.0 to 4.7. In the specimen with the 3 in. staggered splice and the specimen with the 5 in. staggered splice, the failure of the compression strut led to failure of the

specimen as shown in Figure 3.11. The absence of splitting cracks along the bar suggests that the heads mainly transferred the force between the bars. Figure 3.11 also shows how struts were formed for the outer splices although no cracking in the struts between the interior splices could be observed. This suggests that a wedging action forms in the interior splices and that the outer splices fail first due to the lack of confinement from the outer edges of the slab.

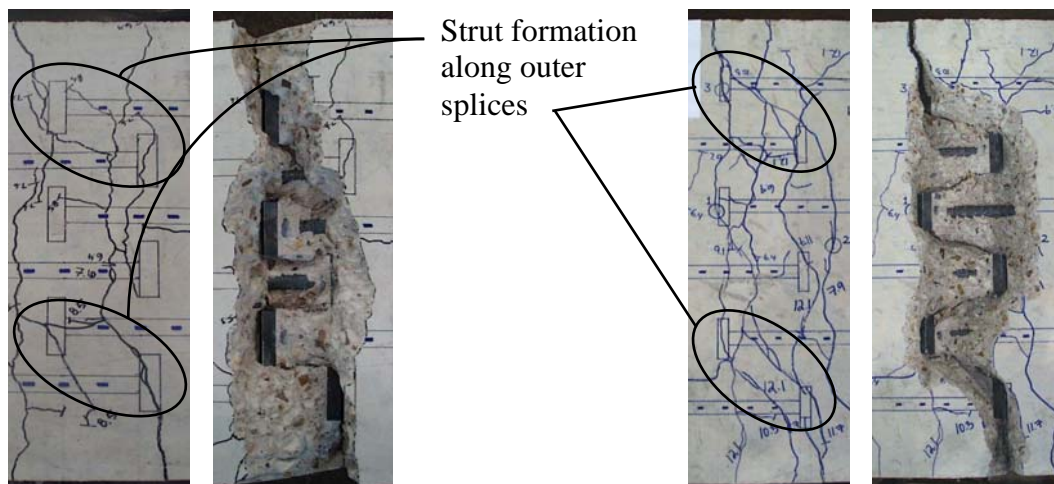


**Figure 3.11 – Failure of ULS-#8-4.7R-6S-3 and ULS-#8-4.7R-10S-5**

Figure 3.12 shows the failure of specimen ULS-#8-4.7R-6S-5. The specimen reached 53% of  $M_y$  although the lap length was only 5/32 (16%) of the AASHTO requirement. A crack propagates from the edge of the head of the outer bar and extends to the head of the opposing bar. It is unclear if the crack started

as a crack in the compression strut or as a splitting crack along the bar. In addition to the crack described above, a second crack was formed at failure of the specimen. This second crack is also located along an outer edge splice.

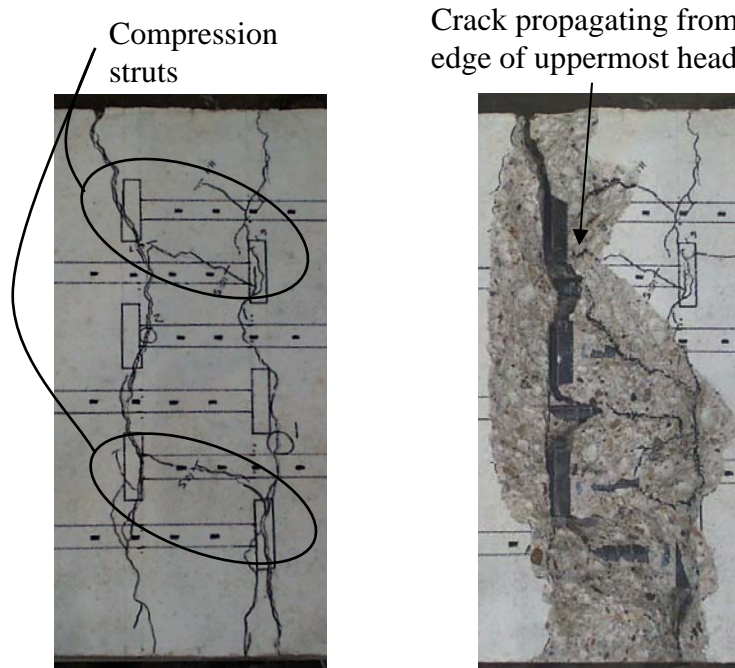


**Figure 3.12 – Failure of Specimen ULS-#8-4.7R-6S-5**

Of the two specimens with 8 in. lap splices, one had circular heads with an  $A_n/A_b = 4.0$  and the other had rectangular heads with  $A_n/A_b = 4.7$ . The specimen with circular heads developed 68% of  $M_y$  and the specimen with rectangular heads developed 62% of  $M_y$  although the lap lengths were only 25% of the AASHTO requirement. The specimen with circular heads was closer to the yield

moment than the specimen with rectangular heads even though both specimens reached roughly the same moment capacity. This was due to the specimen with circular heads having reinforcement with a yield stress of 61 ksi as opposed to the specimen with rectangular heads, which had reinforcement with a yield stress of 68 ksi. Pictures taken at failure show cracks in the compression strut and splitting cracks in front of the circular head as shown in Figure 3.13. With the cover removed, one can see that cracks propagate from the heads on some bars and also propagate from the lugs on other bars. Looking back at the previous specimens discussed that had 8 in. lap splices, all of the specimens show diagonal cracking along the compression strut that propagated from lugs near the middle of the lap splice. This may indicate that an 8 in. lap splice is the beginning of a transition zone where significant development of the bar is achieved by a combination of bearing of the lugs and bearing of the heads on the concrete. The other specimen had rectangular heads with  $A_n/A_b = 4.7$ . Figure 3.14 shows how splitting cracks along the bar led to cover failure of this specimen. The splitting cracks resulting from ring tension surrounding the bars show that significant bar development was achieved by bearing on the lugs in addition to bearing on the heads.

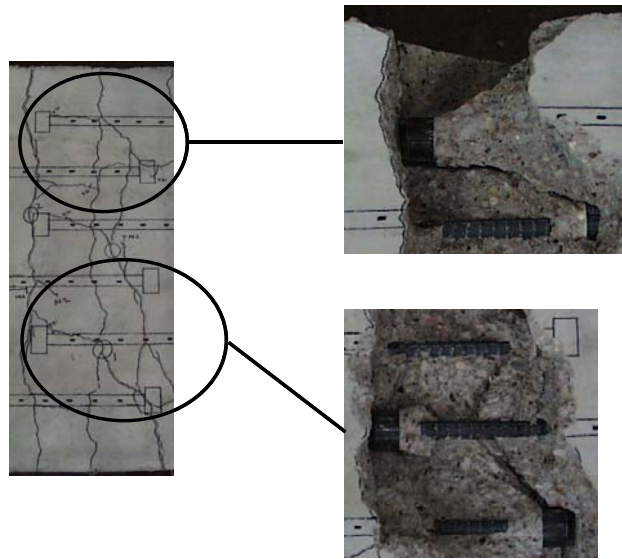


**Figure 3.13 – Failure of Specimen ULS-#8-4.0C-10S-8**

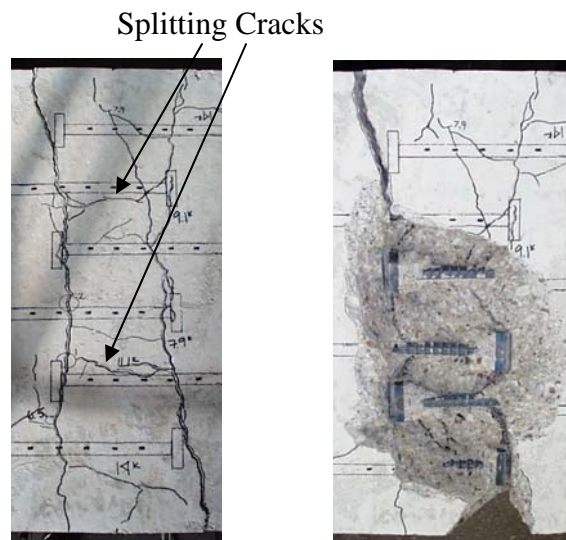


**Figure 3.14 – Failure of Specimen ULS-#8-4.7R-10S-8**



### *Failure of Specimen with Adjacent Splice*

One specimen (ULS-#8-4.7R-10A-5) had 5 in. lap splice length spaced adjacently. The specimen failed as shown in Figure 3.15. The specimen reached 62% of  $M_y$  although the lap length used was only 5/32 (16%) of the AASHTO requirement. No splitting cracks could be observed along the bar before failure suggesting that the force transfer between bars mainly occurred by bearing against the heads of the bars. Pictures taken after the cover was removed show a large diagonal crack extending between the spliced bars. The angle of this cracks is larger than typically observed from previous specimens. The crack may not accurately represent the angle of the compression strut formed between the spliced bars but may have formed due to high tensile stresses that form in the zone between the two opposing pullout cones.

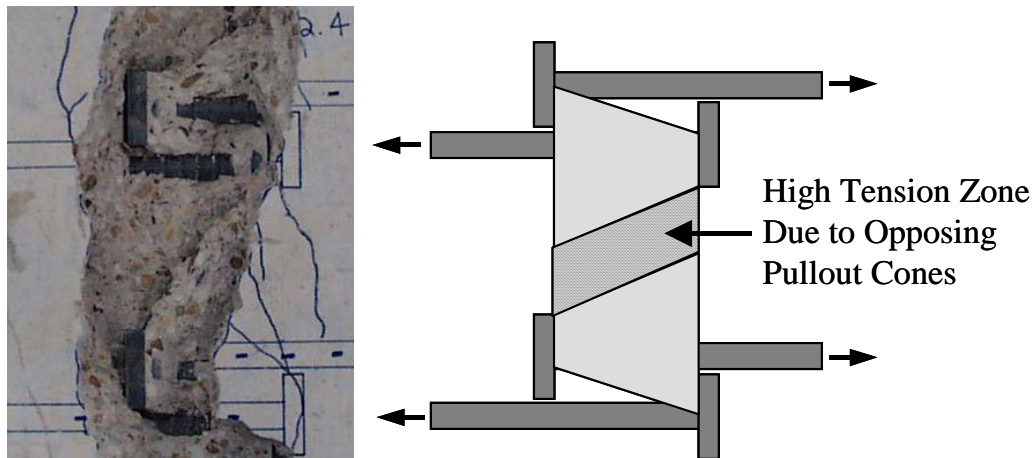


**Figure 3.15 - Failure of Specimen ULS-#8-4.7R-10A-5**

### 3.4 Load-Deflection Response of Specimens with #8 Bars

Load vs. deflection for the 12 specimens reinforced with #8 bars are shown in Figures 3.16 to 3.19. The graphs are divided into four groups with similar properties. Each graph includes the theoretical load vs. deflection response. Comparison between the specimens will be discussed in Chapter 4.

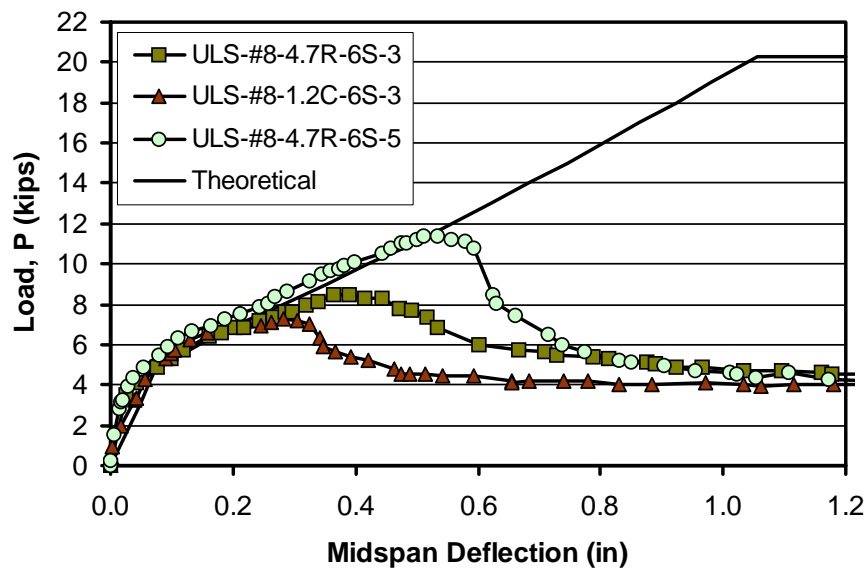


Figure 3.16 – Load vs. Deflection of 25 in. Wide Specimens

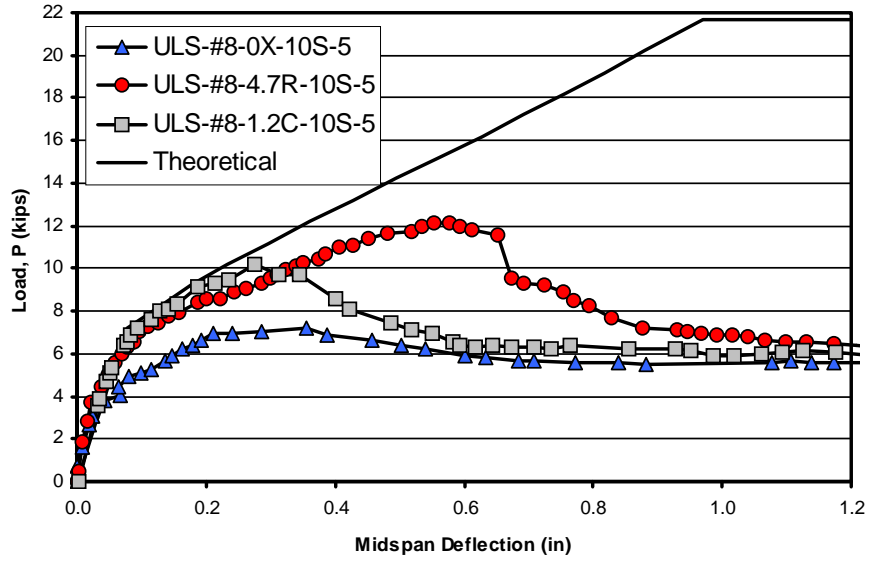


Figure 3.17 – Load vs. Deflection of 36 in. Specimens w/ Staggered  $L_s = 5$  in.

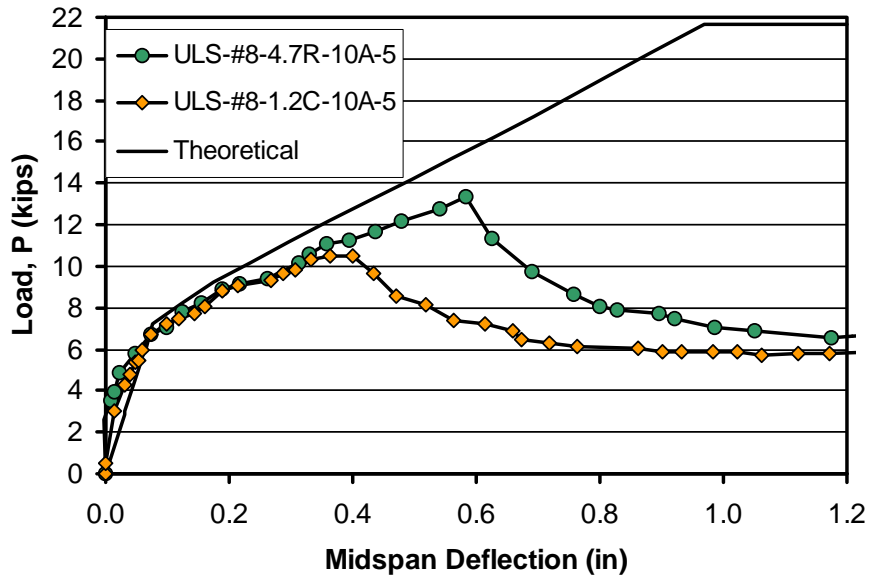
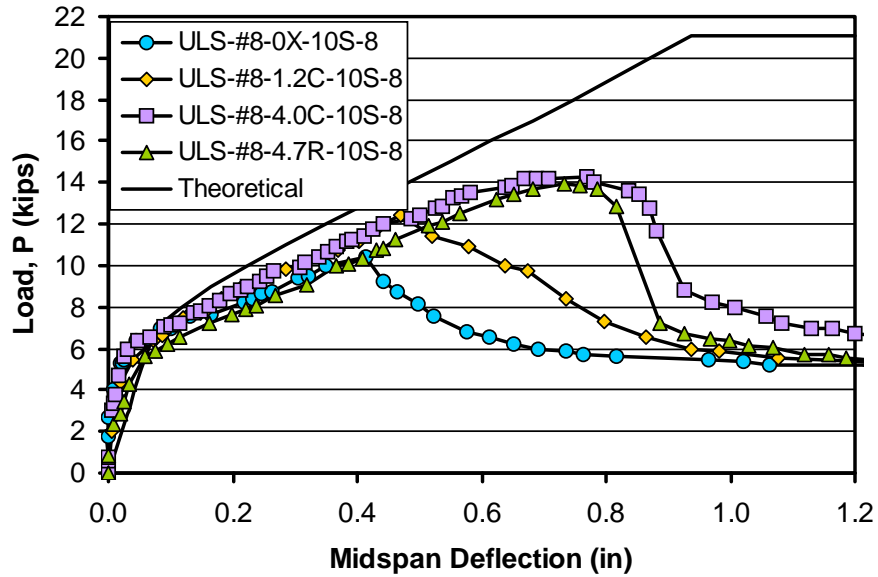
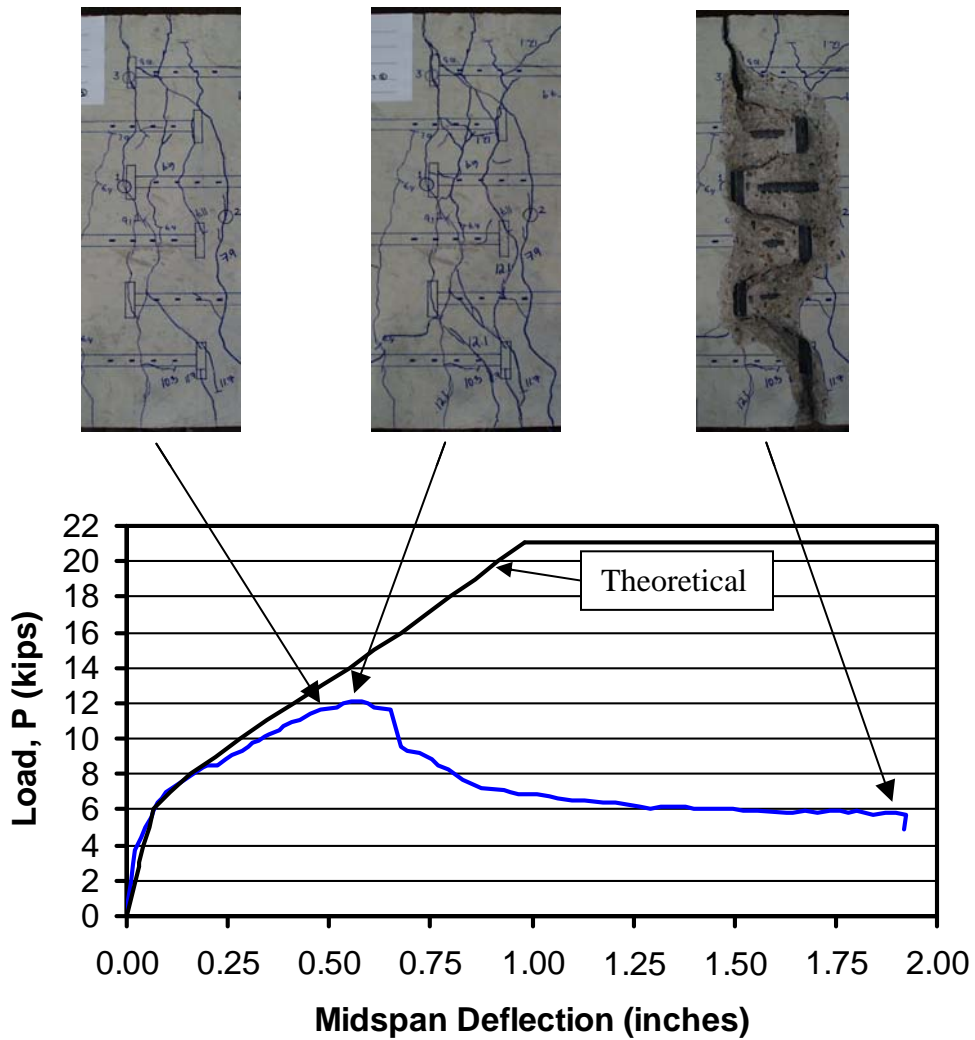


Figure 3.18 – Load vs. Deflection of 36 in. Specimens w/ Adjacent  $L_s = 5$  in.



**Figure 3.19 – Load vs. Deflection of 36 in. Specimens w/ Staggered  $L_s = 8$  in.**

Figure 3.20 shows an example of the individual specimen load vs. deflection graphs located in the appendix. In addition to the graphs, pictures taken before failure, at failure, and after cover removal are presented.



**Figure 3.20 – Load-Deflection Response of ULS-#8-4.7R-10S-5**

### 3.5 Measured Strains

The average measured strain at failure of the specimen does not always coincide with the expected strain at failure. Two reasons why the measured strain

in the reinforcing bars may not accurately reflect the actual strain in the reinforcing bar are: 1) strain gages located near cracks have lower strains because the concrete surrounding the bars transfer tension forces and 2) strain gage readings may not reflect average strain in the bar due to the bending of the bar during loading. Figure 3.21 shows the average measured strain outside of the lap splice when the specimen failed. Figure 3.22 shows the average measured strain at the end of the lap splice when the specimen failed.

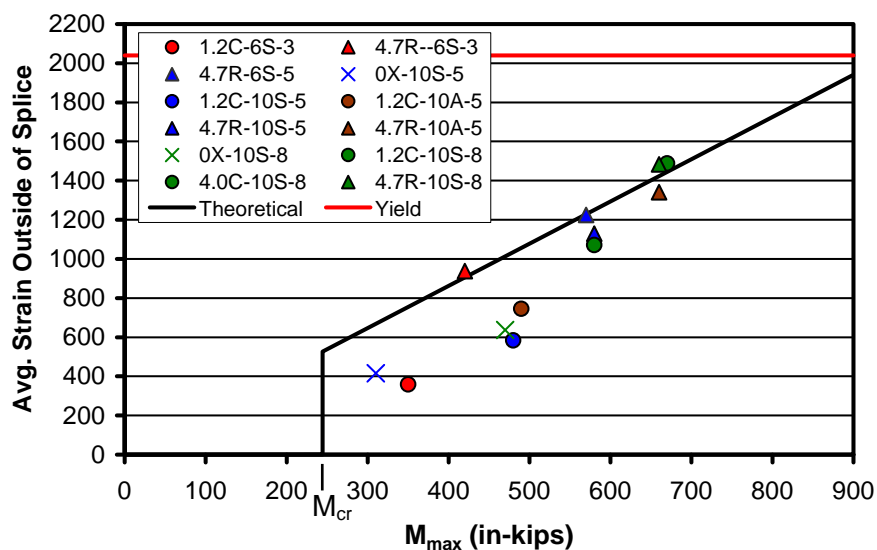


**Figure 3.21 – Strains Outside of Splice at M<sub>max</sub> for Specimens w/ #8 Bars**

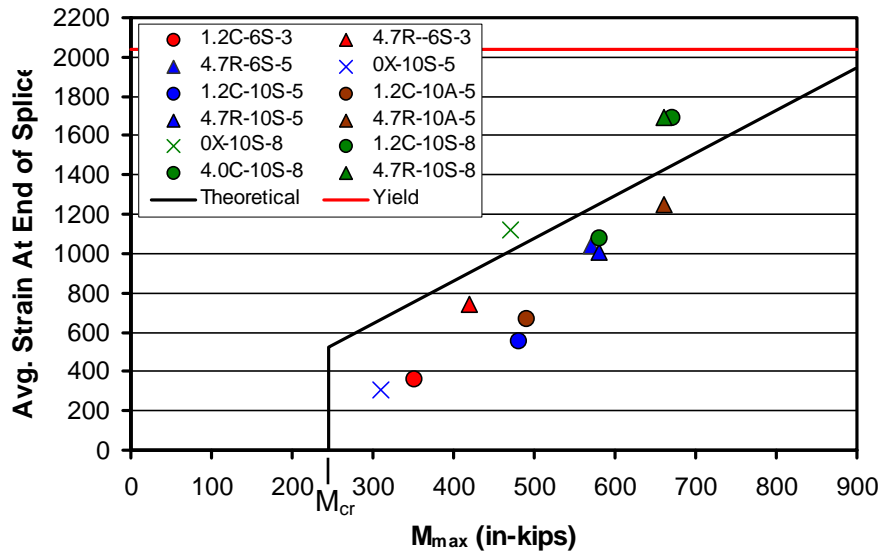


**Figure 3.22 – Strains at End of Splice at  $M_{max}$  for Specimens w/ #8 Bars**

For some specimens, the average strain at failure is well below the theoretical strain. The theoretical estimation of strain is based on cracked section analysis. The location of the strain gage in relation to a crack has a large significance on the measured strain. Strain gages several inches away from cracks have lower strains because the specimen is behaving as an uncracked section. Specimen ULS-#8-0X-10S-8 is a good example of how strain gage location affects the strain readings. Figure 3.23 shows the specimen at failure so that the location of strain gages in relation to cracks can be observed. The

average strain for the gages at the end of the splice is 1100 microstrain while the average strain for the gages outside of the splice is 640 microstrain.

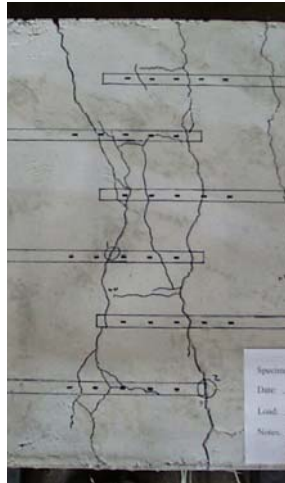


**Figure 3.23 – Location of Strain Gages in Relation to Cracks**

Strain gauges can also read higher or lower than expected strains for another reason. As described in Section 2.7.1, the strain gauges were attached to reinforcing bars along the longitudinal rib of the bar. When the bars were cast in the specimen, the exact orientation of the strain gauges could not be controlled. The bars bend as the specimen deflects during loading. Strain along the top of the bar is higher than strain at the bottom of the bar.



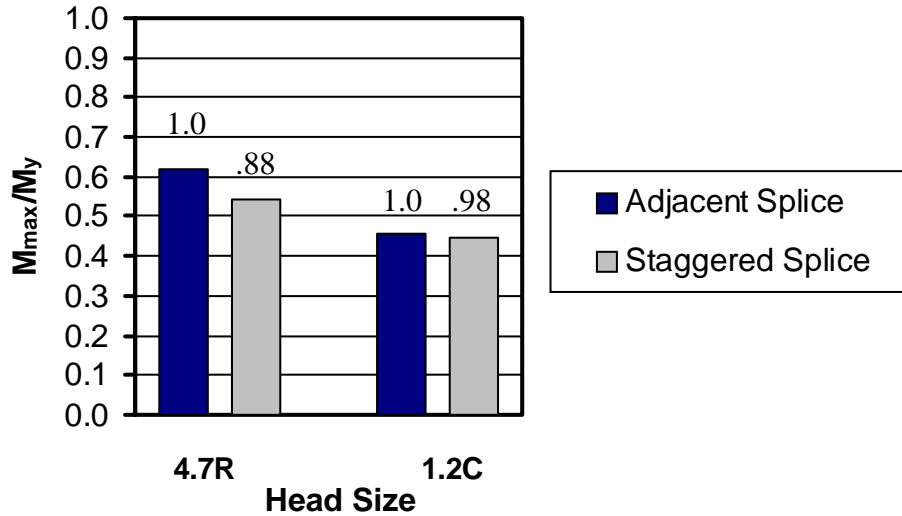
## Chapter 4: Comparison of Test Results

### 4.1 Introduction

Test results are discussed in this chapter and comparisons are made in terms of the strength of staggered vs. adjacent splice arrangement, head size, head shape, bar spacing, lap splice length, and bar size.

### 4.2 Staggered vs. Adjacent Splice Arrangements

Two test groups in which the only variable was lap splice position provide data for direct comparison. Staggered lap splices were spaced so that all bars were equal distances from each other and adjacent splices were spaced so that spliced bars were as close as the heads would permit. Four specimens with #8 bars,  $s_{\text{bar}} = 10$  in., and  $L_s = 5$  in. were tested. Two of specimens had circular heads with  $A_n/A_b = 1.2$  and the other two specimens had rectangular heads with  $A_n/A_b = 4.7$ . Figure 4.1 shows that staggered lap splices did not perform as well as adjacent lap splices. In each plot, the value of the largest moment developed was used to determine the ratio of relative strength. The circular heads had almost the same strength whether adjacent or staggered. The larger rectangular heads ( $A_n/A_b = 4.7$ ) shows the staggered splices to be 12% weaker. The largest staggered spacing used in this study was 5 inches but it is recommended that a maximum allowable staggered spacing be established.



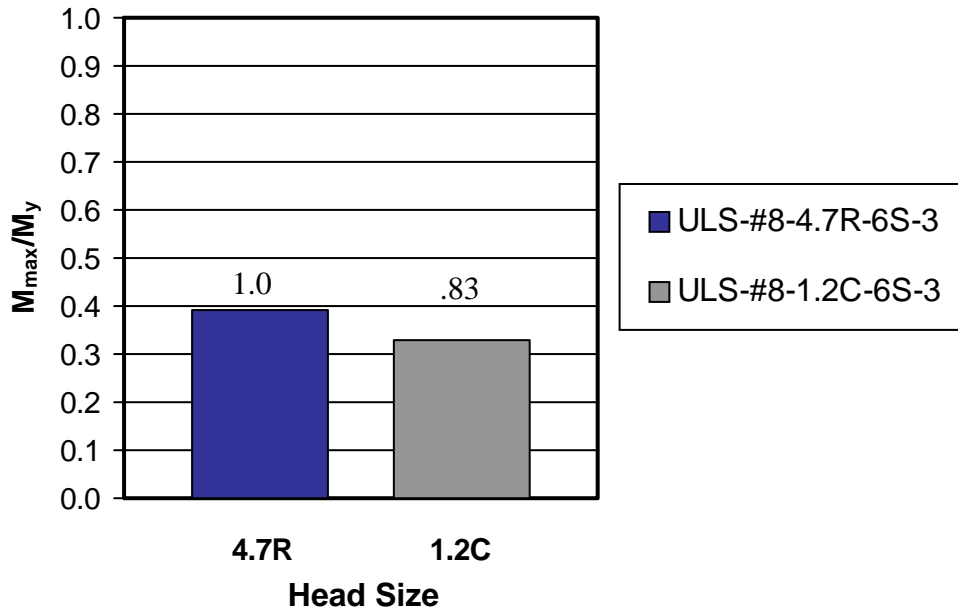
Width (in)	Specimen	$P_{max}$ (kips)	$P_y$ (kips)	$M_{max}$ (in-k)	$M_y$ (in-k)	$M_{max}/M_y$
36	ULS-#8-4.7R-10A-5	13.5	21.8	660	1070	0.62
	ULS-#8-4.7R-10S-5	12.1	21.8	580	1070	0.54
	ULS-#8-1.2C-10A-5	10.5	21.8	490	1070	0.46
	ULS-#8-1.2C-10S-5	10.2	21.8	480	1070	0.45

**Figure 4.1 – Beam Capacities with Staggered and Adjacent Splice Laps**

### 4.3 Head Size

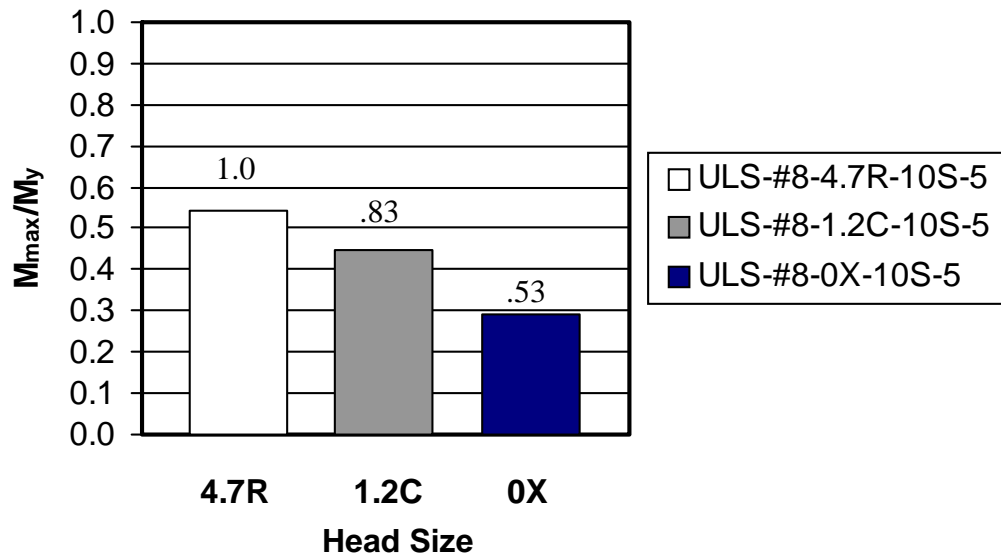
Head sizes used in the study of #8 bar specimens had  $A_n/A_b$  that ranged from 1.2 to 4.7. ASTM A970-98 [4] requires a minimum  $A_n/A_b = 10$ . However, none of the headed bars used in the specimens with #8 bars met this requirement. For research purposes, smaller  $A_n/A_b$  ratios were used in order to determine the effect that head size and development along the bar had on the strength of the lap

splice. As shown in Figures 4.2 to 4.4, moment capacity increased as  $A_n/A_b$  increased. However, the relationship was not linear. Also, as lap length increased, the effect of increased head size on capacity diminished. Three groups of specimens offered direct comparisons between head sizes. All groups of specimens were reinforced with #8 bars spaced at 10 in. with 3, 5, or 8 inch lap lengths. In Figure 4.2, specimens with 3 inch lap lengths are compared. The splices with large heads ( $A_n/A_b = 4.7$ ) were 20% stronger than splices with small heads ( $A_n/A_b = 1.2$ ). In Figure 4.3, specimens with 5 in. lap lengths are compared. Splices with small heads were more than 50% stronger than the non-headed bar splices. With large heads, the capacity was nearly 90% greater than the non-headed bars. In Figure 4.4, the capacity of specimens with 8 in. lap lengths are compared. Bars with small heads ( $A_n/A_b = 1.2$ ) reached a capacity 23% greater than the non-headed bars. With  $A_n/A_b = 4.0$  the capacity increased 43%, and with  $A_n/A_b = 4.7$  the capacity increased by 40%. Figure 4-4 shows that specimen ULS-#8-4.0C-10S-8 reached an  $M_{max}/M_y$  of about 0.69 which was larger than specimen ULS-#8-4.7R-10S-8 even though both had roughly the same capacity. Specimen ULS-#8-4.0C-10S-8 was reinforced with bars that had a lower yield capacity ( $f_y = 61$  ksi) vs.  $f_y = 68$  ksi for the other specimens.



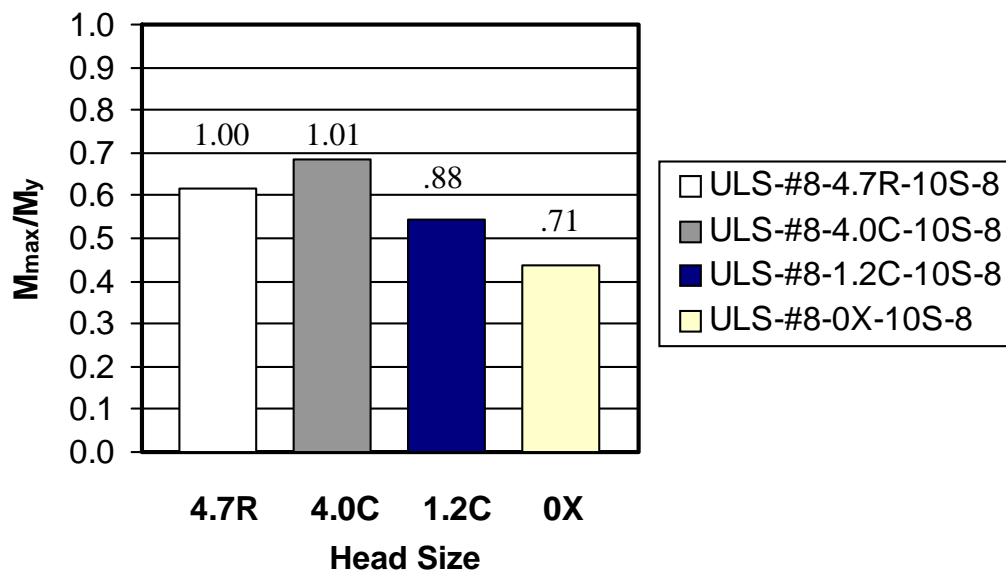
Width (in)	Specimen	$P_{max}$ (kips)	$P_y$ (kips)	$M_{max}$ (in-k)	$M_y$ (in-k)	$M_{max}/M_y$
25	ULS-#8-4.7R-6S-3	8.5	20.7	420	1070	0.39
	ULS-#8-1.2C-6S-3	7.3	20.7	350	1070	0.33

**Figure 4.2 – Beam Capacity vs. Head Size with  $L_s = 3$  in.**



Width (in)	Specimen	$P_{max}$ (kips)	$P_y$ (kips)	$M_{max}$ (in-k)	$M_y$ (in-k)	$M_{max}/M_y$
36	ULS-#8-4.7R-10S-5	12.1	21.8	580	1070	0.54
	ULS-#8-1.2C-10S-5	10.2	21.8	480	1070	0.45
	ULS-#8-0X-10S-5	7.2	21.8	310	1070	0.29

**Figure 4.3 – Beam Capacity vs. Head Size with  $L_s = 5$  in.**



Width (in)	Specimen	$P_{max}$ (kips)	$P_y$ (kips)	$M_{max}$ (in-k)	$M_y$ (in-k)	$M_{max}/M_y$
36	ULS-#8-4.7R-10S-8	14.0	22.4	660	1070	0.62
	ULS-#8-4.0C-10S-8	14.2	20.6	670	980	0.68
	ULS-#8-1.2C-10S-8	12.4	22.4	580	1070	0.54
	ULS-#8-0X-10S-8	10.4	22.4	470	1070	0.44

**Figure 4.4 – Beam Capacity vs. Head Size with  $L_s = 8$  in.**

Figure 4.5 shows the effect that head size has on the strain distribution along the bars in the lap zone at a load of  $P = 7.2$  kips (29% of  $M_y$ ).  $P = 7.2$  kips is also the load at which the non-headed bar specimen failed. Theoretically, the strains at the ends of the bar should be similar if the beams are at the same load.

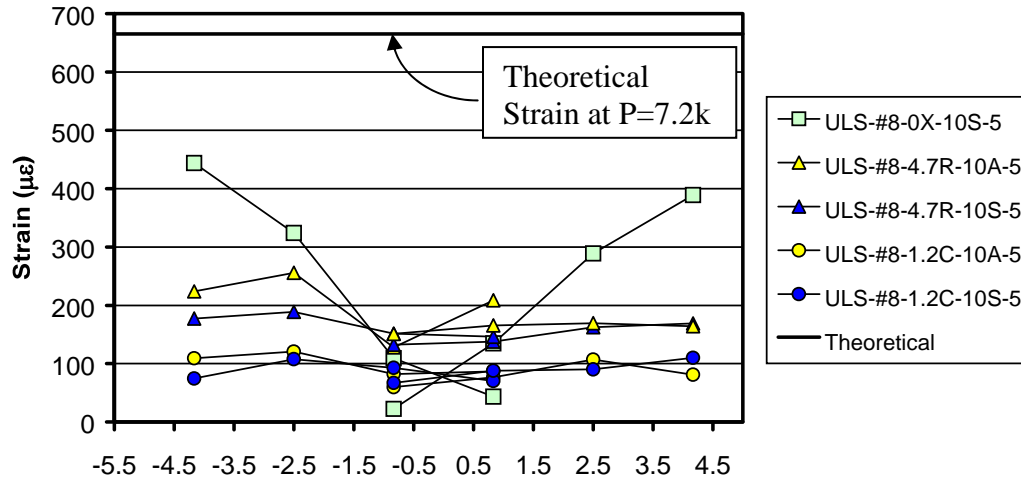


**Figure 4.5 – Strain Along Splice at P = 7.2 kips  
 $b = 36$  in.,  $L_s = 5$  in.,  $s_{bar} = 10$  in., Staggered Splice**

The graph shows that all strains are below the theoretical strain. This is probably due to the influence of cracking patterns. The calculated cracking load of the specimens is approximately 7.0 kips. All of the specimens in Figure 4.5 showed cracking at  $P = 7.2$  kips. However, the headed bar specimens had less cracking than the non-headed bar specimen. The headed bar specimens generally showed little cracking in the lap splice zone at  $P = 7.2$  kips, therefore stresses are largely transferred by tension in the surrounding concrete instead of by the bars. Stress levels of non-headed bars show near linear development over the length of the lap splice while the headed bars show a more constant strain distribution. Strain gages placed near the ends of bars show that strain at the ends of non-headed bars approach zero while the strain at the ends of headed bars show a value greater than zero. Figure 4.6 shows the strain distribution of the headed bar specimens at failure. The headed bars show increased development along the length of the lap splice. This indicates that a combination of bearing of the head and bearing of the lugs on the concrete contribute to the development of the bars. Further testing of specimens with longer lap lengths need to be conducted to determine whether the behavior holds true at higher stresses.



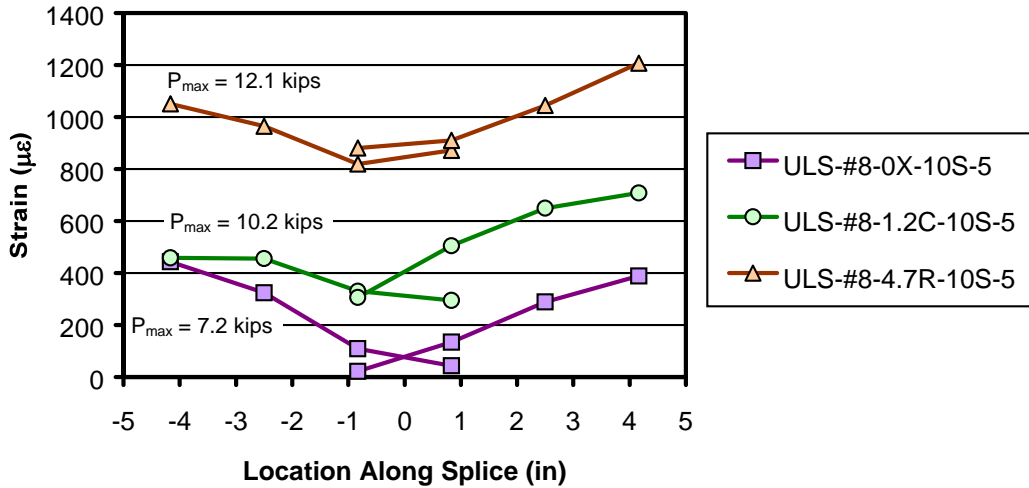


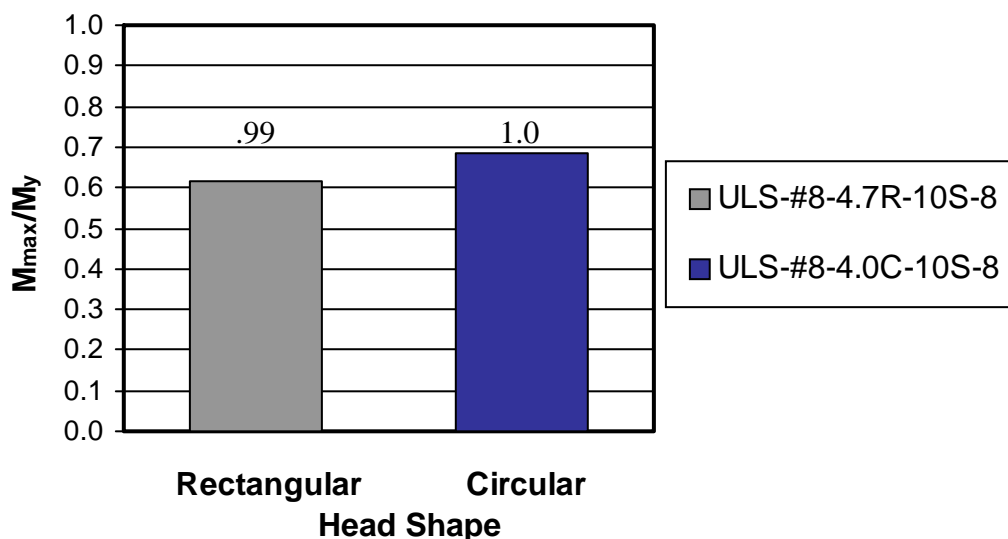
**Figure 4.6 – Strain Along Splice at Failure**  
 **$b = 36$  in.,  $L_s = 5$  in.,  $s_{bar} = 10$  in., Staggered Splice**

#### 4.4 Head Shape

The effect of head shape was studied using the results of tests with circular heads ( $A_n/A_b = 4.0$ ) and rectangular heads ( $A_n/A_b = 4.7$ ). Figure 4.7 shows that the specimens developed nearly the same capacity. The figure shows that the specimen with circular heads was closer to yield than the specimen with rectangular heads even though they both reached roughly the same capacity. The specimen with circular heads used bars with a lower yield strength ( $f_y = 61$  ksi) than the other specimen ( $f_y = 68$  ksi).

Although clear cover to the head was not a variable in this study, minimum clear cover requirements should be met in the field. An advantage to

using circular heads is they are easier to place in situations where the headed reinforcement is close to the concrete surface. When using square or rectangular heads, the orientation of the head may be hard to control. Unless the depth of the bar is sufficient to allow the square or rectangular head to be placed at any orientation and still satisfy cover requirements, clear cover tolerances may not be met if the reinforcing bars rotate during steel cage assembly or when concrete is



Width (in)	Specimen	$P_{max}$ (kips)	$P_y$ (kips)	$M_{max}$ (in-k)	$M_y$ (in-k)	$M_{max}/M_y$
36	ULS-#8-4.7R-10S-8	14.0	22.4	660	1070	0.62
	ULS-#8-4.0C-10S-8	14.2	20.6	670	980	0.68

**Figure 4.7 – Beam Capacity vs. Head Shape**

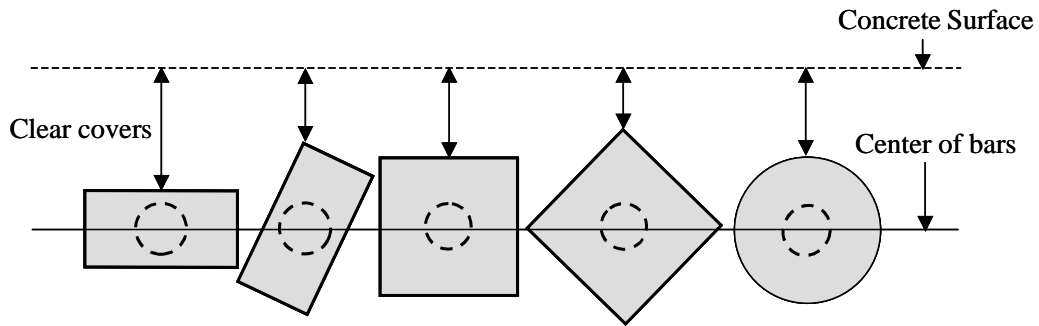
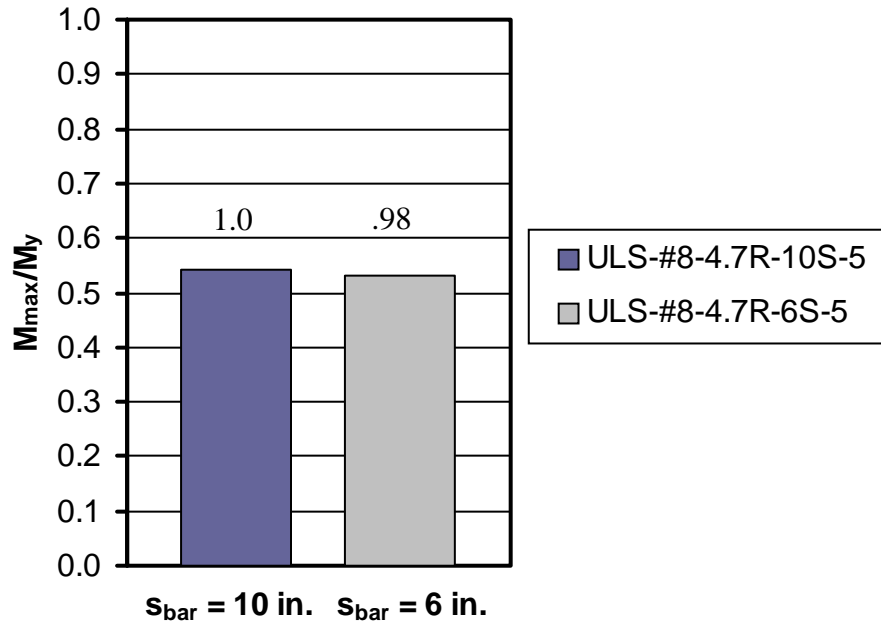


**Figure 4.8 – Clear Cover of Headed Reinforcement**

placed. Figure 4.8 shows how the orientation of rectangular heads and square heads changes the clear cover.

#### **4.5 Bar Spacing**

One direct comparison in which the variables were constant except bar spacing indicated that bar spacing did not affect the performance of headed bar splices. It would be advisable to conduct more tests with varied bar spacing. Figure 4.9 shows the comparison between specimens with #8 bars,  $A_n/A_b = 4.7$ , and 5 in. staggered laps. One specimen had bars spaced at 6 in. on center while the other specimen had bars spaced at 10 in. on center. These specimens developed 53% and 54% of their yield moment capacities, respectively.



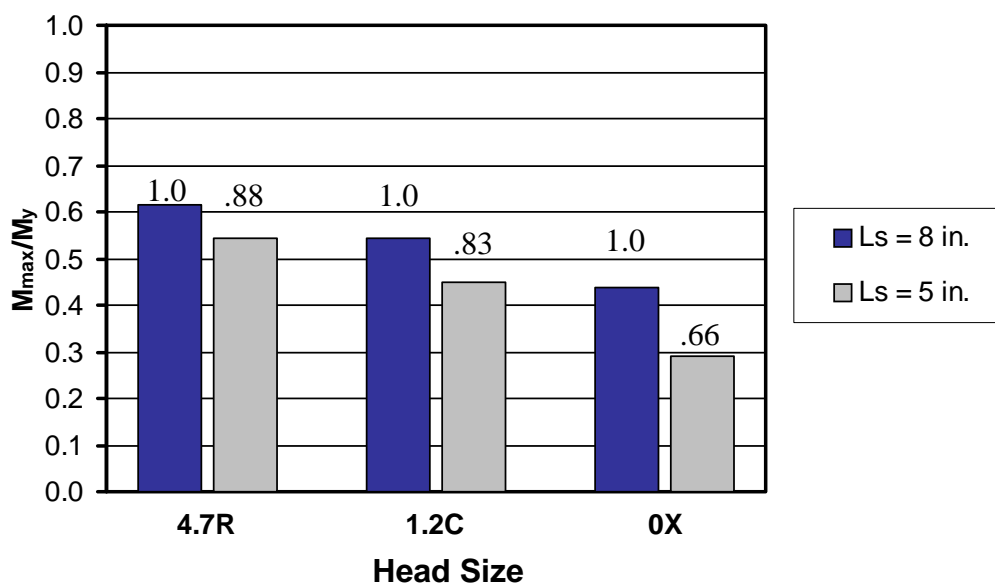
Width (in)	Specimen	$P_{max}$ (kips)	$P_y$ (kips)	$M_{max}$ (in-k)	$M_y$ (in-k)	$M_{max}/M_y$
36	ULS-#8-4.7R-10S-5	12.10	12.10	580	1070	0.54
	ULS-#8-4.7R-6S-5	11.40	11.40	570	1070	0.53

**Figure 4.9 – Beam Capacities with 6 in. and 10 in. Bar Spacing**

#### 4.6 Lap Splice Length

Lap length influenced the performance of the lap splice tests significantly. Three direct comparisons were made in which all variables were kept constant except for lap length. All specimens were reinforced with #8 bars and had 10 in.

staggered splices with lap lengths of either 5 or 8 inches. The capacities are shown in Figure 4.10. Specimens with no heads showed an increase in capacity of 52%. Specimens with small heads ( $A_n/A_b = 1.2$ ) showed an increase in capacity of 21% while specimens with large heads ( $A_n/A_b = 4.7$ ) showed an increase of 14%.



Width (in)	Specimen	$P_{max}$ (kips)	$P_y$ (kips)	$M_{max}$ (in-k)	$M_y$ (in-k)	$M_{max}/M_y$
36	ULS-#8-4.7R-10S-8	14.0	22.4	660	1070	0.62
	ULS-#8-4.7R-10S-5	12.1	21.8	580	1070	0.54
	ULS-#8-1.2C-10S-8	12.4	22.4	580	1070	0.54
	ULS-#8-1.2C-10S-5	10.2	21.8	480	1070	0.45
	ULS-#8-0X-10S-8	10.4	22.4	470	1070	0.44
	ULS-#8-0X-10S-5	7.2	21.8	310	1070	0.29

**Figure 4.10 – Comparison of 5 in. and 8 in. Lap Lengths with Various Heads**

## 4.7 Bar Size

In designing the test program, the influence of bar size on the performance of headed bar splices was included. However, three of the specimens with #5 bars failed by yielding of the reinforcement and the fourth failed after splitting cracks formed along an outer lap splice. Therefore, no comparisons could be made with the #8 bar specimens.

## 4.8 Comparison with Existing Models

### 4.8.1 Comparison with Orangun, Jirsa, and Breen

Based on analyses of data, Orangun, Jirsa, and Breen (O-J-B) [22] determined that the average bond strength along the bar ( $u$ ) for non-headed bars without any transverse reinforcement is:

$$u_c = \left( 1.2 + 3 \frac{C}{d_b} + 50 \frac{d_b}{L_s} \right) \sqrt{f'_c} \quad (\text{Eq. 4-1})$$

$$C = \min(C_b \text{ or } C_s)$$

$$\frac{C}{d_b} \leq 2.5$$

$C_b$  is the clear cover to main reinforcement and  $C_s$  is half the clear spacing between bars or splices or half available concrete width per bar or splice resisting splitting in the failure plane.

Using  $u = \frac{f_s d_b}{4L_s}$ , the equation can be rearranged and solved for  $L_s/d_b$

$$\frac{L_s}{d_b} = \frac{\frac{f_s}{4\sqrt{f'_c}} - 50}{\left(1.2 + 3\frac{C}{d_b}\right)} \quad (\text{Eq. 4-2})$$

Figure 4.11 shows the average stress of specimens with #5 bars at failure vs.  $L_s/d_b$ . The graph shows that the headed bars reached stresses higher than predicted using O-J-B's equation.

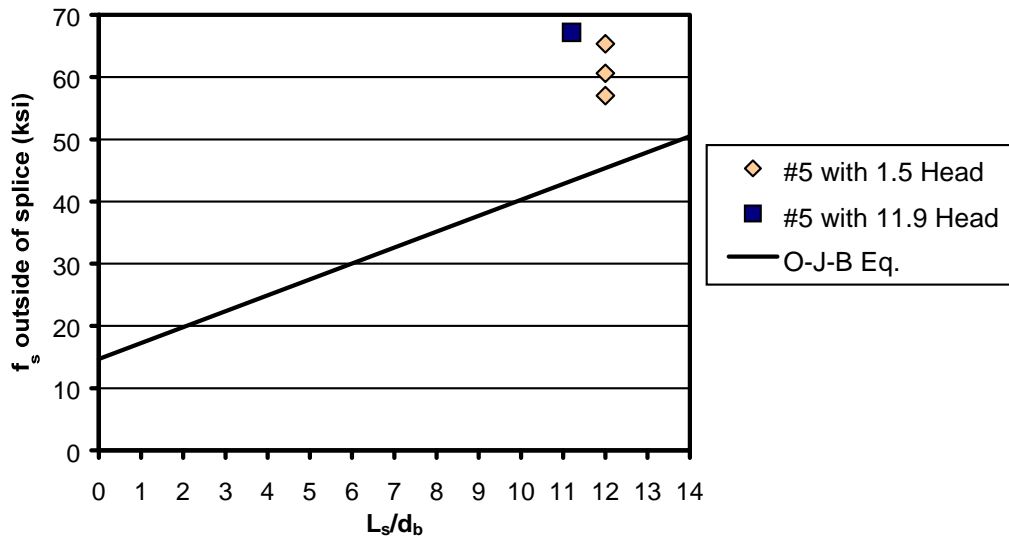


**Figure 4.11 – Comparison of #5 Bar Specimens with O-J-B**

Figure 4.12 shows the average stress of the specimens with #8 bars at failure vs.  $L_s/d_b$ . One problem with the development length equation for non-headed bars by O-J-B is that the analysis was based from  $L_s/d_b$  ratios over 10 and

was not intended for very short development lengths. The lap lengths used in this study were very short. For example, if the development length is zero, the stress in the bar should be zero for non-headed bars, but the computed stress is 12 ksi.

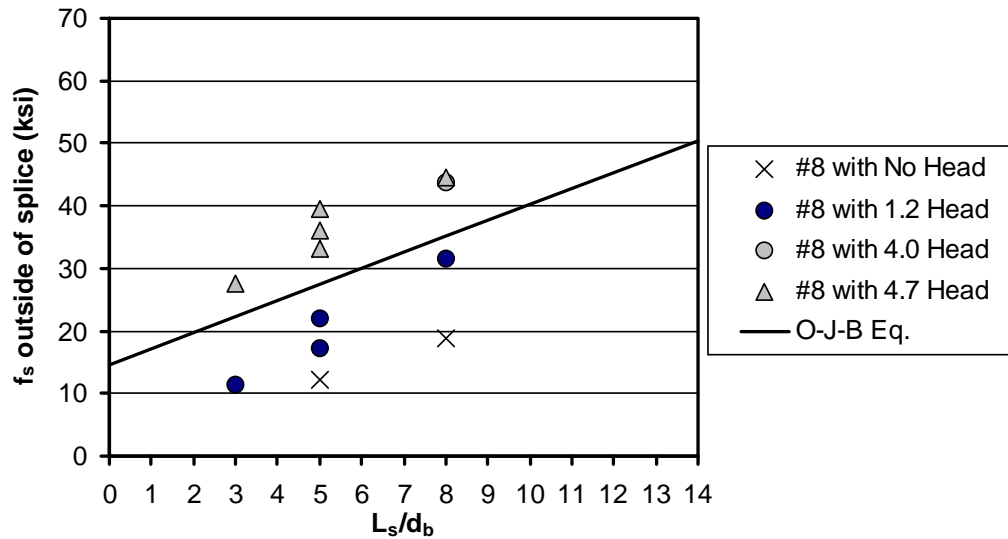


**Figure 4.12 – Comparison of #8 Bar Specimens with O-J-B**

#### 4.8.2 Comparison with AASHTO Basic Development Length Equation

It would be better to compare the measured data of this study with the basic development length equation specified in Section 8.25 of the AASHTO Standard Specifications for Highway Bridges [3]. The basic development length equation in AASHTO was developed from a compilation of research on development and splice lengths but was simplified and incorporated a resistance



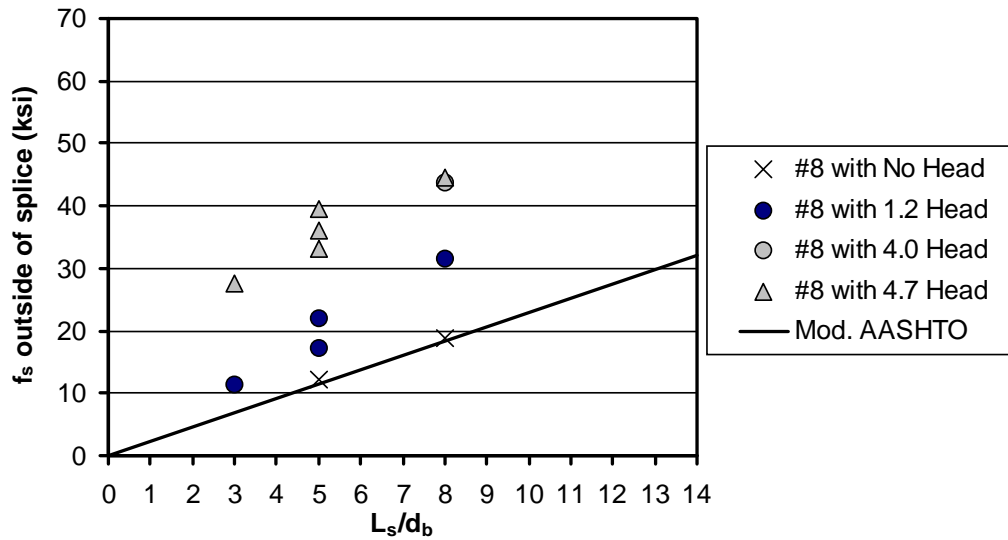
factor of approximately 0.85 for use in design [1,2,22]. The requirement for basic development length of #11 bars and smaller is:

$$l_d = \frac{0.04A_b f_y}{\sqrt{f_c}}, \text{ but not less than } 0.0004d_b f_y \quad (\text{Eq. 4-3})$$

Substituting  $L_s$  for  $l_d$ , modifying to solve for  $L_s/d_b$ , and removing the resistance factor of about 0.85, the equation becomes:

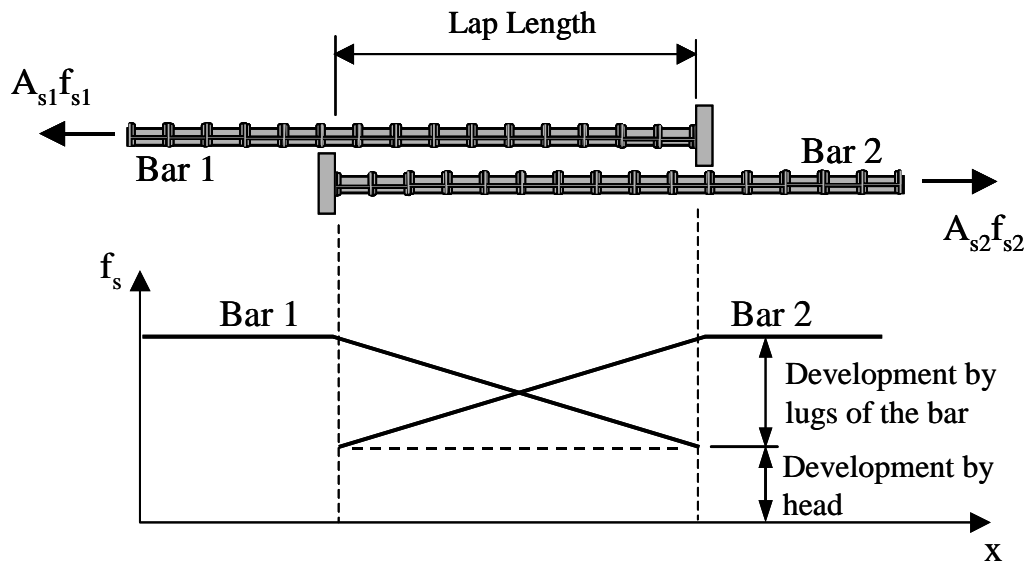
$$\frac{L_s}{d_b} = \frac{0.04A_b f_s}{d_b \sqrt{f_c}} 0.85 \quad (\text{Eq. 4-4})$$

Figure 4.13 shows the test results versus the Modified AASHTO equation. The specimens with non-headed bars follow the Modified AASHTO equation well. The figure also shows that the small heads ( $A_n/A_b = 1.20$ ) increased the stress development of the bar while the larger size heads ( $A_n/A_b = 4.0$  and  $4.7$ ) showed a greater increased in development stress.



**Figure 4.13 – Comparison with Modified AASHTO Equation**

In Chapter 1, Section 1.4, a hypothesis was proposed that the headed bar lap splice develops bar stress by both bearing of the head and bearing of the lugs on the surrounding concrete. Figure 4.14 is a repeat of Figure 1.12 that shows the bar develops a certain amount by bearing of the head and then development of the bar increases linearly by bearing of the lugs on the surrounding concrete. Figure 4.5 showed how stresses along the headed bars do not go to zero at low levels of stress like the non-headed bars. Figure 4.6 showed that at higher levels of stress, the headed bar splice shows development at the head and then development of the bar increases along the lap length. This seems to confirm the hypothesis of how a



**Figure 4.14 – Development of Headed Bar Splice**

headed bar lap splice develops. A simple method for determining the design capacity of headed bar lap splices would be beneficial to designers. The results obtained suggest that development is composed of two parts with a form  $y = A + Bx$ . Part A of the development occurs by bearing of the head. Part Bx occurs by bearing of the lugs of the bar on the surrounding concrete over a lap length  $x$ . Figure 4.15 is the same as Figure 4.13 except that it shows how development by part A (bearing of the head) may be estimated. Part Bx, the development by the lugs of the bar, can be estimated using the Modified AASHTO Equation 4-4. These values of Bx are shown by drawing lines parallel to the Modified AASHTO Equation 4-4 through the data points for  $A_n/A_b = 1.2$  and 4.7 respectively. The

intercept of these lines with the  $f_s$  axis at  $L_s/d_b = 0$  gives a good estimate of the head bearing contribution (A). From the Figure 4.15, a rough approximation shows that the development by bearing of the head with  $A_n/A_b = 1.2$  is approximately 8 ksi and the development by bearing of the head with  $A_n/A_b = 4.7$  is approximately 23 ksi.

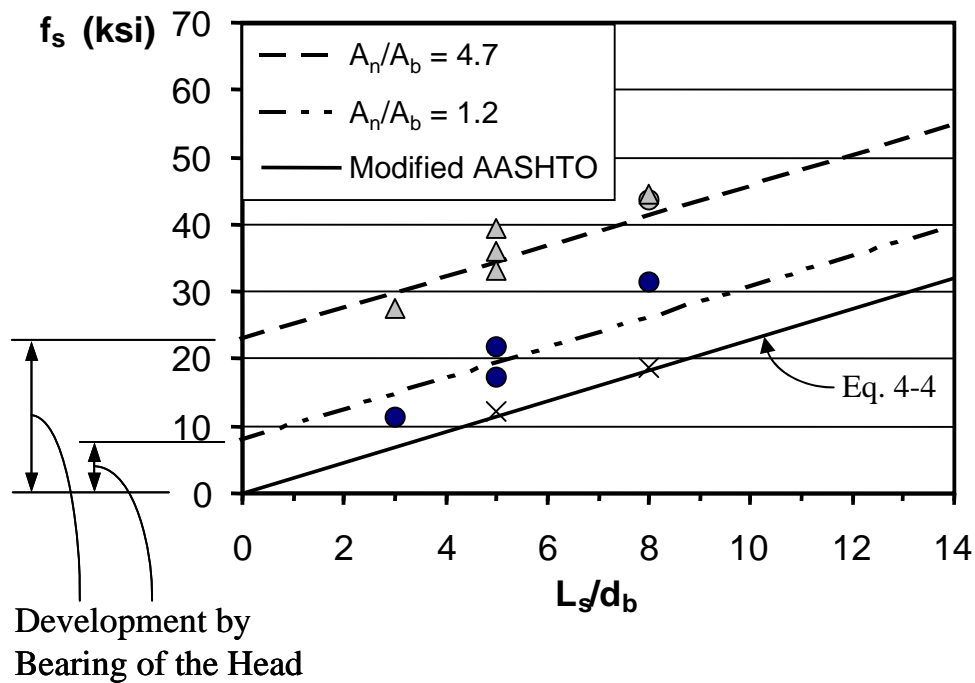


**Figure 4.15 – Development that Parallels Modified AASHTO Equation**

#### 4.8.2 Comparison with DeVries' Side Blowout Capacity Equation

In his research on anchorage of headed bars, DeVries [15] determined the blowout capacity of headed bars. The equation DeVries developed was similar to

the equation that Furche and Eligehausen [18] used to determine the development of headed studs. Variables used in his research such as cover, development length, concrete strength, head size and edge placement are relevant in the use of headed bars in lap splices. In his analysis of development length as a variable, DeVries concluded that the increased capacity provided by development length could be accurately predicted using O-J-B's equation or the development length provisions in ACI 318-95 [1]. However, DeVries conservatively chose not to include development length as a variable in the design equation. DeVries' equation for side blowout capacity of headed reinforcement is:

$$P_U = \frac{A_{bo}}{A_{bon}} 0.017 C_1 \sqrt{A_n f'_c} \quad (\text{SI Units}) \quad (\text{Eq. 4-5})$$

Converting to customary US units gives

$$P_U = \frac{A_{bo}}{A_{bon}} 204.7 C_1 \sqrt{A_n f'_c} \quad (\text{Eq. 4-6})$$

where  $P_U$  is the blowout capacity in lbs,  $C_1$  is the minimum edge distance to the center of the bar in inches,  $A_n$  the net bearing area of the head in  $\text{in}^2$  and  $f'_c$  the concrete compressive strength in psi. The ratio  $A_{bo}$  over  $A_{bon}$  is the ratio of available failure area for a single bar or group of bars to the basic failure area.  $A_{bon}$  equals  $36C_1^2$ , which was determined by the Comite Euro-International du Beton (CEB) [12] as the average failure surface area of a single bolt near an edge and was used by DeVries in his studies of headed bars. Figures 4.16 and 4.17

show graphically how  $A_{bon}$  and  $A_{bo}$  are defined. For lap splices, the available failure area for an interior bar would be:

$$A_{bo} = (3C_1 + \frac{1}{2}L_s)s_{bar} \quad (\text{Eq. 4-7})$$

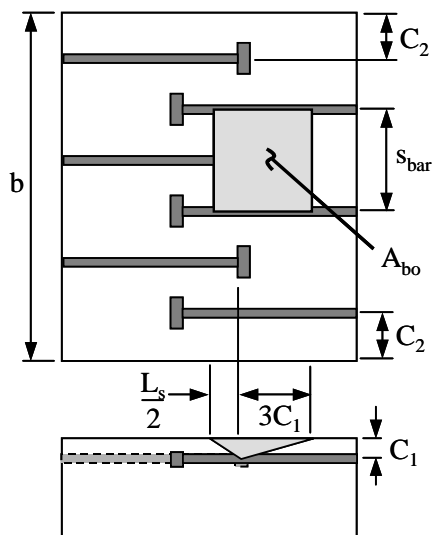


**Figure 4.16 – Definition of Available Failure Area,  $A_{bo}$ , for an Interior Headed Bar**

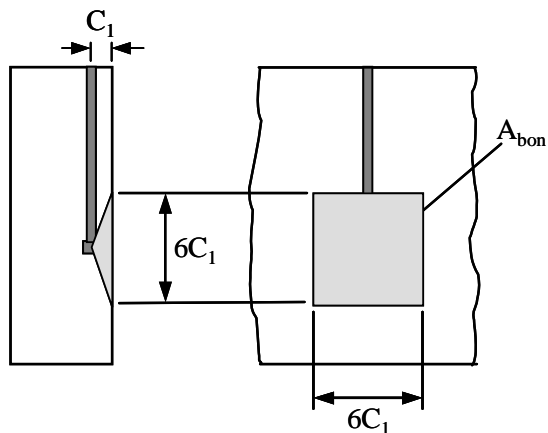


**Figure 4.17 – CEB Definition of Basic Blowout Failure Area,  $A_{bon}$ , Shown for a Single Headed Bar**

Stresses near the heads of the headed bars were calculated using DeVries side blowout model and compared to measured stresses near the heads. Statistical measurements of the comparison are shown in Table 4.1. The predicted stresses are close to the graphically approximated stresses determined in Figure 4.15. Figure 4.18 shows how the predicted stress,  $\sigma_{pred}$ , compares to the measured stress,  $\sigma_{meas}$ . The figure shows that there is a wide range of scatter in the data.

**Table 4.1 – Comparison of Measured Stress at the Head with Predicted Stress Using DeVries’ Side Blowout Model**

Specimen	Measured Strain ( $\mu\epsilon$ )	$\sigma_{meas}$ (ksi)	$\sigma_{pred}$ (ksi)	$\sigma_{meas}/\sigma_{pred}$
ULS-#8-1.2C-6S-3	365	8.4	5.8	1.45
ULS-#8-1.2C-10S-5	300	6.9	10.7	0.64
ULS-#8-1.2C-10A-5	530	12.1	10.7	1.14
ULS-#8-1.2C-10S-8	495	11.3	12.3	0.92
ULS-#8-4.0C-10S-8	1275	29.2	22.1	1.32
ULS-#8-4.7R-6S-3	680	15.6	11.2	1.39
ULS-#8-4.7R-6S-5	960	22.0	12.5	1.77
ULS-#8-4.7R-10S-5	875	20.0	20.8	0.97
ULS-#8-4.7R-10A-5	880	20.2	20.8	0.97
ULS-#8-4.7R-10S-8	1400	32.1	23.9	1.34
		<b>Maximum</b>		<b>1.77</b>
		<b>Minimum</b>		<b>0.64</b>
		<b>Average</b>		<b>1.19</b>
		<b>Standard Deviation</b>		<b>0.32</b>

At least part of the scatter may be attributed to the influence of crack patterns. Strain gages near cracks record higher strains and strain gages located further away from cracks record lower strains. It might be better to compare the development of the headed bar lap splice specimens using moment capacity instead of using bar strain data.

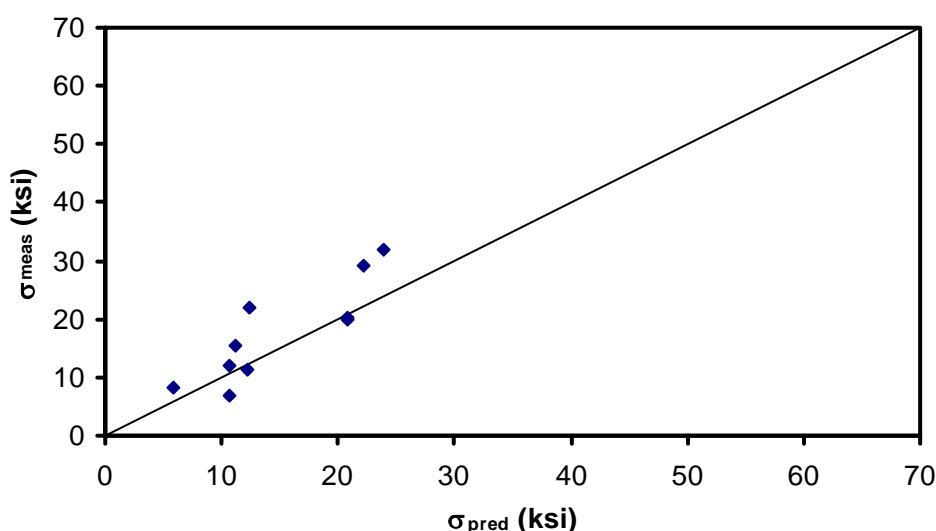


**Figure 4.18 – Comparison of Measured Bar Stress at the Head with Predicted Bar Stress at the Head Using DeVries’ Side Blowout Model**

#### **4.8.3 Calculation of Moment Capacity Using Combination of DeVries’ Model and the Modified AASHTO Development Length Equation**

The development of a headed bar splice could be calculated using a combination of DeVries’ side blowout equation and the Modified AASHTO equation for development length. The proposed model for bar development would be of the form:



$$F = P_u + P_{MA} \quad (\text{Eq. 4-8})$$

where  $F$  is the force developed by the bar in lbs,  $P_u$  is the force developed by the head using DeVries' side blowout equation, and  $P_{MA}$  is the force developed by the lugs of the bar along the lap length using the Modified AASHTO equation. The expanded form of the equation would be.

$$F = \frac{A_{bo}}{A_{bon}} 204.7 C_1 \sqrt{A_n f'_c} + \frac{L_s \sqrt{f'_c}}{(0.04)(0.85)} \quad (\text{Eq. 4-9})$$

The values of  $P_u$  and  $P_{MA}$  were calculated and used to predict the moment capacity of the headed bar specimens. Predicted moment capacities were determined using rectangular stress block theory.  $M_u$  is the predicted moment using  $P_u$  and  $M_{MA}$  is the predicted moment using  $P_{MA}$ . The force developed by the bar ( $F$ ) times the number of bars being spliced ( $n$ ) represents the total tension force developed by the beam section. The predicted moment capacities ( $M_{pred}$ ) were then compared with the measured moment capacities ( $M_{max}$ ).

$$M_{pred} = M_u + M_{MA} \quad (\text{Eq. 4-10})$$

Statistical measures of the comparisons are shown in Table 4.2. Moment capacities were used to compare the specimens instead of bar stresses because measured strain gage data tend to show a wide range of scatter depending on the cracking pattern of the specimen. The combination of DeVries' side blowout model and the Modified AASHTO development length equation gives average

values that are nearly equal to the measured average capacities of the headed bar specimens.

**Table 4.2– Predicted Moment Capacities Based on DeVries’ Side Blowout Model and the Modified AASHTO Development Length Equation**

Specimen	$n \cdot P_u$ (kips)	$M_u$ (in-k)	$n \cdot P_{M.A.}$ (kips)	$M_{M.A.}$ (in-k)	$M_{pred}$ (in-k)	$M_{max}$ (in-k)	$M_{max}/M_{pred}$
ULS-#8-1.2C-6S-3	21.9	140	15.9	102	242	350	1.45
ULS-#8-1.2C-10S-5	40.5	264	26.5	173	437	480	1.10
ULS-#8-1.2C-10A-5	40.5	264	26.5	173	437	490	1.12
ULS-#8-1.2C-10S-8	46.6	304	42.4	276	580	580	1.00
ULS-#8-4.0C-10S-8	84.0	548	42.4	276	824	670	0.81
ULS-#8-4.7R-6S-3	42.6	272	15.9	102	374	410	1.10
ULS-#8-4.7R-6S-5	47.3	303	26.5	169	472	570	1.21
ULS-#8-4.7R-10S-5	78.9	514	26.5	173	687	580	0.84
ULS-#8-4.7R-10A-5	78.9	514	26.5	173	687	680	0.99
ULS-#8-4.7R-10S-8	90.7	592	42.4	276	868	660	0.76

**Maximum 1.45**  
**Minimum 0.76**  
**Average 1.04**  
**Standard Deviation 0.21**

Figure 4.19 shows the measured capacities compared to the predicted moment capacities of the headed bar specimens. The measured capacities were higher than the predicted moment capacities for capacities below 600 in-kips or

approximately 55% of  $M_y$ . For capacities above 600 in-kips, the measured capacities were below the predicted capacities. More tests closer to the yield moment would be helpful to determine if this model is increasingly unconservative at higher capacities. The development length contribution could conservatively be ignored for design purposes. Figure 4.20 shows the measured moment capacities compared to the capacities predicted only using DeVries' side blowout model,  $M_u$ . The yield moment,  $M_y$  for these specimens was 1070 in-k. The measured capacities were higher than the predicted capacities for all tests.

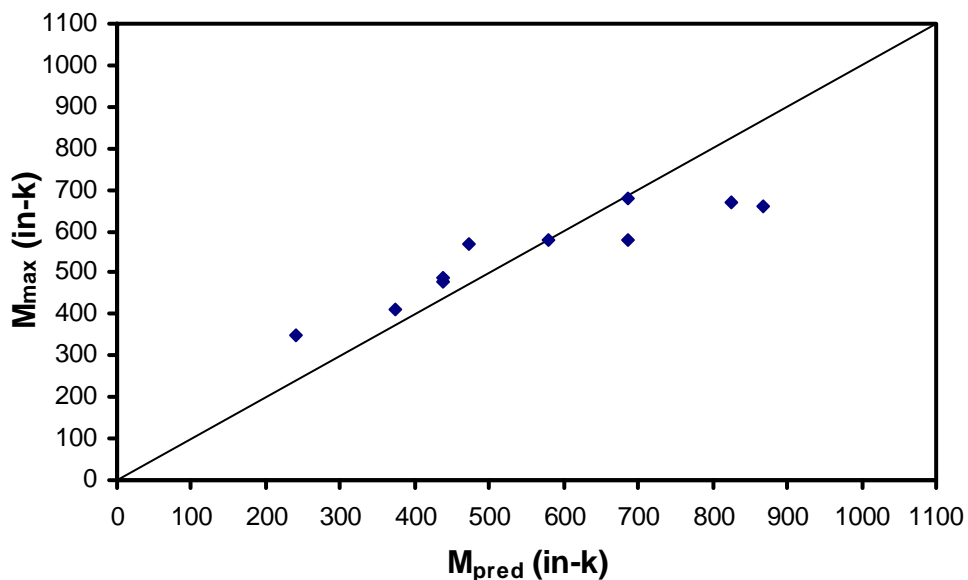


**Figure 4.19 – Comparison of Measured Moment Capacities of Headed Bar Specimens with Predicted Moment Capacities Using Eq. 4-9**

As capacity increases, the measured capacities approach the predicted capacities. Again, further tests near yield failure would be helpful to determine if this model remains conservative at higher capacities. For design purposes, it would be conservative to ignore the contribution of development length. However, some minimum development length should be established to avoid very large heads with extremely short lap splices. Ideally, designers should be able to answer the question; “Given the available development length, how big must the head be to fully develop the bars in tension?”

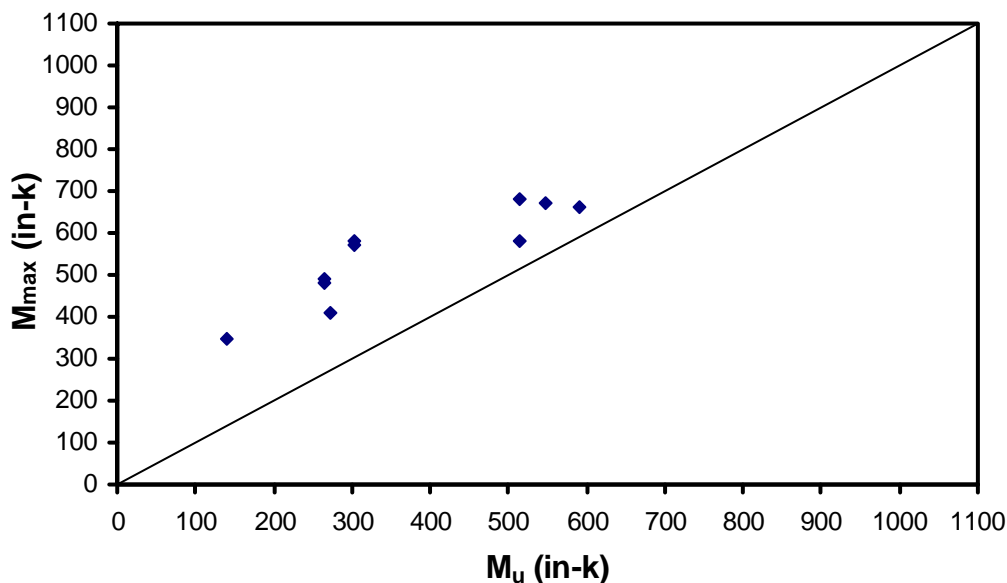


**Figure 4.20 – Comparison of Measured Moment Capacities of Headed Bar Specimens with Capacities Predicted Using DeVries Side Blowout Model**

#### **4.9 Recommendations for Further Research**

More tests are needed to determine the required  $L_s/d_b$  to cause yielding of the reinforcement for the specimens with #8 bars and to determine how the proposed model compares to measured capacities as yield is approached. More tests are also needed with shorter lap splice lengths using #5 bars to determine whether the specimens match trends observed with the #8 bar specimens and to determine the effects of bar size on the headed bar lap splice model. Tests where the bars are sheathed to destroy bond along the bar in the lap zone would be useful for better understanding of the contribution by bearing of the head on the concrete. Tests using confining reinforcement will also need to be evaluated.

## **Chapter 5: Summary and Conclusions**

### **5.1 Summary**

Recent progress in fabricating headed reinforcement provides opportunities for simplifying some details common to bridge structures. This study focused on the use of headed bars in lap splicing applications. Use of headed bars may significantly reduce the required lap length to fully develop the reinforcing bars and therefore, may be a better solution than conventional straight bar development for some splicing applications. Areas that show the most promise for use of headed bar splices are in precast construction and in situations where clearance problems may limit the exposure of steel required to provide continuity, such as retrofit applications or staged construction.

Headed bars were introduced in reinforced concrete construction because provisions for anchorage of bars, splices, and continuity between elements pose significant difficulties for designers and contractors. Use of headed bar anchorages may reduce congestion problems which make the fabrication of reinforcement cages and placement and consolidation of concrete difficult when large amounts of bent bar reinforcement are used.

Sixteen tests were evaluated to determine the behavior of unconfined headed bar lap splices. Variables included strength of staggered splices vs. adjacent splices, head size, head shape, bar spacing, lap length, and bar size.

## **5.2 Conclusions**

The following observations and conclusions were made concerning the behavior of headed bars in lap splices:

- 1) Force transfer between spliced bars occurs by a combination of bearing of the head and bearing of the lugs of the bar through the surrounding concrete.
- 2) Staggered lap splices did not perform as well as adjacent lap splices. The staggered lap splices developed 88% to 98% of the capacities of the adjacent splices. Staggered splices were spaced so that all bars were equal distances from each other and adjacent splices were spaced so that spliced bars were as close as the heads would permit.
- 3) Capacity increased as head size was increased. However, the effect that head size had on capacity diminished as lap length increased due to increased force transfer by bearing of the lugs of the bar on the surrounding concrete. Head size was defined as the ratio of net head area to bar area.  $A_n/A_b$  ratios tested were 1.5 or 11.9 for specimens reinforced with #5 bars.  $A_n/A_b$  ratios ranged from 0.0 to 4.7 for specimens reinforced

with #8 bars. The increase in capacity, due to head size, of specimens could be predicted using DeVries' model for side blowout capacity of headed reinforcement (Eq. 4-6) [15].

- 4) Head shape did not significantly affect the performance of the lap splices. Head shapes tested were square, rectangular, and circular.
- 5) Bar spacing did not seem to affect the performance of the lap splice tests. However, only one comparison of bar spacing was made. Bar spacing,  $s_{bar}$ , was either 6 or 10 inches.
- 6) Splice length,  $L_s$ , had a large influence on the capacity of the specimens. Splice lengths tested were 7 to 7.5 in. for #5 bar specimens and 3 in., 5 in., or 8 in. for #8 bar specimens. The increase in capacity, due to splice length, of the specimens could be predicted using a modified version of the AASHTO Basic Development Length Equation (Eq. 4-4). The AASHTO Basic Development Length Equation (Eq. 4-3) [3] incorporates a resistance factor of approximately 0.85.
- 7) The effect that bar size had on the development of headed bar splices was inconclusive because three of the four specimens reinforced with #5 bars failed by yielding of the reinforcement. Such failures indicate that the splice is fully effective but do not indicate whether a shorter lap length



would have been equally effective. The fourth specimen failed after splitting cracks formed along an outer edge splice.

- 8) The capacity of the specimens could be predicted using a combination of DeVries' side blowout equation and the Modified AASHTO development length equation. The equation for the capacity of headed bar splices is:

$$F = \frac{A_{bo}}{A_{bon}} 204.7C_1 \sqrt{A_n f'_c} + \frac{L_s \sqrt{f'_c}}{(0.04)(0.85)} \quad (\text{Eq. 5-1})$$

F is the force developed by the bar in lbs.,  $C_1$  is the minimum edge distance to the center of the bar in inches,  $A_n$  the net bearing of the head in  $\text{in}^2$ ,  $f'_c$  is the concrete compressive strength in psi,  $L_s$  is the splice length in inches, and the ratio  $A_{bo}$  over  $A_{bon}$  is the ratio of available failure area for a single bar or group of bars to the basic failure area.  $A_{bon}$  equals  $36C_1$ , which was determined by the Comité Euro-International du Béton (CEB) [12] as the average failure surface area of a single bolt near an edge. For lap splices, the available failure area for an interior headed bar would be:

$$A_{bo} = \left( 3C_1 + \frac{1}{2}L_s \right) s_{bar} \quad (\text{Eq. 5-2})$$

- 9) For design purposes, it would be conservative to ignore the contribution of development length. However, some minimum development length should be established to avoid splices with very large heads and extremely short lap lengths. Test results showed that the measured capacities of the

specimens using only the side blowout model were above the predicted capacities of the specimens for all of the specimens reinforced with #8 bars. Because of the number of yield failures, capacities were not predicted for the specimens with #5 bars.

### **5.3 Recommendations for Further Research**

More tests are needed to determine the required  $L_s/d_b$  to cause yielding of the reinforcement for the specimens with #8 bars. More tests are also needed with shorter lap splice lengths of the #5 bars to tell whether the specimens match trends observed with the #8 bar specimens and to determine the effects of bar size on the headed bar lap splice model. Tests where the bars are sheathed to destroy bond along the bar in the lap zone would be useful for better understanding of the contribution by bearing of the head on the concrete. Tests using confining reinforcement will also need to be evaluated.

## Appendix

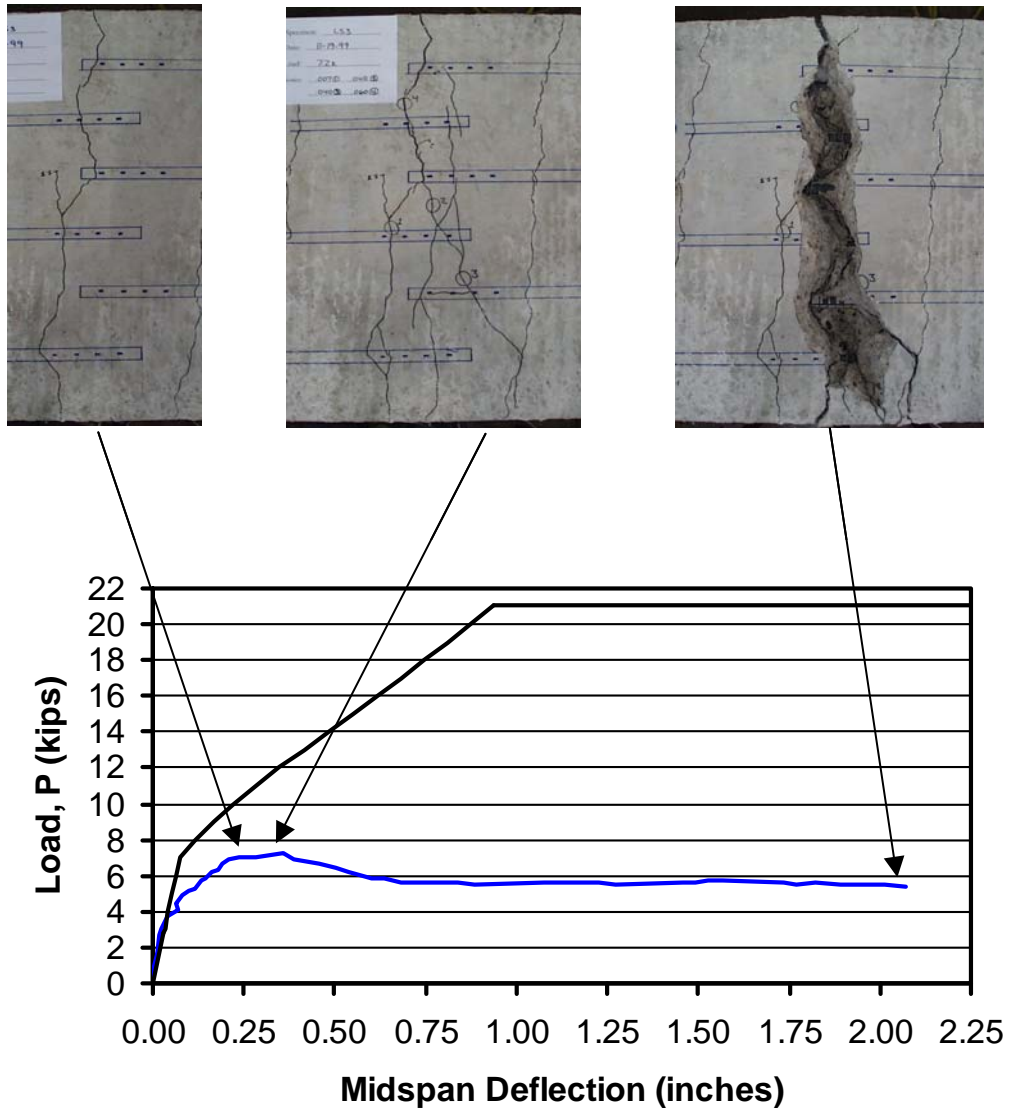


Figure A.1 – Specimen ULS-#8-0X-10S-5

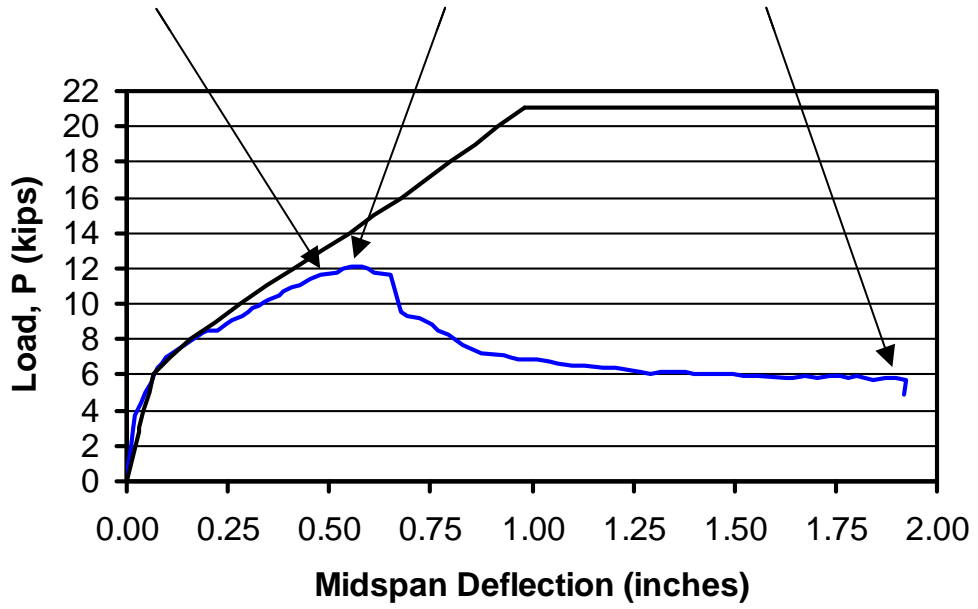


Figure A.2 – SpecimenULS-#8-4.7R-10S-5

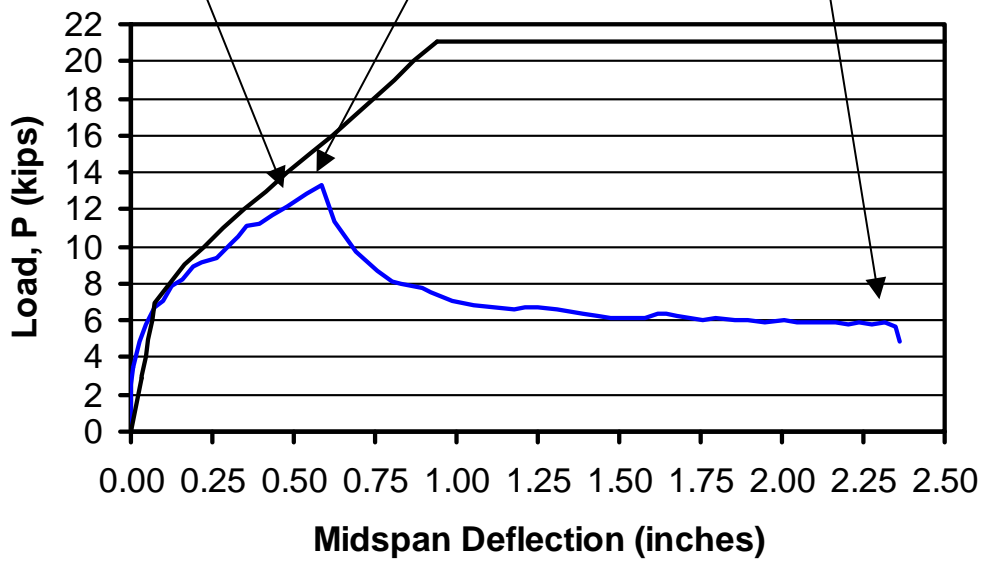
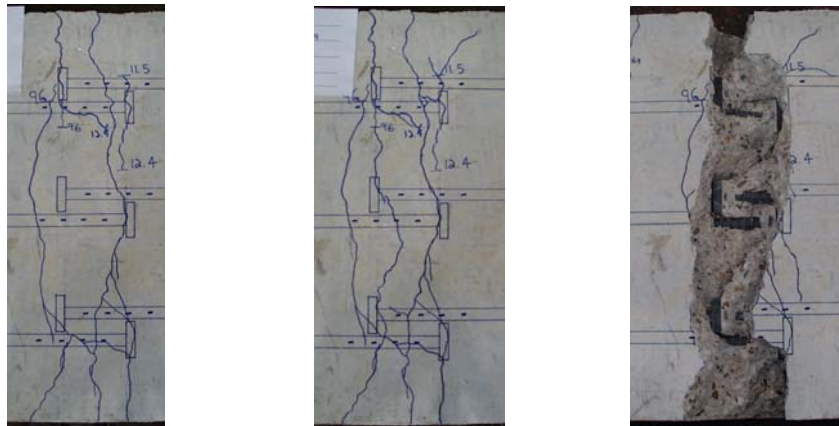


Figure A.3 – Specimen ULS-#8-4.7R-10A-5

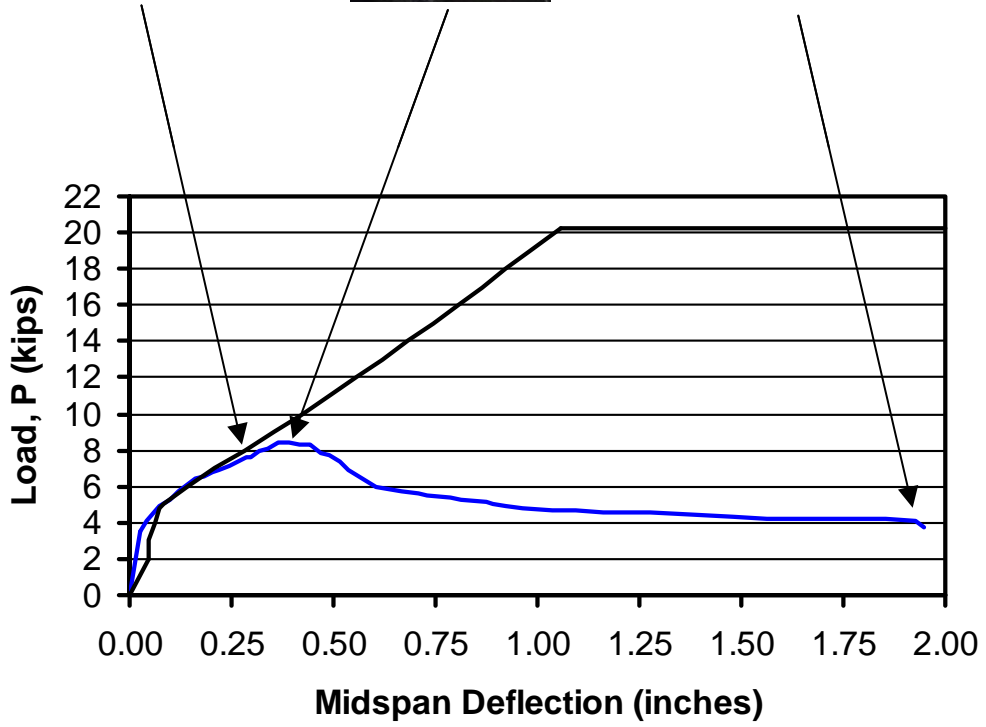
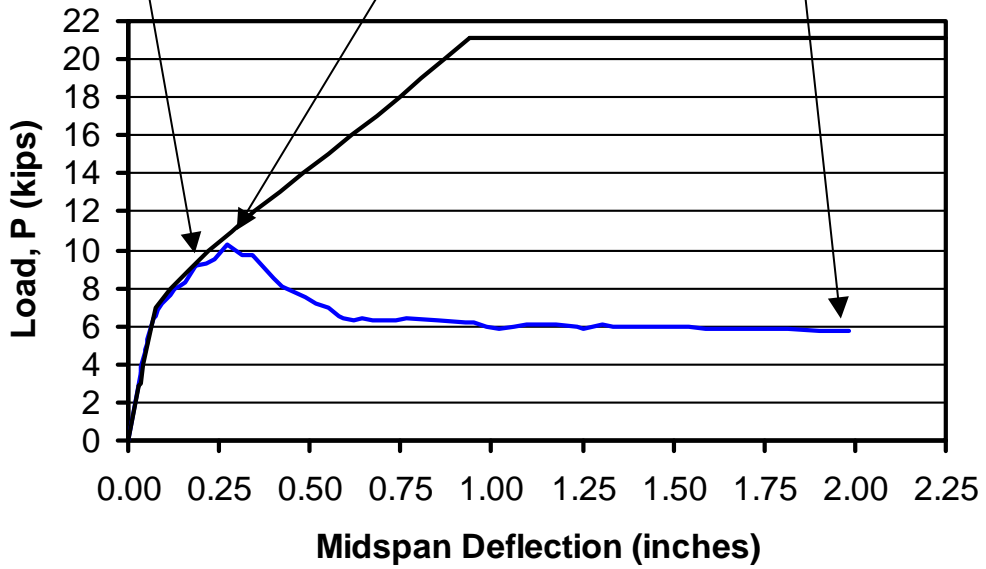


Figure A.4 – Specimen ULS-#8-4.7R-6S-3



**Figure A.5 – Specimen ULS-#8-1.2C-10S-5**

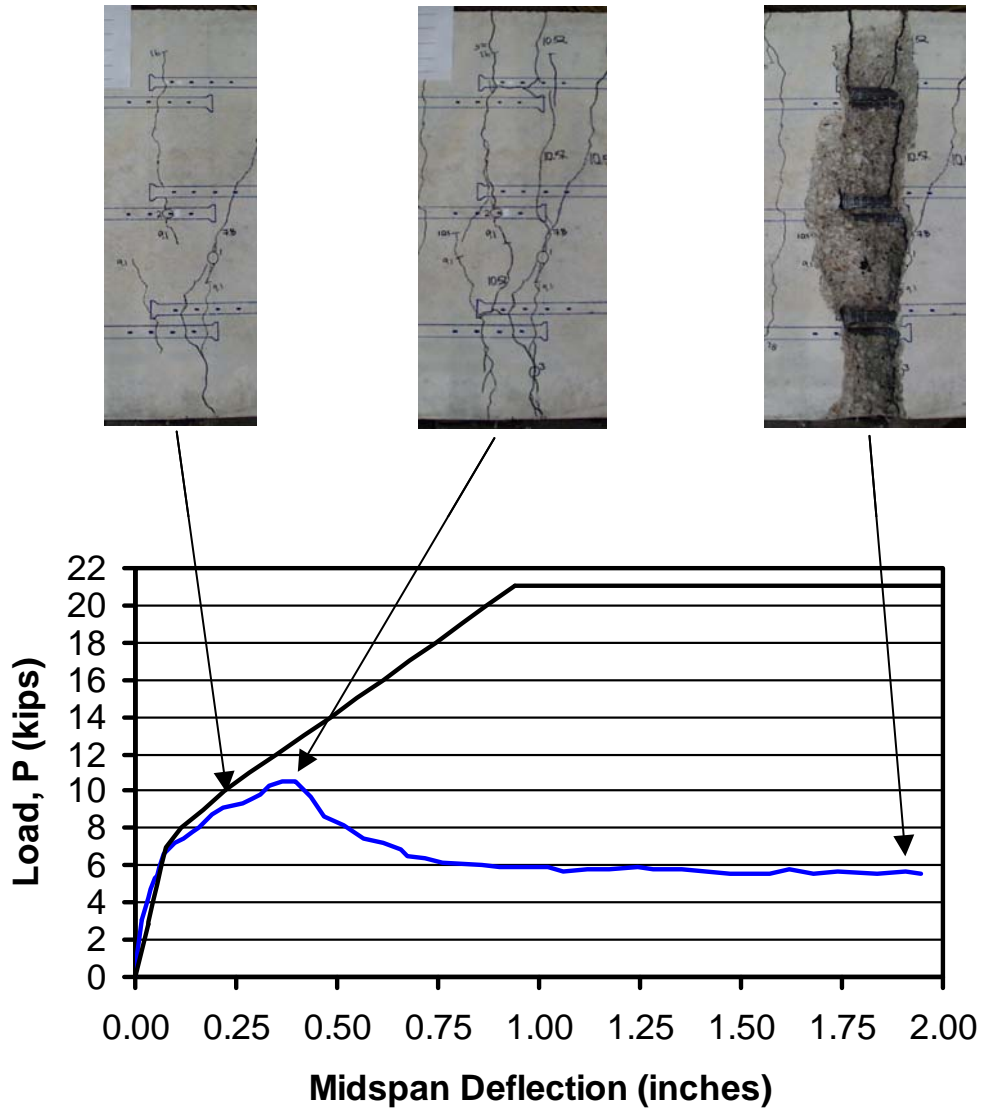


Figure A.6 – Specimen ULS-#8-1.2C-10A-5



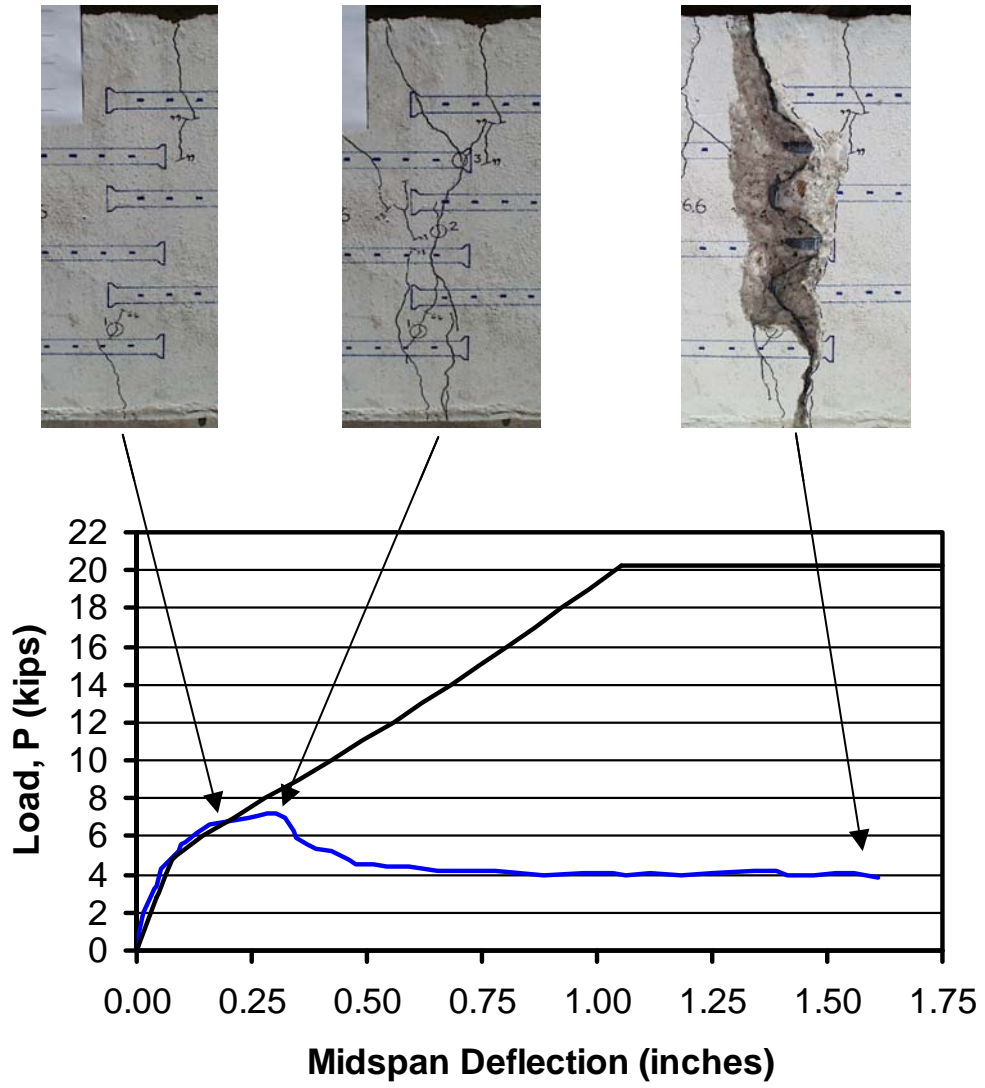


Figure A.7 – Specimen ULS-#8-1.2C-6S-3

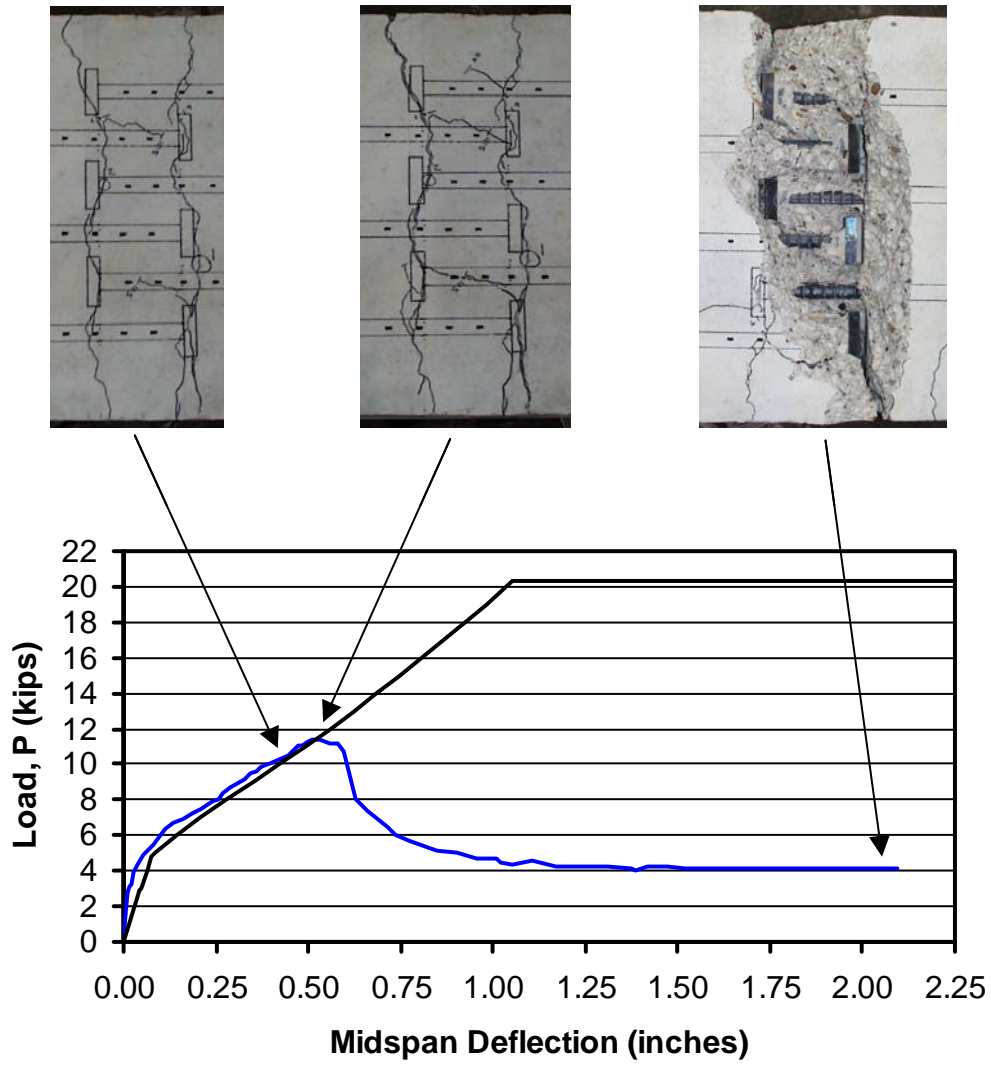


Figure A.8 - Specimen ULS-#8-4.7R-6S-5

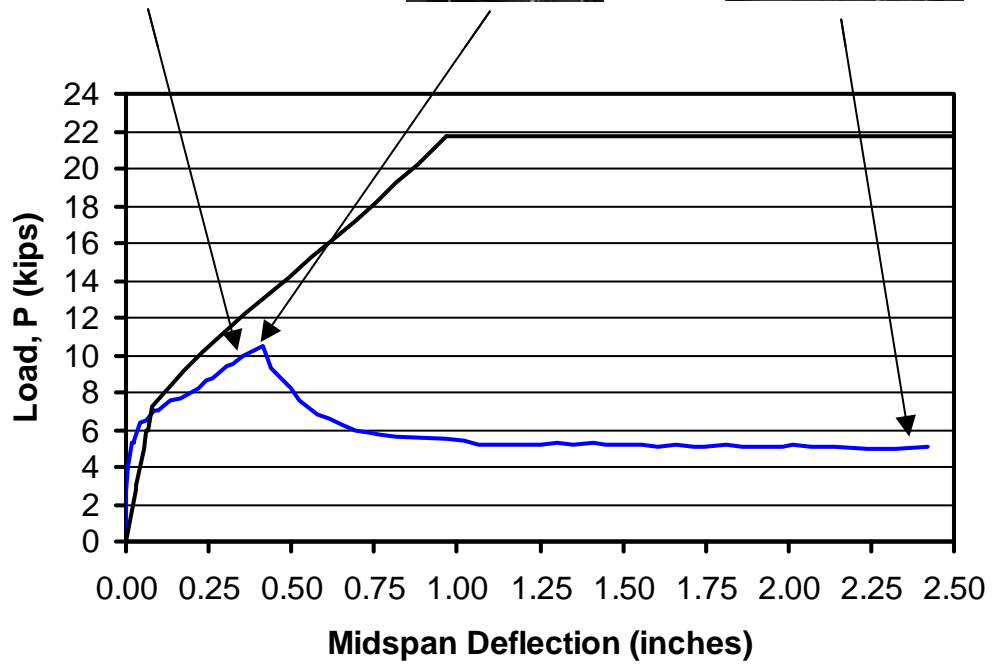
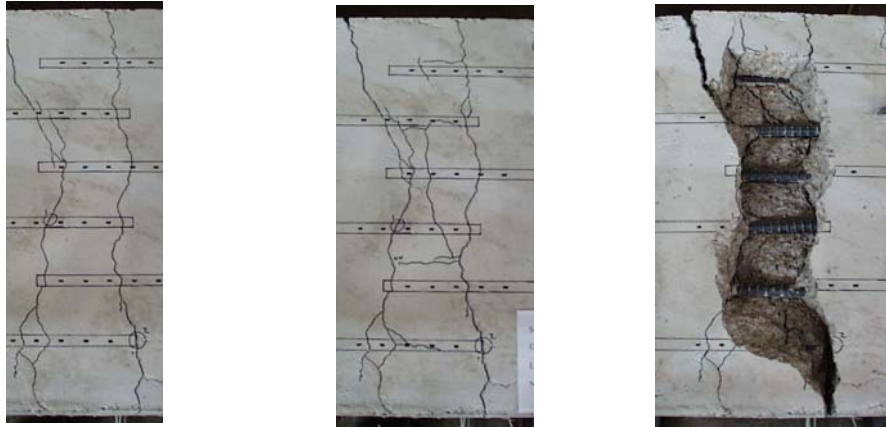


Figure A.9 – Specimen ULS-#8-0X-10S-8

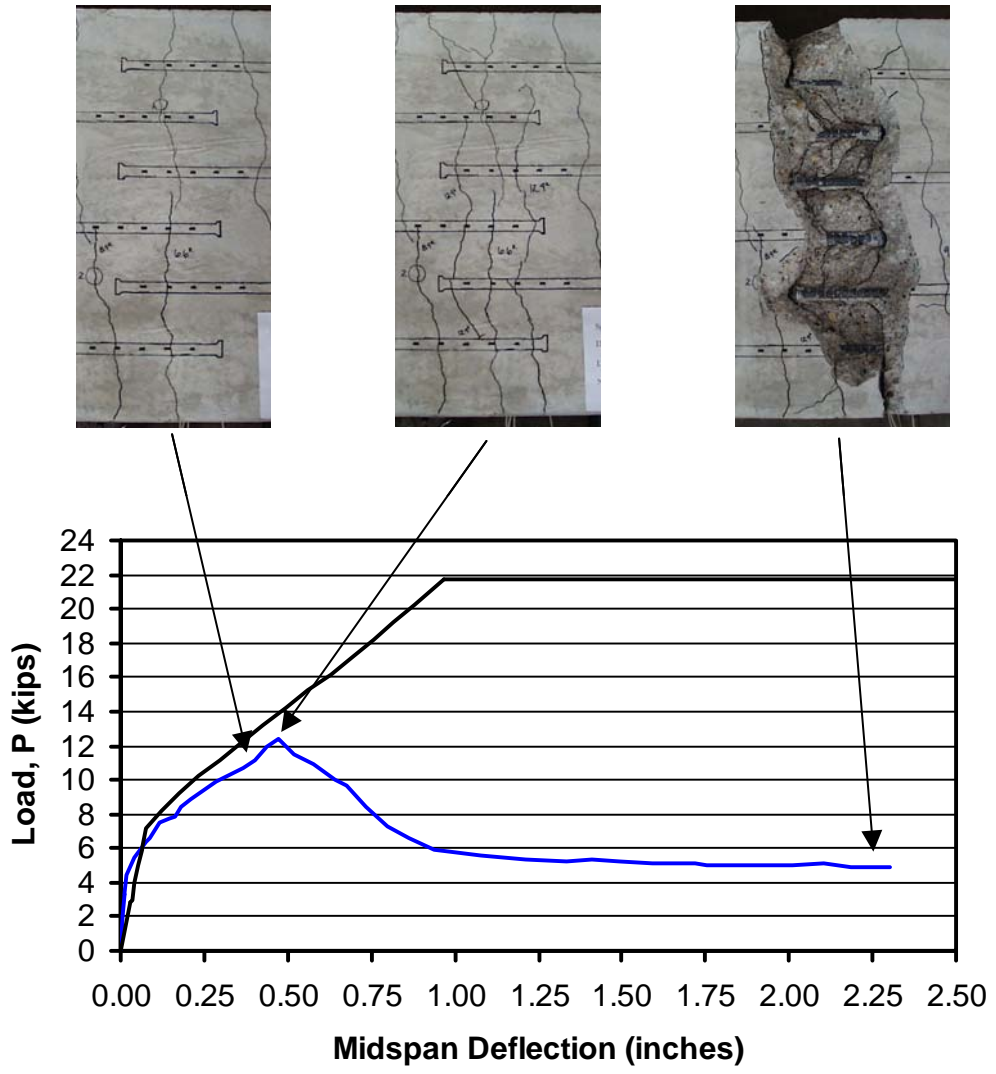


Figure A.10 – Specimen ULS-#8-1.2C-10S-8

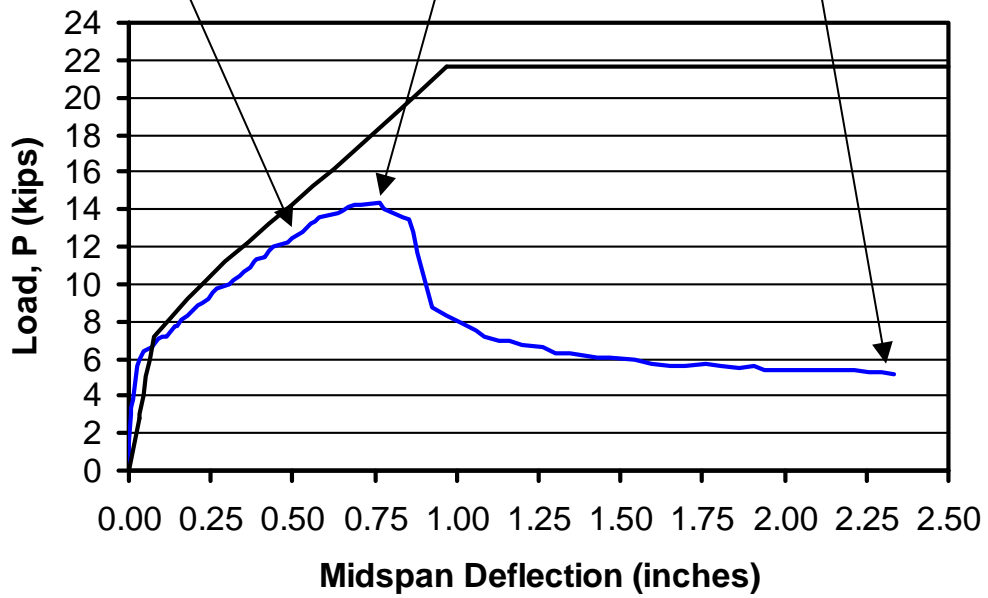
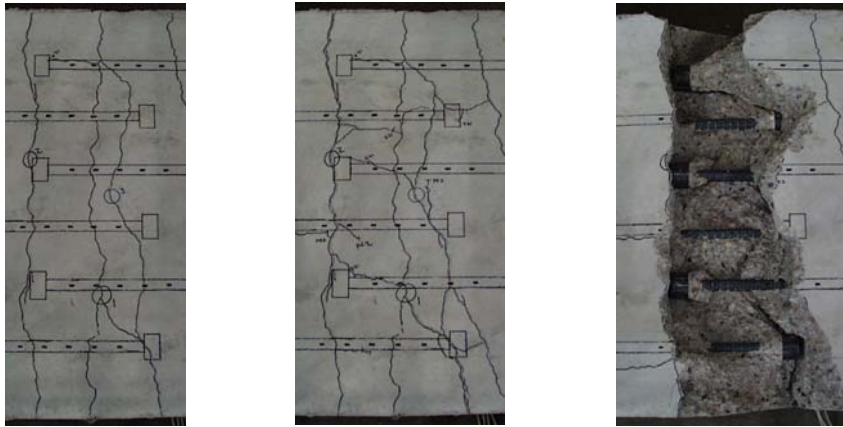


Figure A.11 – Specimen ULS-#8-4.0C-10S-8

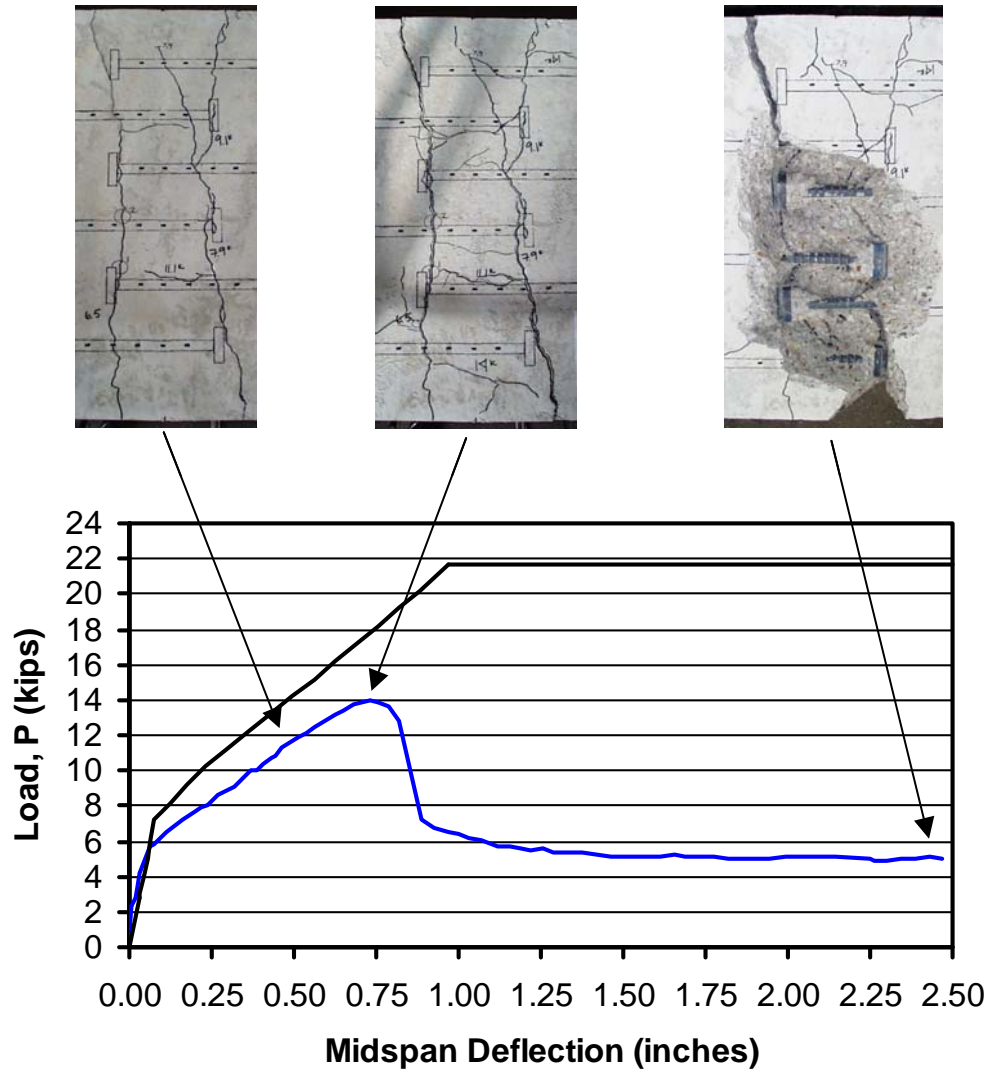


Figure A.12 – Specimen ULS-#8-4.7R-10S-8

## Bibliography

1. American Concrete Institute (ACI 318-95), Building Code Requirements for Structural Concrete and Commentary, American Concrete Institute, Detroit, Michigan, 1995.
2. ACI Committee 408, “Suggested Development, Splice, and Standard Hook Provisions for Deformed Bars in Tension,” (ACI 408.1R-90), American Concrete Institute, Detroit, 1990, 3pp. Also *ACI Manual of Concrete Practice*, Part 3.
3. American Association of State Highway and Transportation Officials (AASHTO), Standard Specifications for Highway Bridges, Fifteenth Edition, American Association of State Highway and Transportation Officials, Washington, D.C., 1993.
4. “ASTM A 970/A 970M-98 Standard Specification for Welded or Forged Headed Bars for Concrete Reinforcement,” 1998 Annual Book of ASTM Standards, American Society for Testing and Materials, Philadelphia, Pennsylvania, 1998.
5. “ASTM C 39/C 39M-99 Standard Test Method for Compressive Strength of Cylindrical Concrete Specimens,” 1999 Annual Book of ASTM Standards, American Society for Testing and Materials, Philadelphia, Pennsylvania, 1999.
6. “ASTM C 78–94 Standard Test Method for Flexural Strength of Concrete (Using Simple Beam with Third-Point Loading),” 1994 Annual Book of ASTM Standards, American Society for Testing and Materials, Philadelphia, Pennsylvania, 1994.
7. “ASTM C 469–94 Standard Test Method for Static Modulus of Elasticity and Poisson’s Ratio of Concrete in Compression,” 1994 Annual Book of ASTM Standards, American Society for Testing and Materials, Philadelphia, Pennsylvania, 1994.

8. "ASTM C 496-96 Standard Test Method for Splitting Tensile Strength of Cylindrical Concrete Specimens," 1996 Annual Book of ASTM Standards, American Society for Testing and Materials, Philadelphia, Pennsylvania, 1996.
9. Bashandy, T.R., "Applications of Headed Bars in Concrete Members," PhD. Dissertation, The University of Texas at Austin, Austin, Texas, December 1996.
10. Berner, D.E., and Hoff, G.C., "Headed Reinforcement in Disturbed Strain Regions of Concrete Members," Concrete International, Vol. 16, No. 1, January 1994, pp. 48-52.
11. Comite Euro-International du Beton (CEB), Model Code for Concrete Structures, English Translation, proposed 1990.
12. Comite Euro-International du Beton (CEB), "Fastening to Reinforced Concrete and Masonry Structures: State of the Art Report," Bulletin d'Information No. 206, August 1991.
13. Cote, P., and Wallace, J. W., "A Study of Reinforced Concrete Knee-Joints Subjected to Cyclic Lateral Loading," Report No. CU/CEE-94/11, Clarkson University, Postdam, New York, February 1993.
14. "Design of Fastenings in Concrete (Draft CEB Guide, Parts 1 to 3)" and "Fastenings for Seismic Retrofitting (State-of-the-Art Report on Design and Application)," Task Group 3.5 (Embedments), Euro-International Concrete Committee (CEB), CEB Bulletin D Information No. 226, Comite Euro-International du Beton, August 1995.
15. DeVries, R.A., "Anchorage of Headed Bars in Concrete Members," PhD. Dissertation, The University of Texas at Austin, Austin, Texas, December 1996.
16. Dr. Techn. Olav Olsen a.s., "Important Aspects for Further Development Concerning the use of T-Headed Bars in Concrete Design and Construction – Final Report" Norway, 1993.



17. Dyken, T., and Kepp, B., "Properties of T-Headed Reinforcing Bars in High Strength Concrete," Nordic Concrete Research Publication No. 7, Nordic Concrete Federation, Oslo, Norway, 1998, pp. 41-54.
18. Furche, J. and Eligehausen, R., "Lateral Blow-out Failure of Headed Studs Near a Free Edge," Anchors in Concrete-Design and Behavior, SP130, ACI, Detroit, 1991, pp. 235-252.
19. Ingham, J.M., "Seismic Design of Knee-Joints Under Transverse Loading," Applications of the T-Headed Bar in Concrete Design and Construction Workshop, St. John's, Newfoundland, 1994.
20. Kuchma, D. A., "Compressive Response of Reinforced Concrete Confined by T-Headed Reinforcement," Applications of the T-Headed Bar in Concrete Design and Construction Workshop, St. John's, Newfoundland, 1994.
21. McConnell, S. W., and Wallace, J. W., "Behavior of Reinforced Concrete Beam-Column Knee-Joints Subjected to Cyclic Loading," Report No. CU/CEE-95/07, Structural Engineering Research Laboratory, Department of Civil Engineering, Clarkson University, Potsdam, NY, June 1995.
22. Orangun, C. O., Jirsa, J. O., and Breen, J. E., "A Reevaluation of Test Data on Development Length and Splices," ACI Journal, Vol. 74, No. 3, March 1977, pp. 114-122.
23. SEQAD Structural Engineers, Solana Beach, California, "Seismic Response of a Bridge Column/Cap-Beam Knee Joint Designed with Headed Reinforcement," Report No. 95/12, Job No. 94/17, Prepared for Headed Reinforcement Corporation, Canada, 1995.
24. SINTEF Report No. STF20 F92020, "Static and Dynamic Pull-Out Tests of T-Headed Bars Embedded in Concrete," SINTEF, Trondheim, Norway, 1992.

## **Vita**

Antonio Lopez Ledesma was born in Seoul, South Korea on October 8, 1974, the son of Arthur and Son Ye Ledesma. He moved to Louisiana and then to San Antonio, Texas. At age 5, he moved to Fayetteville, NC where he graduated from Seventy First Senior High School in June 1993. He received the degree of Bachelor of Science in Civil Engineering from North Carolina State University in December 1997. He began graduate studies at the University of Texas at Austin in August 1998 under the supervision of Dr. John E. Breen and Dr. James O. Jirsa. He has accepted employment with Parsons Brinckerhoff in Tampa, FL.

Permanent address: 1211 Chilton Dr.  
Fayetteville, NC 28314

This thesis was typed by the author.